Institut für Technische Chemie
der Technischen Universität München
Lehrstuhl II

**Nature and stability of aluminum species in HZSM-5:
changes upon hydrothermal treatment and
effect of binder**

Lay Hwa Ong

Vollständiger Abdruch der von der Fakultät für Chemie der Technischen Universität
München zur Erlangung des akademischen Grades eines

Doktors der Naturwissenschaften

genehmigten Dissertation.

Vorsitzender: Univ.–Professor Dr.-Ing. Kai-Olaf Hinrichsen

Prüfer der Dissertation:

        1.   Univ.–Prof. Dr. Johannes A. Lercher

        2.   Univ.–Prof. Dr. Klaus Köhler

Die Dissertation wurde am 09.12.2008 bei der Technischen Universität München
eingereicht und durch die Fakultät für Chemie am 05.02.2009 angenommen.

Abstract:

The nature of Al in high silica HZSM-5 and the influence of alumina binder were studied. Non-statistical distribution of Al was found to precede Al concentration in defining the overall observed acid strength. Heterogeneity of Al distribution resulted in the preferential dealumination of Al in paired sites located at lower T-O-T angle after hydrothermal treatment. The rapid decrease in acid sites concentration observed in early stages of steaming was concluded to be a result of neutralization of acid sites by neighboring Al. Intimate contact between alumina binder and zeolite crystals was found to stabilize part of the framework Al against dealumination under hydrothermal conditions.

Die Eigenschaften von Al in Silizium-reichem HZSM-5 sowie der Einfluß von Bindemitteln auf die Stabilität des Zeolithen wurden in der vorliegenden Dissertation untersucht. Dabei wurde festgestellt, dass die nicht-statistische Verteilung des Al einen grösseren Einfluss auf die Säurestärke des Zeolithen hat als die Konzentration. Unter hydrothermalen Bedingungen führt eine heterogene Al-Verteilung zu einer bevorzugten dealuminierung in gepaarten Struktureinheiten mit kleinen T-O-T Winkeln. Der schnelle Abbau von sauren Zentren in der frühen Phase der Dampfbehandelung wurde darauf zurückgeführt, dass benachbarte Al-Zentren zur Neutralisation beitragen. Enger Kontakt zwischen dem Bindemittel und den Zeolith-Kristallen führt zu einer Stabilisierung des Gerüest-Al gegen dealuminierung unter hydrothermalen Bedingungen.

UBI CARITAS ET AMOR, UBI CARITAS DEUS IBI EST

Acknowledgements

Andy, thank you very much for your suggestions and views on data interpretation. You are a sharp and introspective scientist and I enjoyed (most time ;)) discussions with you in big and small things.

Elvira, a heartfelt thank you. You are one of the few close friends that I have who understood what I went through and provided lots of support. You gave me a place to stay in and drove me at 4 am to the airport for my big interview. I believe you will be successful and happy with your wonderful personality and intelligence wherever you are. Blessings to you and Christoph! Manuel, may your dream come true too!

To a couple of old birds who left TCII: Krishna, Rino, Alex, Oriol. Guys, you have inspired and encouraged me in all things that I do. Difficult to describe my feelings but whenever I think of you guys, a smile comes to my face.

Lueda and Melissa, I do not know what I will become without you girls. Our friendship in the last year in Munich is really special. These memories helped me to survive tough times also in the Netherlands. You girls believed in me and were always there for me. One day, we must meet for the Oktoberfest and challenge the rollercoaster and German beer again! Not to mention the wooden tables of Papasito!

To my family who is a source of deep strength in me. Laopa, Laoma, Geno and Kok Leong, we are very blessed to have one another. I value you guys so much. I am proud of our achievements and I pray that we will hold on and grow together, no matter where we are and what we do. My friends in Singapore, Adeline, Katalin, big big hugs from me.

Andreas, you are the sweetest and kindest person I know. You have been with me in really rough times and stayed with me throughout, supporting me. Your love and support is priceless to me and I have come so far because of you. Thank you my love.

To TCII, thank you. My dream came true with your help. Your encouragements, kind words, coffee together, parties, they are all part of my precious memories. Thank you.

Lay Hwa
November 2008

Table of contents

Chapter 3.

Influence of alumina binder on the acidity of HZSM-5   **66**

Chapter 1.

Introduction

1.0.   Zeolites development

The word "Zeolite" was first used by a Swedish mineralogist Axel Cronstadt. In 1756, he discovered the very first zeolite mineral "stilbite" and observed that the mineral visibly lost water when heated. Accordingly, he named this class of mineral "zeolite" from the classical Greek words "zeo", meaning to boil, and "lithos", meaning stone. At present there are around 40 identified species of naturally occurring zeolite minerals (with Si/Al ratio $y/x = 1$ to 5 depending on the structure) and at least 150 synthetic species with a very wide range of aluminium content [1]. They vary in crystal structure, chemical composition, and some physical properties.

Today, most natural zeolites have been successfully synthesized in laboratory or in commercial plants. At the same time, scientists have synthesized many zeolites that do not exist naturally or at least have not been discovered on the earth. Zeolite is defined by J.V. Smith in 1963 as "an aluminosilicate with a framework structure enclosing cavities occupied by large ions and water molecules, both of which have considerable freedom of movement, permitting ion-exchange and reversible dehydration" [2]. R. Szostak stated in 1989 that "structurally, zeolite is a crystalline aluminosilicate with a framework based on an extensive three dimensional network of oxygen ions." [3].

The current definition of zeolites is specified by the *Subcommittee on Zeolites of the International Mineralogical Association* as follows:

"A zeolite material is a crystal substance with a structure characterized by a framework of linked tetrahedra, each consisting of four O atoms surrounding a cation. This framework contains open cavities in the form of channels and cages. These are usually occupied by H_2O molecules and extra-framework cations that are commonly exchangeable. The channels are large enough to allow the passage of guest species. In the hydrated phases, dehydration occurs at temperatures mostly below 400°C and is largely reversible. The framework may be interrupted by (OH, F) groups; these occupy a tetrahedron apex that is not shared with adjacent tetrahedra." [4].

All the above definitions explicitly imply a zeolite to be an aluminosilicate crystalline material with three dimensional framework structures consisting of SiO_4 and AlO_4 tetrahedra. Because of the unique sizes of pore openings and the channels in zeolites, zeolites are also called molecular sieves. Molecular sieves are materials that can selectively adsorb molecules based on molecule shape and size. Molecular sieve

11

materials involve a variety of micropore and mesopore materials, such as zeolites, metalloaluminates, silicates, metallosilicates, aluminophosphates (AlPO), silicoaluminophosphates (SAPO), carbon sieves, and MCM-41. By definition, any material that can "screen" molecules based on the molecular size can be referred to as molecular sieve.

The development of synthetic zeolites have been fast paced since the first man-made zeolite A and X were synthesized and commercially used as adsorbents by Union Carbide Co. (UCC) in 1948 [5]. In 1972, Mobil Company (now merged with Exxon to ExxonMobil) synthesized the so-called ZSM-n series, a medium pore, high silica content zeolite. Before this invention, no synthetic or natural zeolites had never have a silica-to-alumina ratio of more than 9. Since then, the synthesis of new zeolites or molecular sieves has been a major research area, especially since 1982 when UCC synthesized AlPO4-n and SAPO-n molecular sieves. The invention of AlPO4-n and SAPO-n molecular sieves by the researchers at UCC enlightened and inspired many scientists to make various new hybrid zeolites or molecular sieves.

Since then, many hybrid zeolites have been prepared but the channel openings (apertures) of zeolites or molecular sieves, either natural or manmade, were mainly composed of either 8-, 10-, or 12-member rings. In 1988, Davis et al. synthesized an aluminophosphate molecular sieve (VPI-5) with a channel opening of 18-member ring [6]. Three years later in 1991, Esterman et al. synthesized a gallophosphate (Cloverite) with a bigger channel opening that is composed of 20- member rings [7]. One year later in 1992, researchers at Mobil Research and Development Co. developed a series of novel, mesoporous molecular sieves. One member of this series, MCM-41, possesses uniformly sized mesopores of 1.5 - 10 nm [8]. In addition to zeolite or zeolite-type crystalline materials with pore openings of 8-, 10-, 12-, 18, and 20-membered rings, a 14-membered ring zeolite-type material, AlPO4-8, was prepared in 1990 [9]. Currently, research has been focusing on the catalysis and application of these new zeolites or molecular sieves materials.

1.1. Properties of zeolites

The general oxide formula of a zeolite is $M_{x/n}(AlO_2)_x(SiO_2)_y \cdot m \, H_2O$, where n^+ is the charge of the cation M. It is invariably found that $y \geq x$. The simplest interpretation of this, assuming that all silicate and aluminate tetrahedra are linked via oxygen bridges to

four other tetrahedra, is that two aluminate tetrahedra cannot neighbour each other in a zeolite framework. This interpretation is assumed in the *Loewenstein rule*, which says Al-O-Al bridges are forbidden in a zeolite framework structure [10]. Two adjacent Al tetrathedra would cause a local electrostatic repulsion that would destabilize the zeolite framework. The zeolitic framework is built up of identical repeating structural sub units, so called secondary building units (SBU) (Figure 1.1) [11, 12].
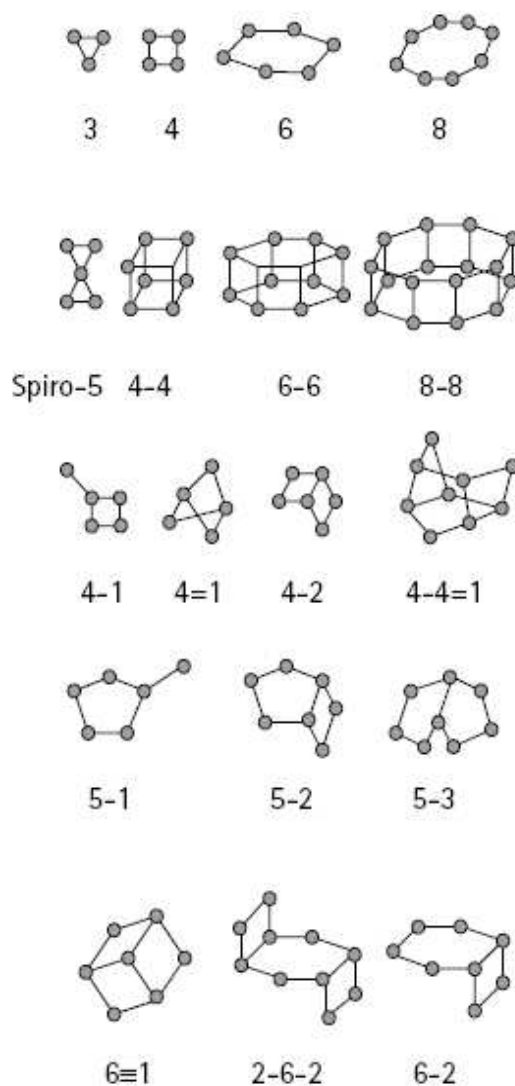
Figure 1.1. Secondary building units (SBUs) [13]

The combination of SBUs larger entities, containing 8, 10 or 12 linked tetrahedra result in systems with well defined pores, channels and cavities. These building units are

characteristic for each zeolite structure and create the typical three dimensional channel systems. The number of linked tetrahedra determines the ring size of the opening and therefore the diameter of the pores (Figure 1.2). For each type of zeolite, the pore diameter of the channel is a characteristic parameter.
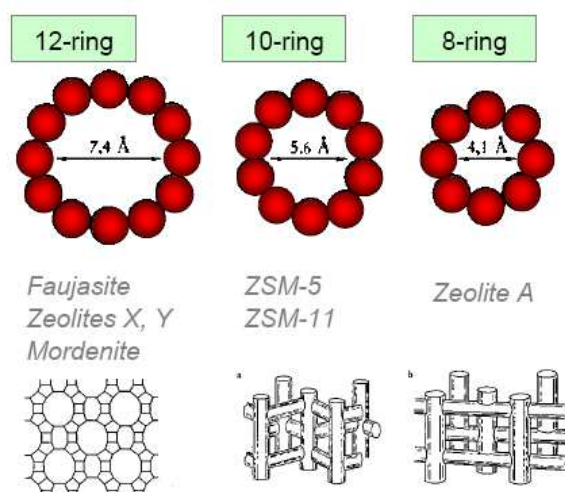
Figure 1.2. Pore openings of common zeolites

The most important advantages of this group of heterogeneous catalyst compared with conventional solid catalysts or catalyst supports stems from the structural properties of zeolites. Zeolites strictly form uniform pore diameters and the pore widths are in the order of molecular dimensions (Figure 1.3).
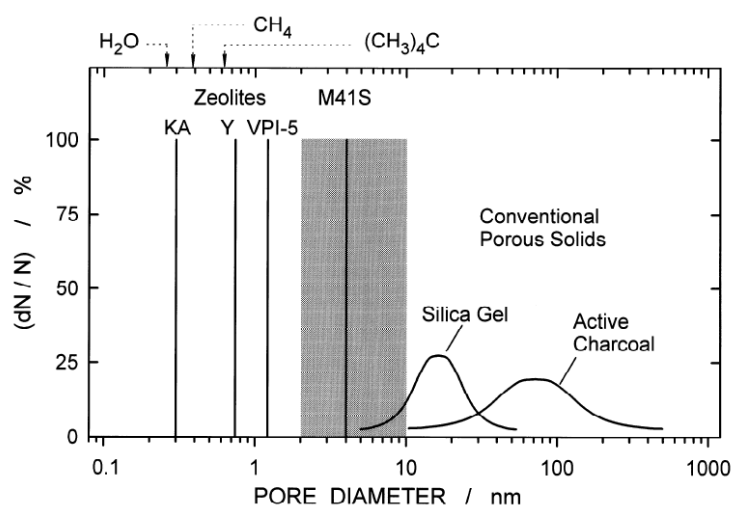
Figure 1.3. Typical pore diameter distributions of porous solids [14].

The pore diameter of zeolites is in the range from 0.2 nm to 1.3 nm. According to IUPAC classification, zeolites are typical microporous materials [15, 16]:

micropores $d_k \leq 2.0$ nm

mesopores: 2.0 nm $\leq d_k \leq 50$ nm

macropores: 50 nm $\leq d_k$

with d_k being the pore diameter. Other conventional porous solids as silica gel have pore diameters from ca. 10 nm with a broad pore diameter distribution compared to zeolites. Because the pore diameters of zeolites are in the range of chemical molecules and the pore size distribution is very narrow, this class of solid materials has the unique ability of being shape selective.

In addition to the defined pore structure, zeolites show acidic character which results from the imbalance of charges in the zeolite structure (SiO_4^{4-} and AlO_4^{5-} tetrahedra). The nature of acid sites, the density or concentration of these sites, their strength or strength distribution and the location of the acid sites influence the overall acidity of the zeolites.

Based on their nature, acid sites can be distinguished in Brønsted acid sites and Lewis acid sites. Brønsted acid sites are bridging hydroxyl groups formed by protons bound to bridging oxygen atoms of Si-O-Al bonds, whereas Lewis acid sites are related to positively charged oxide clusters within the zeolite framework (Figure 1.4).

Brønsted acid site   Lewis acid site
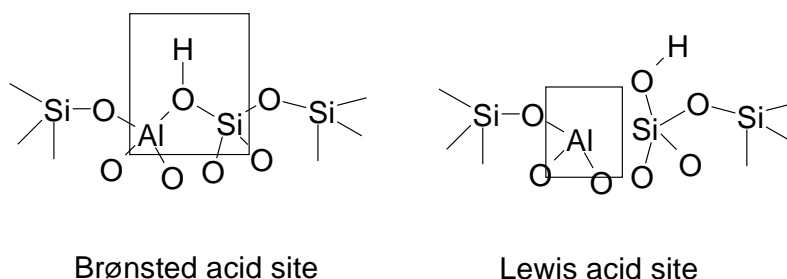
Figure 1.4. Structure of Brønsted and Lewis acid sites.

It has been found that most catalytic activities stem from the Brønsted rather than the Lewis acid sites. R. M. Lago found that under certain circumstances, Lewis acid sites might enhance the strength of nearby Brønsted sites, thereby exerting an indirect influence on the catalytic activity [16].

The density of Brønsted acid sites in a zeolite is related to the framework aluminium concentration, which can be determined by ^{1}H-NMR spectroscopy or IR spectroscopy.

Less readily obtained is the strength distribution of acid sites in zeolites. The most frequently used method is the temperature programmed desorption of bases. Supported by quantum chemical calculations, it is well known that, due to the higher electronegativity of silicon compared to aluminium, the strongest Brønsted acid site in zeolites will occur on completely isolated AlO_4-tetrahedra, i. e. those which lack AlO_4-tetrahedra as next nearest neighbours.

The location of acid sites in a lattice structure is another important characteristic of zeolite. In terms of shape selectivity, it is important whether catalytically active sites occur on the external surface of the crystals or inside the pores. In addition, the presence of compositional gradients, namely, the enrichment or depletion of aluminium in the core or in the outer rim of the individual zeolite crystals is a common phenomenon first observed by Ballmoos et al. in HZSM-5 zeolites [17]. HZSM-5 crystals without significant gradients can be obtained by crystallization from inorganic gels whereas all types of gradients may occur when organic templates are used [18]. J. A. Rabo found that the distribution of the acid sites over the crystals is important for catalytic applications [19].

1.2. Synthesis of zeolites

Natural zeolites are not available ubiquitary but only on special deposits where they are contaminated. The reasons for this fact are the mechanism and the conditions necessary for natural building of zeolites [20]. The age of natural zeolites can not be determined exactly. Usually the geological era of the bedrock formation is declared as the age of the concerning zeolite. Typical geological eras of the creation of bedrocks are quaternary, miocene, pliocene, jurassic or carbon.

A large variety of synthesis routes has been developed for synthetic zeolites. The most convenient method for synthesis of zeolites is the hydrothermal route [21]. A zeolite

was synthesized under hydrothermal conditions by *St. Claire Deville* (1862) and *De Schulten* (1882) for the first time [22]. A difficulty in these times was the lack of analytical methods such as XRD to prove the purity of phases. This problem could only be solved in the 1950s when the group of Barrer developed the basics for modern zeolite synthesis by systematic studies [23]. For zeolite synthesis, five groups of reactants are necessary:

- source for T-atoms (T-atoms means the central atom of each tetrahedron)
- templates
- mineralizer
- solvent
- (possibly) seed crystal

The most common T-atoms are silicon and aluminium. However, also other cations can be used if they fulfil certain conditions [23]:

- $R(T^{n+})/R(O^{2-})$ is between 0.225 and 0.414 (Pauling law)
- electronegativity allows a balanced iono-covalent bonding with oxygen
- the oxidation state is between +2 and +5
- an improvement of the "screening" by polycondensation and "TO_2" units formation
- the resulting framework has a mean charge per tetrahedron between -1 and 0

The T-atoms are generally present in the reaction mixture as amorphous hydroxides, hydrous oxides or related solids (e.g. precipitated gels). Most common sources for silicon are soluble glass, volcanic ashes, colloidal suspensions or fumed silicas. Possible aluminium sources are salts of mineralic acids, aluminium oxides or hydroxides. Different T-atoms may also occur in the same source (e.g. calcined clays for Al and Si).

For templates, inorganic cations (Sr^{2+}, K^+) are often employed but also organic cations are commonly used (tetramethylammonium cation). Templates possess structure directing properties and stabilize the zeolite structure during the synthesis procedure.

OH⁻, the most common mineraliser for silica- and aluminosilica-based zeolites, is often present in the source of the T-atoms. According to the pH required for the reaction, fluoride salts or acids are added as sources of the F⁻ mineraliser. The most important task of mineralisers is the decomposition of the amorphous aluminosilicates during the synthesis. An additional function is to increase the solubility of T-atoms containing species in the reaction mixture.

The most commonly used solvent is water. Its properties are well suited for the dissolution, with the help of the mineraliser, of all species needed for crystallization and thermal conditions of the transformation.

Addition of seeds of the desired zeolite allows, through a reduction of the crystallization time, the formation of a pure metastable phase in competition with more stable phases (kinetic aspect). Furthermore, the crystal size may be adjusted by varying the amount of added seeds.

Different modifications need to be applied to the as-synthesised zeolite product in order to produce the material characteristics required for a given application. When an organic structure directing agent is used for synthesis, it remains in the pores of the precursor zeolite. Therefore, calcination at elevated temperatures is necessary for its removal. Ion exchange can be applied to introduce H^+ or metal cations into non framework positions to balance charges. The H^+ form of a zeolite can also be reached by using an ammonium salt for synthesis and removing ammonia afterwards by heating. The impregnation method can also be used to load the zeolite with catalytically active metal cations.

The Si to Al ratio can also be modified after the actual synthesis of the zeolite. By different types of dealumination, this ratio can be increased to reduce the number of acid sites. On the other hand, aluminium can be inserted into the zeolite framework by treatment with aluminium halides. Furthermore, it has been reported that aluminium can be added by extrusion of high-silica zeolites with aluminium oxide binders to adjust the Si/Al ratio [23-27].

1.3.   Overview of HZSM-5

An intensively studied zeolite framework type of enormous industrial importance is the MFI type. The Si/Al ratio of this type of zeolite can be varied within a broad range via synthesis or post synthesis treatment. Values from approximately 7 up to ∞ can be

reached. The aluminium free form is referred as silicalite-1 [28] and the aluminium containing form as ZSM-5. The great variability of the Si/Al ratio is accompanied by a broad spectrum of zeolite properties such as hydrophilicity/hydrophobicity and catalytic activity or inertness.

1.3.1. Structure of HZSM-5

ZSM-5, together with ZSM-11, is known as the end members of the family of high-silica zeolites. The structure of ZSM-5 zeolite is presented in Figure 1.5. This type of material of formula $Na_n[Al_nSi_{96-n}O_{192}]\cdot\approx16H_2O$ (where $n < 27$) crystallizes with orthorhombic symmetry, space group Pnma, with a=20.1, b=19.9 and c=13.4 Å. The framework is built up from pentasil units resulting in a three dimensional pore channel system [29].
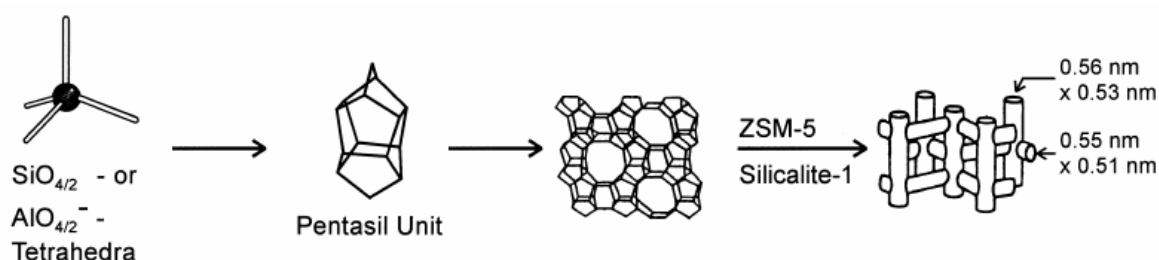
Figure 1.5. Structure of HZSM-5 zeolite and its micropore system and dimensions [14]

In the ZSM-5 framework structure, two kinds of pores occur. One kind of pores is built up by ten membered rings of tetrahedra ending in nearly circular openings with the dimensions of 0.53×0.56 nm. These parallel running pores are crossed perpendicular by the second type of sinusoidal pores of 0.51×0.55 nm. E. M. Flaningen et al. and Argauer et al. determined that by these two types of channels, intersections with diameters of 0.89 nm are created [30, 31].

Because of the small pores of ZSM-5 zeolite and the absence of large cavities, special properties of shape selective catalysis and coke resistance arise and make ZSM-5 an interesting catalyst for industrial processes.

1.3.2. Catalytic application of HZSM-5

The catalytically attractive properties of zeolite ZSM-5 are mainly due to its unique channel system. The channel structure is intermediate between the large pores of faujasite and the small pore of zeolites such as zeolite A and erionite. Additionally, ZSM-5 can be synthesized in a broad range of acidity which corresponds to different activities. Also the shape selective properties and the resistance to coke formation of ZSM-5 play an important role in catalytic applications [32].

The most important and industrial attractive catalytic applications of ZSM-5 zeolite includes dewaxing of paraffins, conversion of methanol to gasoline (MTG), production of light alkenes from methanol (MTO), alkylation of benzene, xylene isomerization and toluene disproportionation.

The principle of the process of dewaxing of paraffins is a shape-selective conversion of wax (long-chain linear and slightly branched alkanes) to branched isomers in order to improve the octane quality in refinery process.

Methanol, produced from synthesis gas ($CO + H_2$), can be converted into synthetic gasoline over ZSM-5 zeolite. However, not only gasoline can be produced from methanol but also olefins, which are an important feedstock for the production of other chemicals.

The conversion of benzene and ethylene to ethylbenzene over a ZSM-5 catalyst is another example of industrial application of ZSM-5. This high-temperature reaction route offers an alternative to the common liquid phase process. The advantages of the zeolite based route are primarily the high energy efficiency and the elimination of corrosive materials ($AlCl_3$ used in the liquid process).

Industrially, the most important xylene isomers are *p*- and *o*-xylene. These can be produced by isomerization of a mixture of xylene isomers by using the shape-selective properties of ZSM-5 zeolite combined with hydrogenation/ dehydrogenation properties of metals in bifunctional catalyst. A further reaction for which the selectivity properties of ZSM-5 are suitable is the disproportionation of toluene to xylene isomers and benzene.

1.4.   Bound HZSM-5 and effect of binder

A zeolite or zeolite-type material is in fine powder form when it is synthesized. Therefore, it has to be incorporated into a matrix, namely a binder, in order to obtain a

large and rigid catalyst of some physical forms. This can avoid a high pressure drop in a fixed-bed reactor or attrition in a moving-bed or fluidized-bed reactor at the industrial level. The most commonly used binders includes refractory oxides such as alumina and silica, and clay such as kaolin and montmorillonite. Being thermally stable, they are also fairly easy to extrude and provide extrudates of good physical strength.

The acidic and physical properties of a zeolite can be influenced by the presence of a binder and thence, the catalytic performance of the final catalysts in terms of activity, selectivity and deactivation. The change in the catalyst performance may be a result of the changes in alkaline metal contents of zeolite, blockage of zeolite channels, decrease in surface area, and trapping of coke precursors on binders. Yet, the influence of binder on the physicochemical and catalytic properties of a zeolite catalyst has been rarely studied in comparison to the non bound zeolites.

It has been claimed that low acidity oxide binders such as SiO_2, TiO_2, and ZrO_2 do not interact with zeolite to increase the acid catalytic activity [33]. More particularly, the binders may reduce the intrinsic acid catalytic activity of zeolites such as ZSM-5, Y, beta of SiO_2/Al_2O_3 ratio of 70 or less. The authors stated in the patents that the oxides may replace alumina in the zeolite, resulting in higher silica content in the framework, smaller ion-exchange capacity, lower hexane cracking rate, and lower α (alpha) value. Unlike the low acidity oxide binders, an alumina binder gives a zeolite a higher intrinsic acid catalytic activity, which is indicated by a higher hexane cracking rate and a higher α value. These patents did not disclose how acidity changes due to the different binders in terms of acid nature, number of acid sites, and strength of acid sites.

Cao et al. [34] studied γ-alumina made by different manufactures as a binder for mordenite. They found that both the strong and medium Lewis acid site densities increased significantly with all three γ-alumina samples, while for Brønsted acid site density, two samples of γ-alumina showed a reduction and only one sample showed a slight increase. Unfortunately, no report on alkaline metal contents for the alumina binders and the zeolite powder was given.

The effects of silica, alumina and kaolin binders on the acidity and activity of H-gallosilicate was investigated by Choudhary et al. [35] and Devadas et al. [36]. Dry-binding method was used instead of the wet-binding method used by the previous authors in the above mentioned works. The catalysts were prepared by physically mixing the binder powder and the zeolite powder, followed by pressing, crushing and finally

calcining at 600°C under nitrogen for 1 hour. Using two model reactions, iso-octane cracking and toluene disproportionation, to check the external acidity and intra-crystalline acidity, respectively, of the bound catalysts, they concluded that the alumina binder had no significant effect on the intra-crystalline acidity but caused an appreciate increase in external acidity. The increase in external acidity was believed to be due to the creation of new zeolitic acid sites at the external surface of the zeolite crystals by substitution of framework Si with Al from the binder. However, external surface of a zeolite is only a very small portion of the total surface. Hence, the increase in external acidity would not make a significant contribution to the total acidity. This result does not seem consistent with Shihabi et al.'s [26] and Cao et al.'s [34] results. That is because Choudary et al. [35] used a dry-mixing method while Shihabi et al. and Cao et al. used a wet-mixing method. Shihabi et al. believed that Al migrated into the zeolite framework in the extrusion process rather than in a solid-solid reaction. In this aspect, both of the results are consistent.

From propane aromatization activity test, it was further concluded that all of the bound catalysts showed better shape-selective catalysis and a lower deactivation rate than the zeolite itself [35]. The alumina-bound catalyst showed a similar activity to the zeolite. The increase in shape-selective catalysis indicated the decrease in effective channel diameter of the zeolite. The authors supposed that this was due to the migration of alkaline and alkaline-earth metal cations from the binders into the zeolite channels and/or due to the formation of non-framework Ga-oxide species formed from degalliation of the zeolite.

The acidities of alumina-bound ZSM-5 of different SiO_2/Al_2O_3 molar ratios (from 5 to 280) was also studied [37]. It was found that the alumina-bound ZSM-5 had more total acidity than the unbound counterparts, which is consistent with most of the previous researchers' results. The increase in total acidity of alumina-bound zeolites primarily came from the increase in Lewis acidity, which may support Zholobenko et al.'s finding of a new Lewis center [38]. The strength of acid sites, which was indicated by the peak temperature in ammonia desorption profile, did not change after the zeolites were bound with alumina.

Al_2O_3-bound zeolite beta for nitration of toluene was also investigated [39]. The bound catalyst showed a higher acidity and activity at the same selectivity to para-isomers and a longer life than the unbound beta. The bound catalyst was found to have

a larger BET surface area, which is different to most of previous observations, and a smaller total pore volume. The activity increase was attributed to the increased acidity by the alumina binder which was believed to contribute to the Lewis acidity of the zeolite beta sample, which originally had only Brønsted acid sites.

Only the wet-embedding method can lead to this effect, while the mechanical mixing method does not provide any significant stabilization of acid sites and textural structure. The alumina-containing matrix preserved the acidity and also increased the acid sites by dealumination---insertion of AlO_4 tetrahedra into the vacancies (defect silanol groups) of the framework and thus improved the crystallinity and decreased the micropore volume. Pure-silica matrix-embedded beta did not have these effects.

In a matrix-base zeolite catalyst, the pore system is also an important factor for reactants and products to diffuse in and out of the zeolite channels. If the matrix or the binder can establish a pore system with a smooth change in pore diameters, that is the so-called "funnel-shaped" pore configuration, the molecules of reactants and products would have a much less surface diffusion barrier.

Thus, the binder or the matrix needs to be in intimate contact with the zeolite to possess such a pore system. With this thought, Le Van Mao [40] and his coworkers conducted research and showed that the catalysts (silica or alumina bound ZSM-5) made under this idea have higher activity and selectivity for aromatization of n-butane than the parent ZSM-5 catalyst.

In most applications of zeolites as catalysts, they are used as solid acidic catalysts, or as materials to provide acidic properties. For a solid acid, acid site density, acid site nature, and acid site strength are the three most important properties. All of the three properties play important roles in acidic catalytic reactions in addition to pore surface area and pore volume. Therefore, if a binder would affect one of these properties of a zeolite, the catalytic property of the zeolite would be altered after it is bound with the binder. Consequently, the results obtained from the unbound zeolite may not be directly applicable to the bound zeolite.

Based on these reports, the major similarities of the results are the significant reduction in the acidity of a bound zeolite when a binder contains a certain threshold of alkaline metals, and the increase of Lewis acidity of the catalyst upon addition of an alumina binder. The differences in observations from the works of the various authors are whether alumina from a binder reacts with silica in zeolites; whether an alumina

binder blocks micropores of zeolites and whether solid-state ion-exchange occurs to a significant degree to reduce the acidity of zeolites.

Complicated physical and chemical processes are involved during the embedding of the zeolite powder into a binder. Binder sources, binder properties, binding methods (dry or wet), and calcination processes (either in air or in steam or in an inert atmosphere) can all affect the properties of the final catalyst. These could explain the different results that have been reported. Therefore, more research is needed to study the effect of the binder on the physicochemical properties of the final zeolite and their behaviors under different application conditions.

1.5. Influence of hydrothermal conditions on zeolites and catalytic processes

The addition of water as a co-feed in several catalytic processes has been investigated by some authors [41-43]. There are several advantages of using water as a co-feed. First, it helps to control the exothermicity of the reaction by absorbing the heat evolved. Second, the partial pressure of reactant can be varied by changing the amount of water used. In certain instances, the selectivity to the desired product was increased and leads to a lower amount of oligomers and aromatics [41].

Water competes with the hydrocarbons for the Brønsted and Lewis acid sites. The adsorption of water on these acid centers reduces their strength and concentration and, thereby, the probability of their interaction with hydrocarbons. As a consequence, the initial conversion of unsaturated hydrocarbons into oligomers, aromatics and coke decreases. Due to the lower yield of coke precursors and the weaker interaction between coke precursors and acid sites, a reduction in deactivation by coke was observed [41]. Nevertheless, the role of water on the deactivation of the catalyst based on HZSM-5 zeolite in the transformation of hydrocarbon is a dual one, depending on the conditions under which the reaction is carried out.

Aguayo et al [44] and Gayubo et a.l [42] found a beneficial effect of using water as a co-feed because it attenuates the deactivation by coke deposition. Hall et al. [45] speculates that the attenuating effect is due to the transformation of Lewis acidic sites into Brønsted ones (which have higher activity for the main reaction and lower for coke formation). Gayubo [46] found that it may also be a consequence of attenuating the evolution of the coke precursors towards polyaromatic structures, as water competes with these precursors in adsorption on the strong acidic sites (required for the

oligomerization reactions, Diels–Alder condensation and polyaromatic formation). This latter hypothesis is supported by the proven fact that water competes, in the adsorption on the acid sites, with all the components of the main reaction, the consequence of which is the attenuation of all the reaction steps. Benito et al [47] and Aguayo et al. [48, 49] proved the attenuation of deactivation by coke by measuring the coke in the MTG process on HZSM-5 zeolite, in the MTO process on SAPO-34 and in the transformation of ethanol on HZSM-5 zeolite [50].

On the other hand, under extreme conditions (at high reaction temperatures) the presence of water has an unfavourable effect on deactivation because, it dealuminates the zeolite [51]. This can also happen to coked catalysts subjected to frequent regeneration whereby the water formed from combustion of aromatics can result in further dealumination of the catalysts [52, 53]. Aukett [54] studied the effect of steam on zeolite structure and proposed that steam attacks the Al–O–Si bonds and produces a rearrangement of the structure of the aluminosilicate. De Lucas [51] found a decrease in the number of Brønsted sites produced and new Lewis sites corresponding to AlO^+ species are created as a result of dealumination. Nayak and Choudhary [27] found that the total effect of steaming is a decrease in the total number of Brønsted and Lewis sites due to dealumination; specifically, the Lewis sites located in the intersections of the channels are affected.

1.5.1. Dealumination of unbound zeolites

The dealumination of zeolites involves the removal of framework aluminium to form extraframework species. Despite the dealuminating effect of water on HZSM-5, it can be utilized as a post-synthesis treatment to tune the acidic properties of a zeolite. In principle, several different methods of dealumination are established and described in literature. Thermal treatment, extraction of framework aluminium with acid [55, 56] and hydrothermal treatment are the most common procedures but also direct replacement of aluminium with silicon by silicon halides has been described [57, 58].

The most common method of dealumination, also applied in this work, is the hydrothermal treatment, also known as steaming. For ZSM-5 zeolite, the Si/Al ratio can be varied in a wide range by synthesis. Despite this fact, preparative dealumination is a widespread technique for this kind of zeolite because ZSM-5 with low Si/Al ratio can be synthesized without using organic templates, making the synthesis easier. Starting from

this high acidic material, the desired acidity can be adjusted by steaming treatment [51, 59-63].

Steaming of the acid form causes a decrease in the amount of tetrahedral framework aluminium while octahedral extra-framework aluminium species are generated [64]. By steaming, terminal SiOH groups and non framework aluminium species will be created from the original Brønsted acid sites, as can be observed by using ^{1}H MAS NMR [65] and ^{27}Al MAS NMR spectroscopy [66, 67]. In literature, different models for the dealumination process are suggested. Gilson et al. explained the extraction of aluminium from the framework via a pentacoordinated aluminium species with a signal at 30 ppm in the ^{27}Al MAS NMR spectrum [68]. However, other authors described the intermediate species as distorted tetrahedral aluminium [69-71]. Till now, the nature of the intermediate hydrolysed aluminium species is highly debatable. The nature of extraframework aluminium is also ambiguous and up to three different kinds of octahedral aluminium species have been described according to ^{27}Al MAS NMR spectroscopy [72].

In addition, during the dealumination process, silicon migrates into the created tetrahedra vacancies of the zeolite framework. With increasing steaming severity, the concentration of Brønsted acid sites decreases. Because every Brønsted acid centre is generated by the substitution of one aluminium atom into the zeolite framework, the concentration of Brønsted acid sites is generally equated to the concentration of framework aluminium. Thus, the progress of dealumination has been commonly monitored by determination of the Brønsted acid sites concentration via IR spectroscopy.

Masuda et al. found that the concentration of strong acid sites caused by tetrahedral framework aluminium decreases whereas the amount of relatively weaker acid sites, which would be induced by the partially distorted octahedral aluminium atoms remains almost constant in steamed HZSM-5 zeolite [73].

Because acidity is the key property of zeolite materials for their catalytic activity, much effort is spent to investigate the change of acid sites concentration by steaming. In the process, the kinetic of dealumination can be derived and is of relevant importance for two main reasons. First, dealumination can be applied as pre-treatment to tune the catalytic properties of zeolites. Second, dealumination occurring under reaction conditions can lead to zeolite deactivation. Hence a correlation of activity to the

dealumination rate can be made to predict a catalysts lifetime and enables one to understand the thermal stability of the bound and unbound zeolites.

The kinetics of dealumination of HZSM-5 zeolite has been investigated by some groups [73-76]. The rate of dealumination by steaming treatment for high acid HZSM-5 catalysts using materials with Si/Al ratios down to 20 was studied. For quantification of the dealumination extent, TPD analysis and ^{27}Al-MAS NMR spectroscopy were used. Brunner *et al.* [77] showed the dependence of the number of remaining framework aluminium on the steam partial pressure, steaming time and steaming temperature (Figure 1.6).
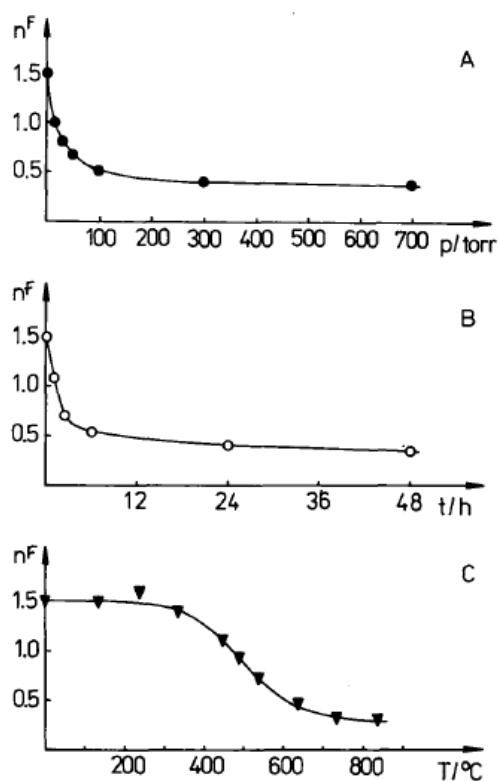
Figure 1.6. Dependence of remaining framework Al (n^F= Al left in the unit cell $Na_xSi_{96-y}O_{196}\cdot18H_2O$) on p ($H_2O$), time and temperature

The following equation for the dealumination process of a HZSM-5 with a Si/Al ratio of 20 was obtained by Masuda *et al.* [73]:

$$-r_{Al} = 0.016 \cdot p(H_2O)^{1.5} \cdot n_{Al}{}^3 \qquad\qquad \text{Eq. 1.1}$$

where n_{Al} is the concentration of remaining framework aluminium and $p(H_2O)$ the water partial pressure. However, Sano *et al* found a rate order of 2 with respect to the concentration of framework Al.

Steaming treatment can enhance the catalytically activity. After mild steaming, aluminium pairs are present. One of these is proposed as non tetrahedral by *Lago et al* [78]. It acts as a strong electron-withdrawing centre for the other tetrahedral aluminium, thus creating a stronger Brønsted acid site. The above results are derived from steaming of pure zeolites of relatively low Si/Al ratio. There are only few detailed investigations on the dealumination of high silica zeolites, which are actually of high industrial importance as the degree of coking in high silica zeolites is lower.

1.5.2. Dealumination of bound zeolites

Depending on the binding method and type of binder, the physicochemical properties of zeolites are altered on being bound. It is hence critical to understand if the presence of the binder has an influence on the hydrothermal stability of the bound zeolites when used under steaming conditions. So far, there are few literature studies that discuss the influence of binder on the thermal stability of bound catalysts. This is an important factor for application in the industry because the presence of binder could interact with the zeolite catalysts under steaming conditions to alter the properties of the catalysts in terms of density of acid sites, strength of acid sites and pore size volume.

As an example, the stability of Fluidized Catalytic Cracking (FCC) catalysts can be enhanced by steam-treatment, which may provide conditions in which some components in a matrix react with the zeolite. Therefore, the study on embedded FCC catalyst might be of help in understanding the relation between binder and zeolite especially since FCC catalysts contain about 50~90 wt% of a binder (matrix) and 10~50 wt% of zeolite [79].

Corma et al. did research on embedding Y zeolites in silica. After steaming, the embedded catalysts [80-82] were tested for gas oil cracking. Silicon from the matrix reacted with extra-framework aluminum to form a new silica/alumina phase, which was external to the zeolite crystal and showed weak Brønsted acidity. The steamed silica-embedded Y catalysts showed enhanced activity and improved gasoline and especially diesel selectivity. Acid leaching, which removed extra-framework aluminum, produced

catalysts with higher micropore volume and more acidic sites [81, 82], which resulted in a higher activity in cyclohexene cracking [83].

Recently, Noronha et al. [84] studied mordenite embedded in a silica-alumina gel. By comparing a physical mixture of the mordenite and the matrix with the catalyst made by binding with the silica-alumina gel (wet-binding method), they further demonstrated that "intimate" contact between the matrix and the zeolite is necessary for the matrix to exert a protecting effect on the zeolite structure (the wet-binding method would provide an "intimate" contact between the matrix and the zeolite). The analysis of the volume of micropores (determined by the t-plot method) showed that the catalyst (only calcined at $500°C$ with no additional steaming) made from a gel-mixture had a slightly smaller micropore volume (0.031 cc/g_{cat}) than the micropore volume of the physical mixture(0.035 cc/g_{cat}). The later value was closely in line with the predicted value. It was concluded that zeolite pores were not significantly blocked.

In the work of Kubecek et al. [85], steaming the silica-alumina embedded catalyst caused the activity and acidity to increase. They concluded that the catalyst made by wet-embedding in alumina or silica-alumina gels followed by calcination at $600°C$ leads to the generation of new zeolite acidic sites which are active sites in cracking reactions. Moreover, the changes of textural properties occurring during the catalyst preparation, particularly when both aluminum and silicon were available in the matrix, supported the assumption that these new sites are created via extensive recrystallization of the zeolite component. This re-crystallization could occur at mild temperatures of around $330°C$.

1.6.   Motivation of thesis

The shape selectivity and high acid strength of HZSM-5 makes it an attractive catalyst for the petroleum refining and chemical industry. However, because of its poor self-binding property, HZSM-5 must be bound with a binder (matrix), such as silica, alumina, clay, or their mixture, to produce the desired shape and mechanical strength for industrial applications.

Synthetic zeolites have had a history of about half a century, and much research has been focused on the synthesis, acidic properties and catalysis with zeolites. There have been several books dedicated to this area, in addition to a tremendous number of papers in journals and professional proceedings. Compared to the extensive research work done on the acidic and catalytic properties of zeolites, not much study has been

carried out on the physicochemical and catalytic properties of bound zeolites, which are more often used in commercial applications. In academia, the acidic and catalytic properties or even kinetic models were studied primarily for pure zeolite (unbound zeolite). In these studies, the binder effect was often neglected.

In most catalysis cases, zeolites are applied as an acidic catalyst. For a solid acidic catalyst, three important properties should be addressed, that is, acid site density, nature of acid sites (i.e., Brønsted acid and Lewis acid), and strength of acid sites. Since most zeolite catalysts are utilized in the bound form, it is important to address whether the binder has any effects on the physicochemical properties such as surface area, pore volume, and acidities, and further on the catalytic properties of the zeolites.

Complicated physical and chemical processes are involved during the embedding of the zeolite powder into a binder. Binder sources, binder properties, binding methods (dry or wet), and calcination processes (either in air or in steam or in an inert atmosphere) can all affect the properties of the final catalyst. Depending on the nature of the binder and the binding method, the zeolite may not experience any change on binding because the binder is "inert" when the zeolite is "mechanically" mixed with the binder. However, it has been shown that the zeolite underwent some changes when bound by wet mulling method. This could explain the different results that have been reported in literature. Therefore, more research is needed to study the effect of the binder on the physicochemical properties of the final zeolitic catalysts and their behaviors under different application conditions. Understanding those phenomena is the key for successful design and synthesis of zeolite tailored for specific industrial applications.

In the 2nd chapter of this thesis, the broad multitechnique characterization of a series of unbound high silica HZSM-5 of different Si:Al ratios is described. A wide range of Si:Al ratios was investigated to explore the subtle variations of the acidic properties of the HZSM-5 as the acid sites are progressively diluted in a silica matrix. In this way, the influence of minor variations in the local environment of the tetrahedral aluminum on the acid-base properties of the HZSM-5 can be studied.

In the 3rd chapter of this thesis, an in depth study of the influence of alumina binder on the final physicochemical properties of HZSM-5 with different Si:Al ratios is presented. Our aim was to demonstrate the sensitivity of the final physicochemical properties of a bound zeolite towards the presence of a binder. Our basic understanding

of the influence of the alumina binder on high silica HZSM-5 would allow us to estimate the behavior of the bound HZSM-5 under specific reaction conditions e.g. under hydrothermal conditions.

Chapter 4 of this thesis presents the detailed study of the dealumination of a high silica unbound HZSM-5. The drive for the fundamental understanding of dealumination under hydrothermal conditions was the insufficient literature available to date on the behavior of a high silica HZSM-5 under steaming conditions. In this chapter, the elementary steps involved in the dealumination process are mapped out and the specific location and distribution of labile aluminium atoms involved at the beginning of this process are identified.

Chapter 5 attempts to identify the critical influence of alumina binder on the dealumination of a high silica HZSM-5. Specifically, in the first section of this chapter, the kinetics of Brønsted acid sites removal upon steaming of the zeolite, in pure powder form and bound with Al_2O_3, is studied.. The second part of this chapter deals with the effect of steaming temperature and duration on the hydrothermal stability of the HZSM-5. The effect of the binder is also discussed.

Overall, the information derived from this thesis allows one to gain a fundamental understanding of the microscopic and macroscopic effect of local variations of aluminium distribution on the acidity of the zeolite and the influence of a binder on the acidity of high silica HZSM-5. This serves as a first step towards the successful design of a robust catalyst that is of high commercial interest due to its stability under hydrothermal conditions.

1.7.   References

1.   http://www.iza-structure.org/databases/NewCodes.htm

2.   Smith, J.V., American Mineral society, Special paper, **1963**, 1, 281-305.

3.   Szostak, R., Molecular Sieves, Principles of Synthesis and Identification, Van Nostrand Reinhold Catalysis Series., **1989**, New York: Van Nostrand Reinhold.

4.   Coombs, D.S., Alberti, A., Armbruster, T., Artioli, G., Colella, C., Galli, E.,Grice, J. D., Liebau, F., Mandarino, J. A., Minato, H., Nickel, E. H., Passaglia, Peacor, E., D. R., Quartieri, S., Rinaldi, R., Ross, M., Sheppard, R. A., Tillmanns, E. and Vezzalini, G., Can. Mineral, **1997**, 35, 1571.

5.   Corma, A., J. Catal., **2003**, 216, 289-312.

6. Davis, M.E., Saldarriaga, C., Montes, C., Garces, J. and Crowder, C., Nature, **1988**, 331, 698-701.

7. Esterman, M., McCusker, L. B., Baerlocher, C., Merrouche, A. and Kessler, H., Nature, **1991**, 352, 320-322.

8. Beck, J.S., Vartuli, J.C., Roth, W.J., Leonowicz, M.E., Kresge, C.T., Schmitt, K.D., Chu, C.T.W., Olson, D.H., Sheppard, E.W., McCullen, S.B., Higgins, J.B. and Schlenker, J. K., J. Am. Chem. Soc., **1992**, 114, 10834.

9. Dessau, R.M., Schlenker, J. L. and Higgins, J. B., Zeolites, **1990**, 10, 522-530.

10. Loewenstein, W., Am. Mineral., **1954**, 39, 92-96.

11. Dyer, A., An Introduction to Zeolite Molecular Sieves, **1988**, New York: John Wiley & Son Inc.

12. Hollemann, A. F., 101. Aufl., Berlin, **1995**, Lehrbuch der Anorganischen Chemie 101. Aufl. 1995, Berlin: Walter de Gruyter.

13. Rakoczy, R.A., Hydrothermalsynthese ausgewählter Zeolithe und ihre Charakterisierung durch Adsorption, **2004**, Universität Stuttgart.

14. Weitkamp, J., Zeolites and catalysis. Solid State Ionics, **2000**, 131, 1-2, 175-188.

15. Everett, D.H., Pure Appl. Chem., **1972**, 31, 579-638.

16. Lago, R.M., Haag, W. O., Mikovski, R. J., Olson, D. H., Hellring, S. D. and K. D. Schmitt, New Developments in Zeolite Science and Technology, Studies in Surface Sience and Technology, ed. A.I. Y. Murakawi, J. W. Ward. Vol. 28. **1986**, Tokyo/Amsterdam: Kodansha/Elsevier. 677.

17. von Ballmoos, R. & Meier, W. M., Nature, 1981, 289, 782–783

18. Tissler, A., Polanek, P.,Girrbach, U., Müller, U. and Unger, K. K., In: Karge, H.G. and Weitkamp, J., Editors, Studies in Surface Science and Catalysis, Elsevier, Amsterdam, **1989,** 46, 399–408.

19. Rabo, J. A. and Gajda, G. J., Guidelines for Mastering the Properties of Molecular Sieves, NATO ASI Series B, ed. Barthomeuf, D., Derouana, E. G. and Hölderich, W., New York: Plenum Press, **1990**, 221, 273.

20. Barrer, R.M., Hydrothermal Chemistry of Zeolites, **1982**, London: Academic Press. 1.

21. Barrer, R.M., Zeolites, **1981**, 1, 130-140

22. Breck, D.W., Zeolite Molecular Sieves (Structure, Chemistry and Use), **1974**, New York: John Wiley & Sons Inc.

23. Kühl, G., Catalysis and Zeolites (Fundamentals and Applications), ed. Puppe, L. and Weitkamp, J., **1999,** Berlin: Springer.

24. Zholobenko, V.L., Kustov, L. M., Kazansky, V. B., Loeffler, E., Lohse, U. and Oehlmann, G., Zeolites, **1991**, 11, 2, 132-134.

25. Chang, C. D., Chu, C. T. W., Miale, J. N., Bridger, R. F. and Calvert, R. B., J. Am. Chem. Soc., **1984**, 106, 26, 8143-8146.

26. Shihabi, D.S., Garwood, W. E., Chu, P., Miale, J. N., Lago, R. M., Chu, C. T. W. and Chang, C. D., J. Catal., **1985**, 93, 2, 471-474.

27. Nayak, V.S. and Choudhary, V.R., Appl. Catal., 1984, 10, 2, 137-145.

28. Grose, R. W. and Flaningen, E.M., **1977**, U.S. Patent 4061724.

29. Kokotailo, G.T., Lawton, S. L., Olson, D. H., Olson, D. H. and Meier, W. M., Nature, **1978**, 272, 5652, 437-438.

30. Flaningen, E. M. and Patton, R. L., **1978**, U.S. Patent 4073865

31. Argauer, R. J. and Landolt, G. R., **1972**, U.S. Patent 3702886.

32. Blauwhoff, P.M.M., Gosselink, J. W., Kieffer, E. P., Sie, S. T. and Stork, W. H. J., Catalysis and Zeolites (Fundamentals and Applications), ed. Puppe, L. and Weitkamp, J., **1999**, Berlin: Springer.

33. Absil, R.P.L., Angevine and P.J, Herbst, J.A, **1991**, U.S. Patent 5053374

34. Cao, Y., Lu, L., Cheng, W. and Yang, D., Acta Petrolei SINICA (Petroleum Processing Section), special issue, **1997**, 111-117.

35. Choudhary, V.R., Devadas, P., Kinage, A. K. and Guisnet, M., Appl. Catal., A, **1997**, 162, 1-2, 223-233.

36. Devadas, P., Kinage, A.K. and Choudhary, V.R., Stud. Surf. Sci. Catal., **1998**, 113, 425-432.

37. Wu, X., Alkhawaldeh, A. and Anthony, R. G., Scientific Bases for the Preparation of Heterogeneous Catalysts, **2002**, 143, 217-225.

38. Zholobenko, V.L., Kustov, L. M., Isaev, S. A. and Kazanskii, V. B., Kinet. Catal., **1992**, 33, 1, 194-196.

39. Dagade, S.P., Waghmode, S. B., Kadam, V. S. and Dongare, M. K., Appl. Catal. A, **2002**, 226, 1-2, 49-61.

40. Le Van Mao, R., Microporous Mesoporous Mater.,**1999**, 28, 9-17.

41. Marchi, A. J. and Froment, G. F., Appl. Catal., A, **1993**, 94, 1, 91-106.

42. Gayubo, A.G., Aguayo, A. T., Moran, A. L., Olazar, M. and Bilbao, J., AIChE J., **2002**, 48, 7, 1561-1571.

43. Aguayo, A.T., Gayubo, A.G., Ortega, J.M., Olazar, M. and Bilbao, J., Catal. Today, **1997**, 37, 239-248.

44. Aguayo, A.T., Gayubo, A.G., Ortega, J.M., Olazar, M. and Bilbao, J., Catal. Today, **1997**, 37, 239-248.

45. Hall, W.K., Lutinski, F. E. and Gerberich, H. R., J. Catal, **1964**, 3, 6, 512-527.

46. Gayubo, A.G., Aguayo, A.T., Castilla, M., Morán, A.L., Bilbao, J., Chem. Eng. Commun., **2003**, 58, 23-24, 5239-5249

47. Benito, P.L., Gayubo, A. G., Aguayo, A. T., Olazar, M. and Bilbao, J., Ind. Eng. Chem. Res., **1996**, 35, 11, 3991-3998.

48. Aguayo, A.T., Benito, P.L., Gayubo, A.G., Olazar, M. and Bilbao, J., Studies in Surface Science Catalysis, **1994**, 88, 567-572.

49. Aguayo, A.T., Sánchez del Campo, A.E., Gayubo, A.G., Tarrío, A. and Bilbao, J., J. Chem. Technol. Biotechnol., **1999**, 74, 315-321.

50. Aguayo, A.T., Gayubo, A.G., Atutxa, A., Olazar, M. and Bilbao, J., Ind. Eng. Chem. Res., **2002**, 41, 4216-4224.

51. de Lucas, A., Canizares, P., Duran, A. and Carrero, A., Appl. Catal., A, **1997**, 154, 1-2, 221-240.

52. Occelli, M.L., Kalwei, M., Wolker, A., Eckert, H., Auroux, A. and Gould, S. A. C., J. Catal., **2000**, 196, 1, 134-148.

53. Aguayo, A. T., Gayubo, A. G., Erena, J., Atutxa, A. and Bilbao, J., **2003**, 42, 17, 3914-3921.

54. Aukett, P.N., Cartlidge, S. and Poplett, I. J. F., Zeolites, **1986**, 6, 3, 169-174.

55. Sand, L.B. Molecular Sieves, Soc Chem Ind., **1968**, London.

56. Frilette, V.J. and M.K. Rubin, J. Catal., **1965**, 4**,** 2, 310-311.

57. Beyer, H.K., Belenykaja, I. M., Hange, F., Tielen, M., Grobet, P. J. and Jacobs, P. A., J. Chem. Soc., Faraday Trans. 1, **1985**, 81, 2889-2901.

58. Grobet, P.J., Jacobs, P. A. and Beyer, H. K., Zeolites, **1986**, 6, 1, 47-50.

59. Trombetta, M., Armaroli, T., Alejandre, A. G., Solis, J. R. and Busca, G., Appl. Catal., A, **2000**, 192, 1, 125-136.

60. Campbell, S.M., Bibby, D. M., Coddington, J. M., Howe, R. F. and Meinhold, R. H., J. Catal., **1996**, 161, 1, 338-349.

61. Erofeev, V.I., Adyaeva, L. V. and Ryabova, N. V., Russ. J. Appl. Chem., **2003**, 76, 1, 95-98.

62. Alsdorf, E., Feist, M., Gross, T., Jerschkewitz, H. J., Lohse, U. and Schwieger, M., Z. Phys. Chem.-Leipzig, **1990**, 271, 2, 267-275.

63. Sendoda, Y. and Ono, Y., Zeolites, **1988**, 8, 2, 101-105.

64. Debras, G., Gourgue, A., Nagy, J. B. and Declippeleir, G., Zeolites, **1986**, 6, 4, 241-248.

65. Engelhardt, G., Jerschkewitz, H. G., Lohse, U., Sarv, P., Samoson, A. and Lippmaa, E., Zeolites, **1987**, 7, 4, 289-292.

66. Fyfe, C.A., Gobbi, G. C. and Kennedy, G. J., J. Phys. Chem., **1984**, 88, 15, 3248-3253.

67. Fyfe, C.A., Gobbi, G.C., and Kennedy, G.J., **1983**, 10, 1551-1554.

68. Gilson, J.P., Edwards, G. C., Peters, A. W., Rajagopalan, K., Wormsbecher, R. F., Roberie, T. G. and Shatlock, M. P., J. Chem. Soc., Chem. Commun., **1987**, 2, 91-92.

69. Samoson, A., Lippmaa, E., Engelhardt, G., Lohse, U. and Jerschkewitz, H. G., Chem. Phys. Lett., **1987**, 134, 6, 589-592.

70. Engelhardt, G., Fahlke, B., Mägi, M. and Lippmaa, E., Zeitschrift für Physikalische Chemie Leipzig, **1985**, 266, 239.

71. Menezes, S.M.C., Camorim, V. L., Lam, Y. L., San Gil, R. A. S., Bailly, A. and Amoureux, J. P., Appl. Catal., A, **2001**, 207, 1-2, 367-377.

72. Yingcai, L., Mingyang, J., Yaojun, S., Tailiu, W., Liping, W. and Lun, F., J. Chem. Soc., Faraday Trans. 1, **1996**, 92, 1647.

73. Masuda, T., Fujikata, Y., Mukai, S. R. and Hashimoto, K., Appl. Catal., A, **1998**, 172, 1, 73-83.

74. Sano, T., Suzuki, K., Shoji, H., Ikai, S., Okabe, K., Murakami, T., Shin, S., Hagiwara, H. and Takaya, H., Chem. Lett., **1987**, 7, 1421-1424.

75. Sano, T., Yamashita, N., Iwami, Y., Takeda, K. and Kawakami, Y., Zeolites, **1996**, 16, 4, 258-264.

76. Sano, T., Ikeya, H., Kasuno, T., Wang, Z. B., Kawakami, Y. and Soga, K., Zeolites, **1997**, 19, 1, 80-86.

77. Brunner, E., Ernst, H., Freude, D., Hunger, M., Krause, C. B., Prager, D., Reschetilowski, W., Schwieger, W. and Bergk, K. H., Zeolites, **1989**, 9, 4, 282-286.

78. Lago, R. M., Haag, W. O., Mikovski, R. J., Olson, D. H., Hellring, S. D. and K. D. Schmitt, New Developments in Zeolite Science and Technology, Studies in

Surface Science and Technology, ed. Murakawi, A.I. Y., Ward, J. W., **1986**, 28, Tokyo/Amsterdam: Kodansha/Elsevier, 677.

79.   Scherzer, J., Fluid Catalytic Cracking: Science and Technology, Studies in Surface Science and Catalysis, ed. Magee, J. S. and Mictchell, M. M., Vol. 76. **1993**, New York: Elsevier Science B.V., 145-182.

80.   Corma, A., Melo, F. V. and Rawlence, D. J., Zeolites, **1990**, 10, 7, 690-694.

81.   Corma, A., Grande, M., Fornes, V. and Cartlidge, S., Appl. Catal., **1990**, 66, 2, 247-255.

82.   Corma, A., Grande, M., Fornes, V., Cartlidge, S. and Shatlock, M. P., Appl. Catal., **1990**, 66, 1, 45-57.

83.   de la Puente, G., Sousa-Aguiar, E. F., Costa, A. F. and Sedran, U., Appl. Catal., A, **2003**, 242, 2, 381-391.

84.   Noronha, Z.M.M., Monteiro, J. L. F. and Gelin, P., Microporous Mesoporous Mater., **1998**, 23, 5-6, 331-344.

85.   Kubecek, N., Vaudry, F., Chiche, B.H., Hudec, P., Renzo, F. Di, Schultz, P. and Fajula, F., Appl. Catal., **1998**, 175, 159-171.

Chapter 2

Effect of aluminum concentration on the acidity of HZSM-5 zeolite

Abstract

The effect of the aluminum content of zeolite HZSM-5 on the acid site concentration and strength was investigated for Si/Al ratios between 20 and 250 (herein referred to as SAMPLE A, SAMPLE B, SAMPLE C and SAMPLE D). Temperature programmed desorption of NH_3, IR spectroscopy of adsorbed pyridine, ^{1}H NMR and thermogravimetry were used to quantify the linear increase of the concentration of acid sites with the concentration of aluminum. Heterogeneity of acid sites was observed in all HZSM-5 samples even for very low concentration of Brønsted acid sites. ^{1}H NMR spectroscopy and desorption of ammonia indicate that in this series of HZSM-5 samples, the acid strength is the highest in HZSM-5 with the highest concentration of framework aluminum (SAMPLE A), while the sample with the lowest concentration of framework Al (SAMPLE D) has the lowest acid strength. The presence of extraframework aluminum and paired aluminum sites are identified as causes for these unusual observations for SAMPLE A and SAMPLE D, respectively. The results indicate how minor variations in the local environment of the tetrahedral aluminum may subtly influence the acid-base properties.

2.0   Introduction

Zeolites are crystalline aluminosilicates with regular microporous systems [1]. Negative charges are generated when SiO_4 tetrahedra are replaced by AlO_4 tetrahedra and the compensation by protons yields acid sites. The concentration, strength, and distribution of these sites greatly influence catalytic properties and thus are topics of various studies [2-5].

The general notion with regards to zeolite acidity is that the decrease in the framework aluminum content is accompanied by an increase in Brønsted acid strength [6]. This is associated with the lower polarity of the lattice, causing increase in proton lability. The validity of this statement requires that the Brønsted acid sites are well distributed and far apart within a zeolite framework. However, experimental results have shown that the above assumption is not always true.

One of the most direct methods to access acid strength is the determination of heat of adsorption using basic probe molecules in microcalorimetry [7-14]. Results are controversial, as some authors found clear differences in the heat of adsorption of zeolites with different Si/Al ratio [15] while others report a constant heat of adsorption [4]. Heterogeneity of OH groups was also suggested by the relatively large half width of IR band of free hydroxyls [16], but the differences in the acid strengths of the different OH groups was hard to determine.

Theoretical calculations performed by van Santen et al. have shown that changes in the zeolite aluminum content have a relatively large influence on proton affinity of neighboring sites [17]. However, it is difficult to predict the overall observed acid strength, when the aluminum is not randomly distributed in the zeolite structure. Hence, the attempt to determine the acid strength purely based on the number of framework Al is oversimplifying the situation in real zeolitic materials.

When a non random distribution of aluminum in the zeolite occurs, enrichment of Al at certain locations in the crystal can give rise to paired aluminum sites. This has been attributed to the use of organic templates as structure directing agents [18, 19]. The distribution of aluminum as a function of the type of templating agent was explored by Sastre et al. who proposed that preferential T sites occupation by the Al atoms in the lattice structure is affected by the energetics of the synthesis process [20].

The varying results derived from theoretical and experimental works prompted us to combine several characterization techniques, such as TPD of ammonia, IR spectroscopy of pyridine, as well as ^1H, ^{27}Al and ^{29}Si MAS-NMR and microcalorimetric

measurements to determine the variations in strength and concentration of acid sites of HZSM-5 with Si/Al ratios between 20 and 250 synthesized using organic templates. The wide range of Si/Al ratios allows exploring subtle variations of the properties as the acid sites are apparently progressively diluted in a crystalline silica matrix. The combination of the techniques allows to assess not only the variations, but also to track better the reasons for these variations.

2.1. Experimental

2.1.1. Materials

Na-ZSM-5 zeolite was prepared according to the following procedure. In a 150 ml flask, 0.075~0.375 g of $Al(NO_3)_3 \cdot 9H_2O$, 0.4 g of NaOH, 2.66 g of TPABr, and 63 g of H_2O were mixed under stirring until a clear solution was obtained. To this solution, 15 g of Ludox HS-40 was added with agitation to give a reaction mixture of 100 SiO_2: 0.1-0.5 Al_2O_3: 5 Na_2O:10 TPABr: 4000 H_2O. The sol or gel obtained was stirred for 2 hours. The mixture was then transferred to a 100 ml Teflon-lined autoclave and kept at 180 °C for 48 hours. The autoclave was cooled to room temperature; the product was filtered and washed with deionized water until a pH value of 8 was reached. Finally, the product was dried at 110 °C overnight and the organic template was removed by first heating in He with a temperature increment of 10°C/min to 550 °C cooling to ambient and repeating the procedure in flowing air.

H-ZSM-5 zeolite was obtained by ion-exchange. Typically, 1 g of calcined Na-ZSM-5 was added to 60 ml of 1 M ammonium nitrate and the solution was stirred at 70 °C for 12 hours. The solution was then filtered and washed several times with deionized water. The above procedures were repeated 3 times. Finally, the ion-exchanged sample was dried at 110 °C overnight and calcined at 550 °C for 6 hours in s tatic air.

2.1.2. IR spectroscopy

IR spectra were measured with a *Perkin Elmer 2000* spectrometer. All spectra were recorded in the region between 4000 and 800 cm^{-1} at a resolution of 2 cm^{-1}. From all spectra, the background spectrum was subtracted.

For IR spectroscopy of adsorbed pyridine, the samples were pressed into self-supporting wafers (density 13-25 mg/cm^2). After activation in vacuum (10^{-6} mbar) for 1 h at 450 °C (heating rate 10 °C /min), the sample was cooled to 150 °C and pyridine was adsorbed in small dosages until full saturation of the bridging OH group at 3606 cm^{-1} was

observed. The system was then equilibrated for 0.5 h. All IR spectra were recorded at 150 °C before adsorption of pyridine, during the ad sorption of pyridine and after outgassing (10^{-6} mbar) at temperature of 250, 350 and 450 °C (holdi ng at the maximum temperature for 0.5 h). The concentration of Brønsted and Lewis acid sites was estimated from the areas of the bands at $1565 - 1515$ cm^{-1} and $1470 - 1435$ cm^{-1}, respectively, by applying Equation 1 and 2 originally derived in ref [21][1].

$$c(BAS) = 4.32 \cdot 1000 \cdot r^2 \cdot \frac{IA(1565 - 1515\,cm^{-1})}{m} \qquad \text{Eq. 1}$$

$$c(LAS) = 3.27 \cdot 1000 \cdot r^2 \cdot \frac{IA(1470 - 1435\,cm^{-1})}{m} \qquad \text{Eq. 2}$$

where:

c = concentration of acid sites [μmol/g]

IA = integral of the respective peak [cm^{-1}]

r = radius of the wafer [cm]

m = mass of the wafer [mg]

Similar experimental steps were also carried out using ammonia as probe molecule with the exception that quantification of acid sites was not done due to overlapping of peaks attributed to Brønsted and Lewis sites.

2.1.3 Temperature programmed desorption (TPD) of ammonia

For TPD experiments, 50-100 mg catalyst was pressed as wafers and loaded in the quartz tubes of a 6 fold TPD set-up. After activation at 550 °C for 1 h (heating rate 10 °C/min) at a pressure of 10^{-3} mbar, 1 mbar of ammonia was adsorbed and equilibrated

[1] The factor used in reference [21] is 1.88 and 1.42 for equation 1 and 2, respectively. However, our results show a constant value of 2.3 times lower acid sites concentration when using the values from reference [21] compared to acid sites concentration derived from nmr, microcalorimetry and TPD of ammonia. We suspect this discrepancy to be due to the definition of absorbance as a function of lg (I/I_o) or ln (I/I_o) which gives exactly a factor of 2.3 lower value if the former is used. Hence, we have modified the factor used in reference [21] by multiplying by 2.3 in order to account for the logarithmic definition of absorbance in this work.

for 1 h at 100 °C. To remove gaseous and physisorbe d ammonia, the pressure was reduced to 10^{-3} mbar for 2 h. The temperature was then increased at a rate of 10 °C/min to 750°C. Desorbing molecules were analyzed by a *Balzers QMG 420* mass spectrometer. Mass 16 was used for ammonia. A HZSM-5 standard with known acid sites concentration (derived from microcalorimetry) was used as a reference for quantification.

2.1.4 MAS NMR spectroscopy

MAS NMR spectroscopy measurements of the zeolites were carried out using a *Bruker Avance AMX-500* NMR-spectrometer with a magnetic field of 11.75 T. The samples were packed in 4 mm ZrO_2 rotors and spun at 15 kHz.

For ^{1}H-MAS NMR spectra, the samples were activated in vacuum at 400 °C for 14 h to eliminate adsorbed water. The sample was transferred to a glove box and the rotor filled in water and oxygen free atmosphere. At the magnetic field of 11.75 T, the Larmor frequency for ^{1}H was 500 MHz. Adamantane $C_{10}H_{16}$ was used as reference material, (δ = 2.0 ppm). For spectra recording, an excitation pulse with a power level of 6.00 dB and a length of 1.60 µs was applied. The relaxation time was 2 ms. For all spectra, 100 scans were recorded. For quantification, the 1D spectra were simulated with Gaussian peaks using the program dmWinfit2001 developed by Massiot [22].

For ^{27}Al-MAS and MQMAS NMR measurements, the samples were hydrated for at least 48 h. The reference for the measurements was Al $(NO_3)_3 \cdot 9\ H_2O$ (δ = -0.543 ppm). An excitation pulse with power level of 7 dB and a length of 0.6 µs was applied for the 1D spectrum. The relaxation time was 250 ms. For all 1D spectra, 2400 scans were recorded. MQMAS spectra were recorded with a three pulse sequence. The power level was 7 dB for the first two pulses and 35 dB for the last one. The pulse lengths were p_1 = 8 µs, p_2 = 3.2 µs and p_3 = 52 µs. The evolution time t_1 was incremented in intervals of 1 µs and data were processed with XWINNMR. For quantification of the ^{27}Al-MAS NMR spectra, the chemical shift and the quadrupolar coupling constant (QCC) were obtained from the MQMAS spectrum and used to deconvolute the 1D spectra using dmWinfit2001.

For ^{29}Si-MAS, the Larmor frequency was 99.36 MHz. The samples were packed in 4 mm ZrO_2-rotors and spun at 15 kHz. The reference for the measurements was solid Si $(OSi\ (CH_3)_3)_4$ (δ = -9.843 ppm). For 1D spectra, an excitation pulse with a power level of 7 dB and a length of 0.6 µs was applied. The relaxation time was 250 ms. For all 1D

spectra, 2400 scans were recorded. For determination of Si/Al ratio, the 1D spectra were simulated using dmWinfit2001.

2.1.5 Microcalorimetric measurements

The adsorption isotherms were measured in a SETARAM TG-DSC 111 instrument. Approximately 25 mg of pellets was charged into the quartz crucible used in the TG-DSC system. The sample was activated by heating to 450 °C with an increment of 5 °C/min and maintaining at 450 °C for 2 h in va cuum (p<10^{-6} mbar). After activation, the temperature was stabilized at 150 °C. Ammonia w as introduced into the closed system in small doses and allowed to equilibrate with the HZSM-5 until a further mass increase was not observed. The ammonia pulses were repeated until a decrease in the differential heat of adsorption was observed.

2.1.6 Atomic absorption spectroscopy (AAS)

The silicon and aluminum contents of the zeolites were determined by AAS using a *UNICAM 939* spectrometer. Before measurement, 20-40 mg of each sample was dissolved in a mixture containing 0.5 mL of hydrofluoric acid (48%) and 0.1 mL of nitrohydrochloric acid and heated to the boiling point of the mixture. From the amounts of silicon and aluminum measured from AAS analysis, the Si/Al ratio was calculated.

2.2.   Results

2.2.1. IR spectroscopy of adsorbed ammonia

The normalized IR spectra of the activated HZSM-5 samples are shown in Figure 1. The band at 3606 cm^{-1} is attributed to the stretching vibration of the bridging hydroxyl groups (Brønsted acid sites), while the band for terminal silanol groups is found at 3743 cm^{-1}. The area of the bridging OH group at 3606 cm^{-1} progressively decreased with the decrease of the framework aluminum concentration. The relatively large half width of the band of the bridging OH groups suggests the presence of different OH groups.

In the IR spectrum of HZSM-5 with the highest Al content (SAMPLE A), a small band was observed at 3660 cm^{-1}, which is attributed to extraframework aluminum hydroxyl groups. The presence of extraframework aluminum is not clearly visible in the spectra of the other activated HZSM-5 samples.
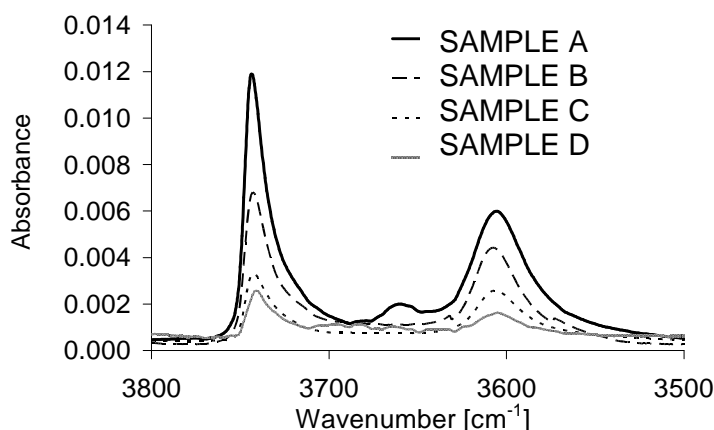
Figure 1. Normalized IR spectra of activated HZSM-5.

Small dosages of ammonia were pulsed into the IR cells at 150 °C until the bridging OH group disappeared. The adsorption temperature of 150°C was chosen in order to complement results of microcalorimetry.

The IR spectra during adsorption of ammonia are depicted in Figure 2. Upon contact with ammonia the OH band at 3606 cm^{-1} decreased in intensity and in parallel a narrow band at approximately 3357 cm^{-1} appeared, which is attributed to the stretching vibration of unperturbed NH groups together with a broad and composite band in the 3280 - 3085 cm^{-1} range which is due to weakly H-bonded NH. In addition, a broad and intense adsorption in the 1530-1402 cm^{-1} range in which a triplet can be distinguished when the spectra are enhanced is observed.
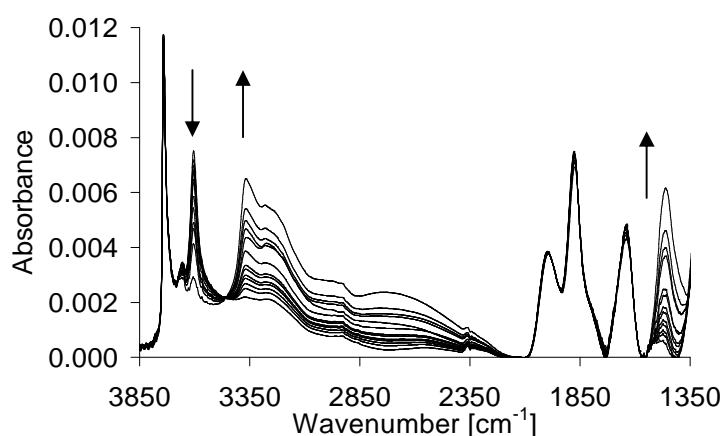
Figure 2. IR spectra during ammonia dosing on SAMPLE A (arrows indicate band intensity change with increasing ammonia partial pressure from 5x10^{-4} to 1x10^{-1} mbar)

Increasing ammonia exposure led to a gradual irreversible disappearance of the bands associated with the strong acid sites. In order to investigate, if ammonia redistributes among the OH groups of different acid strengths, small pulses of ammonia were introduced to the zeolite at 150 °C and IR spe ctra were measured immediately after pulsing of ammonia and 15 minutes after adsorption. No significant shift in the OH band to higher frequency was observed (Δv_{max} = 2 cm^{-1}) within each pulse and between the pulses indicating that no significant redistribution of adsorbed ammonia has taken place (Figure 3a).
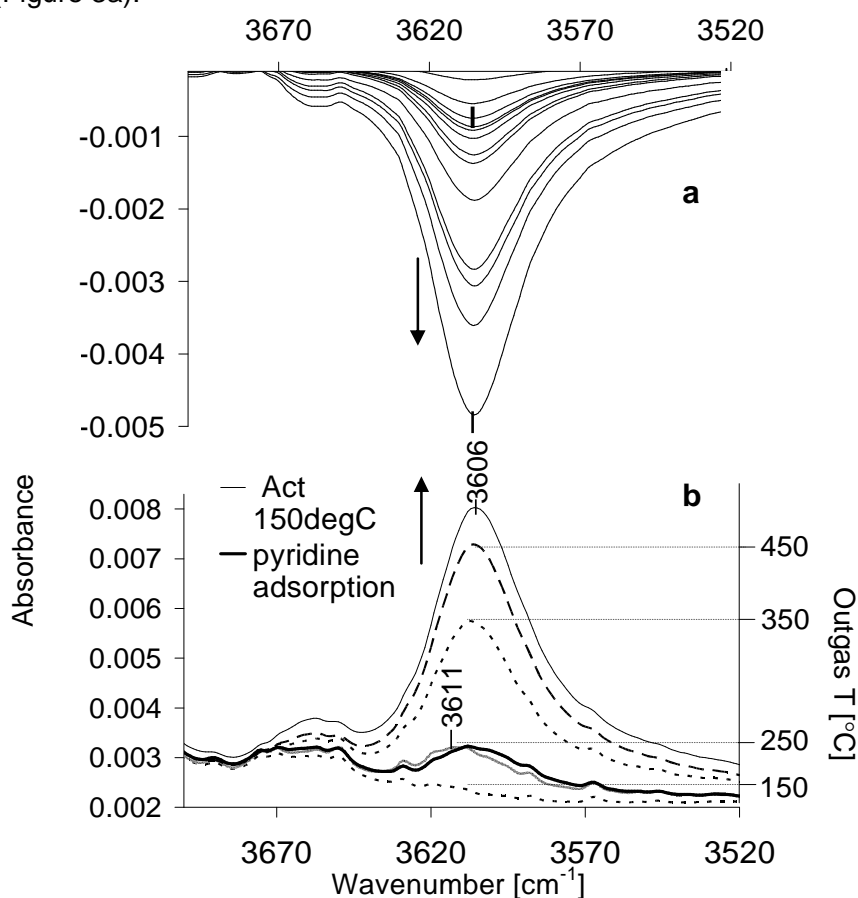
Figure 3a) Difference IR spectra [(spectrum after NH$_3$ dose)-(spectrum after activation)] after adsorption of increasing amount of ammonia (from 10^{-4} to 10^{-1} mbar); b) IR spectra of subsequent desorption of ammonia at increasing temperature of SAMPLE A. All spectra were measured at 150 °C

The sample was outgassed after the bridging OH groups were fully saturated with ammonia. The heterogeneity of OH groups within each zeolite sample was investigated by following the positions of the bridging OH band progressively restored after desorption of ammonia in vacuum at increasing temperature (250, 350 and 450 °C)

(Figure 3b). All the OH groups were subsequently restored by stepwise heating. IR spectra were recorded at 150℃ after the complet ion of each desorption step.

If OH groups were heterogeneous, then the least acidic OH groups (i.e., those of the highest wavenumber) should release ammonia at desorption temperature lower than that of the more acidic OH groups (those with lower wavenumber). Hence, the IR bands of OH groups that are restored upon ammonia desorption should shift to lower frequency with increasing desorption temperature.

Indeed, the restored OH band shifted to lower frequency by 5 cm^{-1} suggesting a minor heterogeneity of OH groups in the HZSM-5 samples. The shift in the OH band after desorption of ammonia are presented in Figure 3b. The comparison at the same pyridine coverage during the adsorption and desorption step shows that the shift in wavenumber (indicating difference in acid strength) is only observable during desorption.

Figure 4a and b shows that not only heterogeneity of acid sites exists in each sample, but also that there is a difference in the relative distribution of acid site strength among zeolites. All zeolites tested have the same concentration of weak acid sites. However, while the concentration of hydroxyl groups free after progressive heating above 250 ℃ (strong Brønsted acid sites) increases for SAMPLE A to SAMPLE C, it leveled above 350 ℃ for SAMPLE D. In consequence, SAMPLE A, B, and C show similar acid strength distribution with SAMPLE A having a higher percentage of strong Brønsted acid sites, which are not restored after ammonia outgassing at 450 ℃. On the other hand, SAMPLE D has a higher proportion of weak Brønsted acid sites (60% restored after outgassing at 250 ℃). In essence, t his results from the larger relative concentration of weakly Brønsted acidic bridging hydroxyl groups.
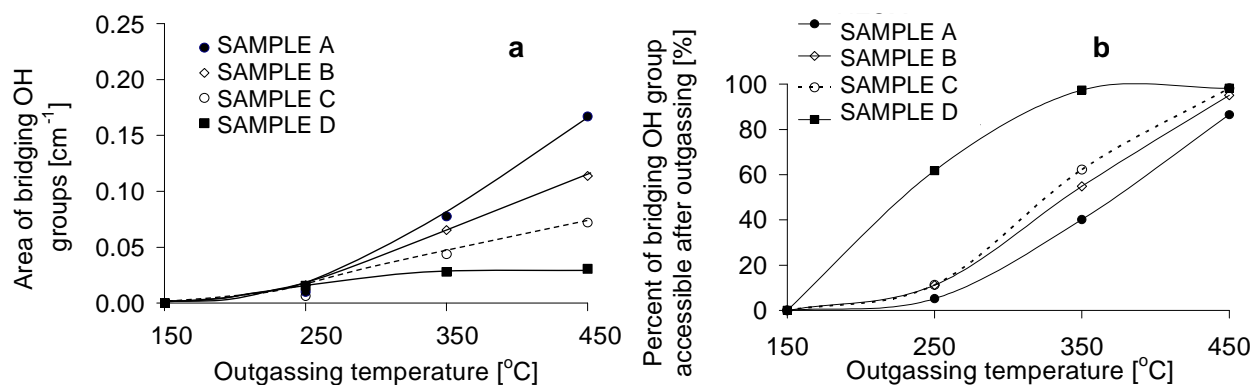
Figure 4. (a) Area of bridging OH group restored at different outgassing temperatures. (b) Percentage of bridging OH remaining after desorption of ammonia at 250, 350 and 450 °C. All spectra were recorded at 150 °C.

2.2.2. IR spectroscopy of adsorbed pyridine

IR spectroscopy of pyridine was used to quantify the concentration of Brønsted and Lewis acid sites using the 19b vibration mode of the adsorbed molecule. The band which appears at 1440 cm^{-1} in liquid like or physically adsorbed pyridine shifts to 1450 cm^{-1} upon formation of coordinated species by adsorption on Lewis acid sites and to 1550 cm^{-1} upon formation of pyridinium ions by protonation at Brønsted sites.

Spectra of progressive adsorption of pyridine on SAMPLE A are presented in Figure 5. The bands due to chemisorbed pyridine appeared in the region 3400-2400 cm^{-1} for the N-H and C-H stretching vibrations and in the region 1680-1430 cm^{-1} for the ring vibrations. The aromatic C-H and N-H vibrations appeared above 3000 cm^{-1}. The two bands at 3265 and 3180 cm^{-1} are typical of pyridinium ions. In addition, a doublet at 2914 and 2849 cm^{-1} was observed, characteristic of symmetric and asymmetric saturated C-H stretching vibrations, respectively, as well as a band at 2979 cm^{-1} corresponding to the overtone vibration of the 1490 cm^{-1} peak. The formation of pyridinium ions was indicated by bands at 1635 and 1544 cm^{-1}, and the presence of species coordinated to Lewis sites by the bands at 1622 and 1455 cm^{-1} from the 8a and 19b modes, respectively. The signal at 1490 cm^{-1} is common to both species.
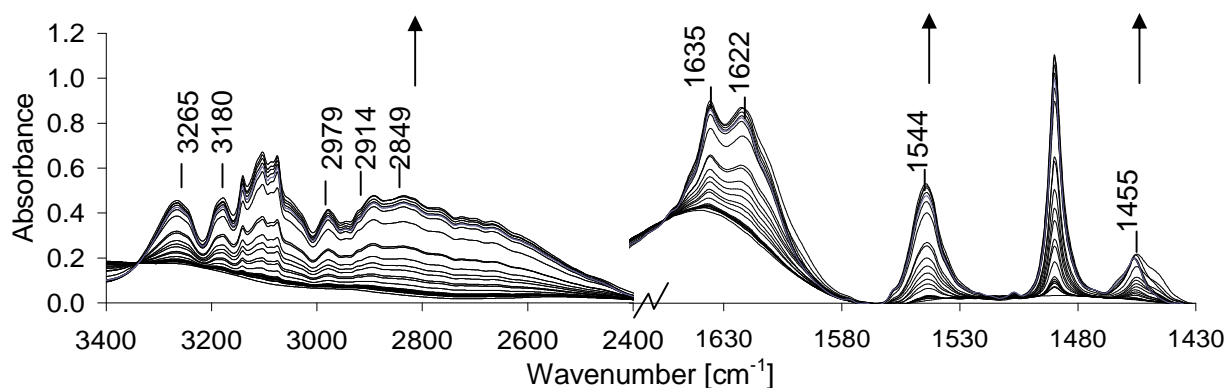
Figure 5. N-H and C-H stretching vibration of pyridine (3400-2400 cm^{-1}) and ring vibration of chemisorbed pyridinium ions (1680-1430 cm^{-1}) on SAMPLE A. Arrows indicate band intensity change with increasing pyridine partial pressure.

Adsorption of pyridine was carried out in small pulses until the band at 3606 cm^{-1} disappeared. After each pulse, the system was allowed to equilibrate for 15 minutes to detect eventual redistribution of pyridine on the HZSM-5. No clear indication of redistribution of pyridine was observed within each pulse. A Δv_{max} of 5 cm^{-1} in the bridging OH group was detected (Figure 6). The shift of up to 5 cm^{-1} was observed for all the investigated samples, even for SAMPLE D as shown in Figure 6b.
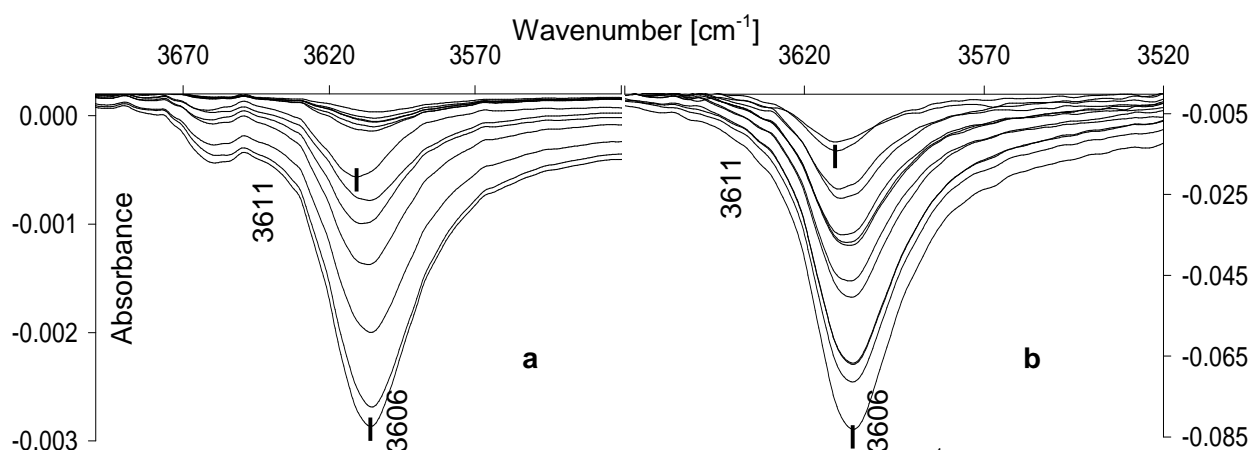
Figure 6. Difference IR spectra [(spectrum after pyridine adsorption) – (spectrum after activation)] with progressive adsorption of pyridine: a) SAMPLE A and b) SAMPLE D.

After outgassing at 150 °C for 1h, the intensity of the band at 1544 cm^{-1} attributed to ring vibration of the protonated pyridinium ion decreased with increase in Si/Al ratio

(Figure 7). In addition, SAMPLE B, C and D appeared to have very low concentrations of extra-framework aluminum for which coordinative adsorption of pyridine would have led to a band at 1455 cm^{-1}.
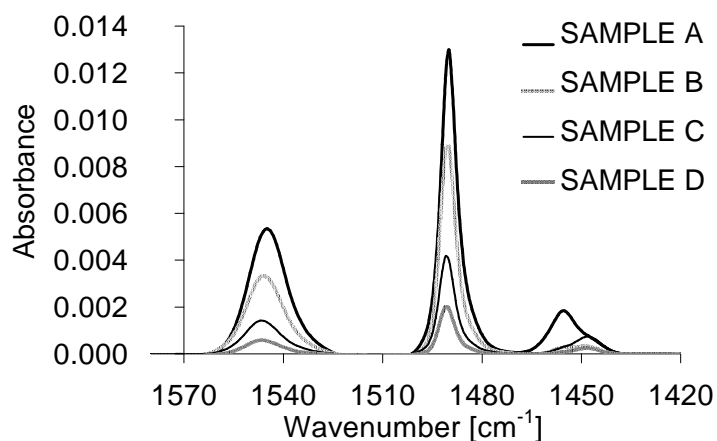
Figure 7. Normalized spectra of chemisorbed pyridine on SAMPLE A, B, C and D

Referring to the band at 1455 cm^{-1}, the strength of Lewis acid site is higher in SAMPLE A compared to the other samples. This is due to the presence of extraframework octahedrally coordinated aluminum in the catalyst, which is associated to the band at around 3660 cm^{-1} in the spectrum of the activated samples (Figure 1). The weak Lewis acid sites observed in SAMPLE B, C and D are attributed to the adsorption of pyridine on Na$^+$ and Fe^{2+} cation impurities present in small concentrations in the zeolites [23].

The concentration of Brønsted and Lewis acid sites are calculated using equations 1 and 2 and the results are presented in Figure 8. A linear correlation of Brønsted acid sites with framework aluminum is observed.
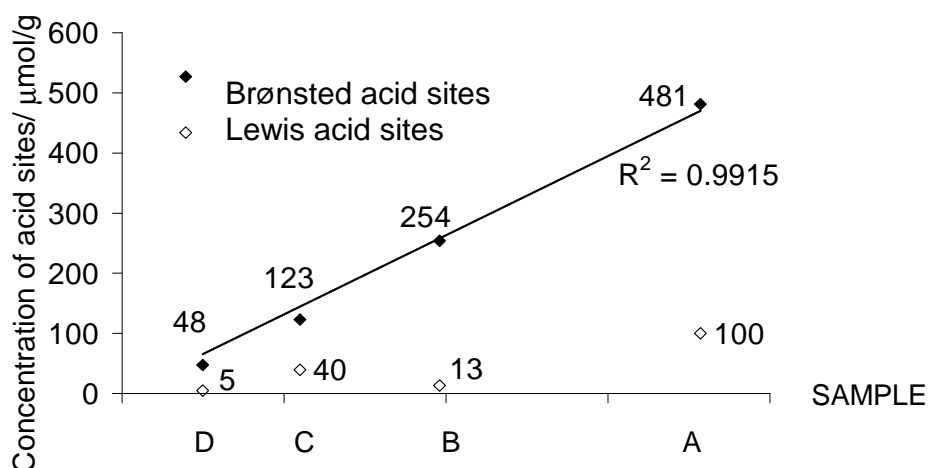
Figure 8. Concentration of Brønsted and Lewis acid sites of HZSM-5 vs. aluminum concentration from IR spectroscopy of adsorbed pyridine (outgassed at 150 °C)

The desorption of pyridine was investigated starting from 150 °C. Initially, the bands of hydrogen bonded species at 1445 cm^{-1} decreased, while those corresponding to chemisorbed pyridine on Brønsted and Lewis sites were hardly affected (Figure 9).
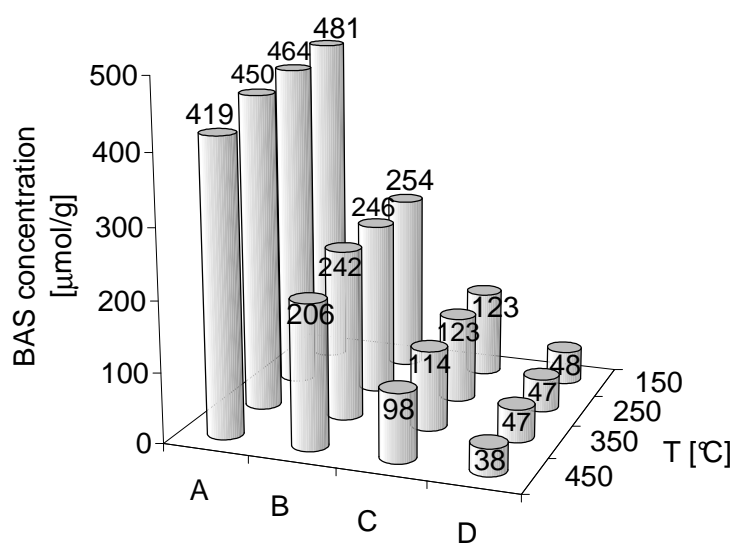
Figure 9. Concentration of remaining Brønsted acid sites at different outgassing temperatures

Nevertheless, in SAMPLE A, a new signal, appearing as a shoulder at 1465 cm^{-1}, developed and increased in intensity with higher desorption temperature (Figure 10).
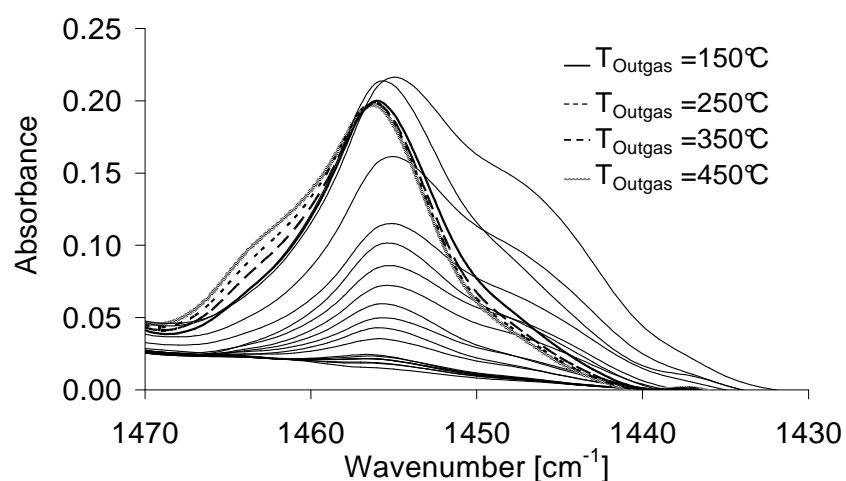
Figure 10. IR spectra of pyridine during adsorption (solid lines) and after desorption at 250, 350, and 450 °C (dotted lines) on SAMPLE A

These new sites are stronger than the original ones and their formation appeared to be favored by the presence of extraframework species in SAMPLE A. Chiche et al proposed this new band to be due to the formation of conjugated iminium ions at paired Lewis and Brønsted acid sites [24]. The observation for this band only for the sample with the highest concentration of Lewis acid sites supports the hypothesis that Lewis centers are involved in the adsorption process.

2.2.3. Temperature programmed desorption of HZSM-5

SAMPLE A to D were characterized by TPD of ammonia to determine the total acid sites concentrations (Figure 11). A linear increase in total acid sites concentration with increase in concentration of framework aluminum was observed (Figure 12).
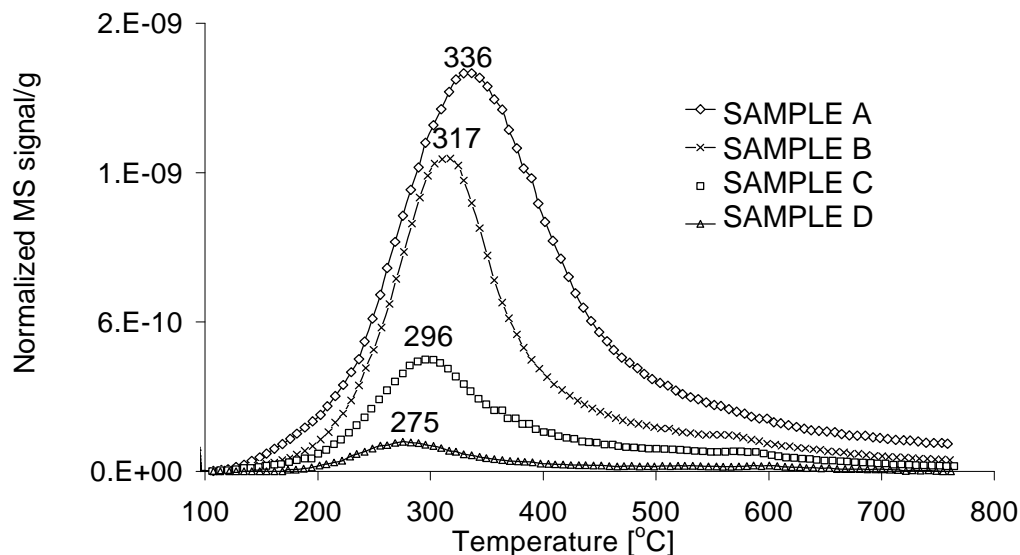
Figure 11. TPD of ammonia of powder HZSM-5 samples
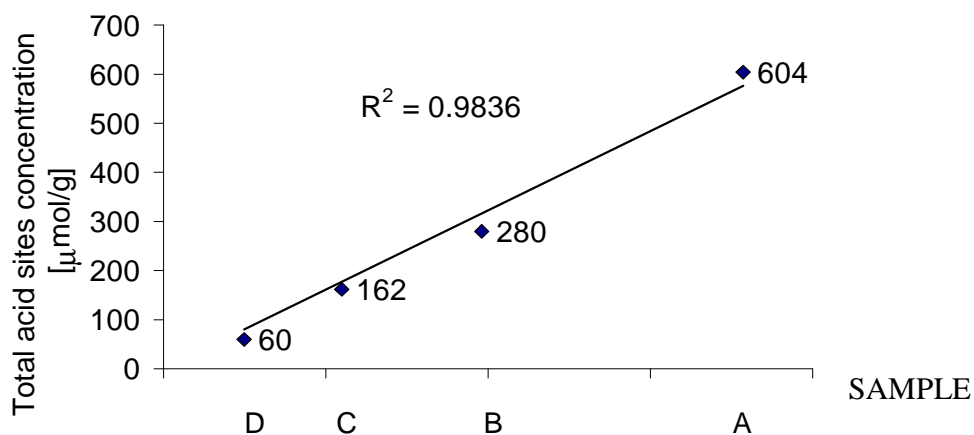
Figure 12. Total acid sites concentration from TPD of NH_3 vs. aluminum concentration

Some authors have attempted to relate the strength of acid sites with the maxima peak temperature obtained from TPD data [25, 26] but others have argued that the readsorption and/or slow diffusion of ammonia usually renders complex the interpretation

51

of peak shape and position of TPD profiles [27]. Thus, the increased chance of readsorption of ammonia onto neighboring acid sites in HZSM-5 with higher Brønsted acid sites concentration during the desorption process can shift the peak maximum to higher temperature. The desorption of ammonia is also controlled by intracrystalline surface diffusion and hence can be strongly dependent on crystal structure [28]. Thus, we did not interpret the TPD results in terms of differences of acid strength between samples.

2.2.4. Microcalorimetric measurements

All microcalorimetric measurements were carried out at 150 °C. The corresponding adsorption isotherms of ammonia on HZSM-5 are shown in Figure 13.
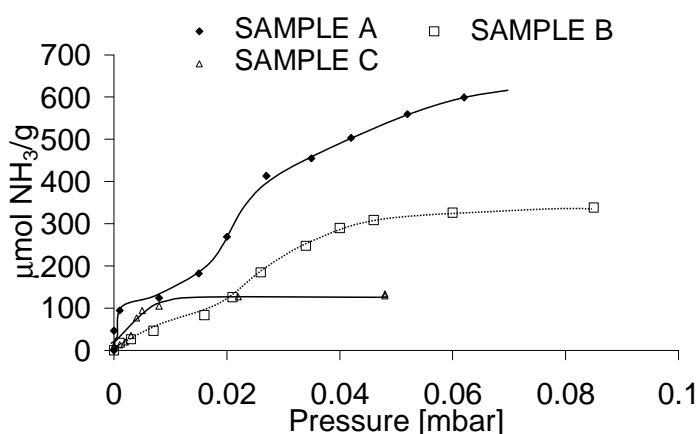
Figure 13. Adsorption isotherms of ammonia on HZSM-5 at 150 °C

A relatively steep increase in the acid sites coverage was observed in the adsorption isotherm of SAMPLE A at low ammonia adsorption pressure, indicating the strong interaction of ammonia with these acid sites. This is correlated with the higher initial differential heat of adsorption of around 160 kJ/mol in SAMPLE A, which is attributed to adsorption on strong Lewis acid sites generated from extraframework aluminum species. The IR spectra of adsorbed pyridine on SAMPLE A suggest that 15% of the acid sites are Lewis acid sites. This corresponds quite closely to the data from the microcalorimetric measurements. The overall differential heat of adsorptions of SAMPLE A and SAMPLE B are similar at around 138 kJ/mol (Figure 14). However, SAMPLE C

exhibited slightly lower differential heat of adsorption of around 132 kJ/mol. The sharp decrease in the differential heat of adsorption after full saturation of the acid sites is due to hydrogen bonding interaction of the ammonia molecule and the zeolite [15]. Due to the poor signal to noise ratio, the differential heat of adsorption of SAMPLE D was not determined.
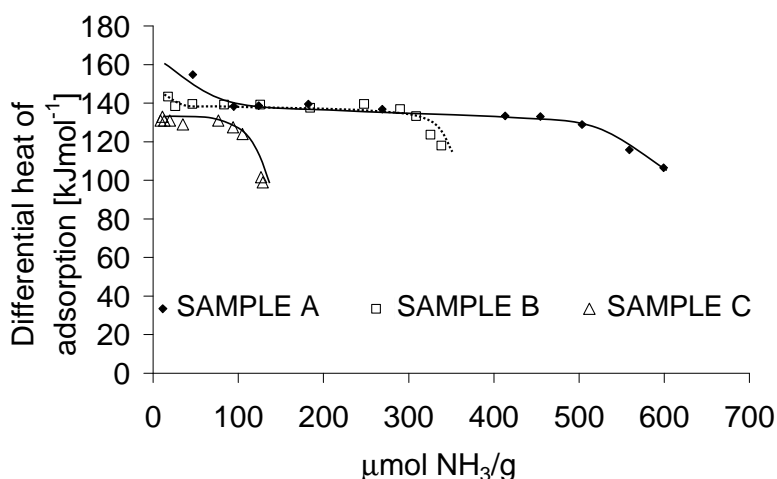
Figure 14. Differential heat of adsorption of ammonia on SAMPLE A, B and C

2.2.5. ^{1}H MAS NMR spectroscopy

Figure 15 shows the ^{1}H MAS NMR spectra of the HZSM-5 samples. Deconvolution was carried out using the parameters reported in Table 1 [29-32]. The resulting values of chemical shifts of bridging OH groups are shown in Table 2. An example of the deconvolution for the spectrum of SAMPLE A is shown in Figure 15. For this sample, two peak maxima in the region of bridging OH group were observed. This is due to the interaction of Brønsted acid sites with lattice framework oxygen or the interaction of SiOH groups with that of nanocavities.
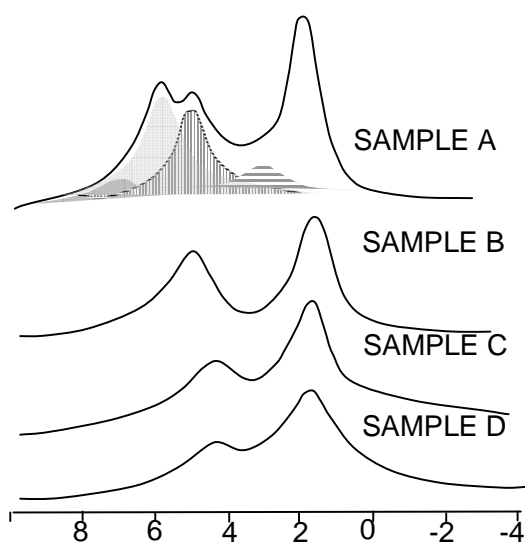
Figure 21. ^{1}H NMR of HZSM-5

Table 1. Assignments of ^{1}H NMR spectrum

Chemical shift/ppm	Assignments
0.5-2	Non acidic terminal SiOH group
2.6-3.6	Extraframework Al-OH
3.5-5.6	Brønsted acid sites
5-6	Bridging OH group interacting with framework oxygen/ hydrogen bonding interaction of SiOH group at lattice imperfect sites
6.5-7.5	NH_4^+

Table 2. Chemical shifts of Brønsted acid sites in HZSM-5

Sample	Chemical shift/ppm
SAMPLE A	5.28
SAMPLE B	5.08
SAMPLE C	4.67
SAMPLE D	4.56
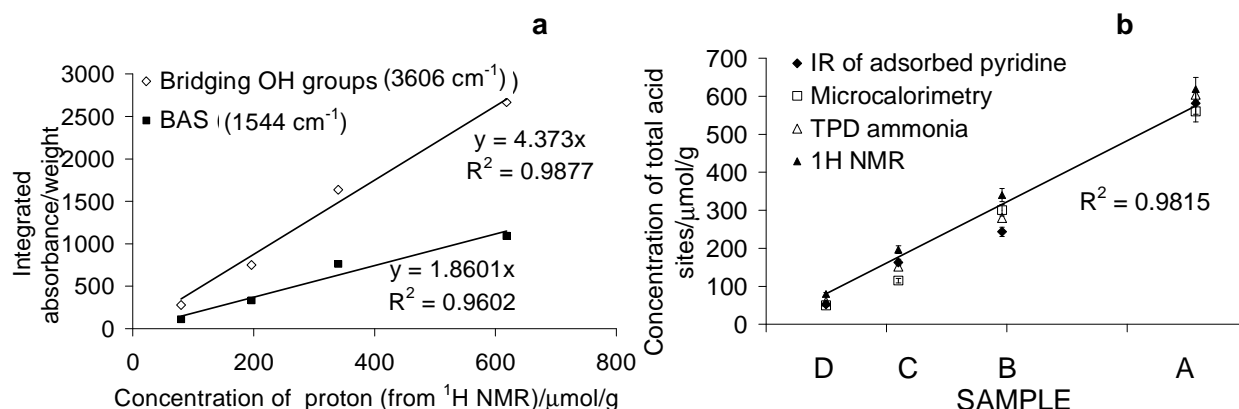
Figure 16 a) Correlation between the area of bridging OH group (3606 cm^{-1}) and area of Brønsted acid sites (1544 cm^{-1}) from IR and concentration of ^{1}H in NMR for HZSM-5 ; b) Comparison of total acid sites concentration determined by IR, microcalorimetry, TPD of ammonia and NMR.

2.2.6. ^{27}Al MAS NMR spectroscopy

The coordination of aluminum in the HZSM-5 was analyzed using ^{27}Al MAS and MQMAS. As shown in Figure 17, most of the aluminum is in tetrahedral coordination with a chemical shift range of 80 to 40 ppm. However, significant tailing of the main tetrahedral peak of SAMPLE A to 20 ppm was observed. The asymmetry of the tetrahedral peak with 2 maxima observed in some of the spectra is due to aluminum in different T sites [33].

Extraframework octahedrally coordinated aluminum is observed at around 0 ppm for all samples even though its contribution in SAMPLE B, C and D is 1% or below. This hexacoordinated aluminum of SAMPLE A however consists of a sharp peak superimposed on a small broad peak at around 0 ppm. This sharp peak experiences small quadrupolar interaction and has a small distribution in isotropic chemical shifts. On the other hand, the broadness of the second hexacoordinated aluminum indicates a larger quadrupolar interaction.
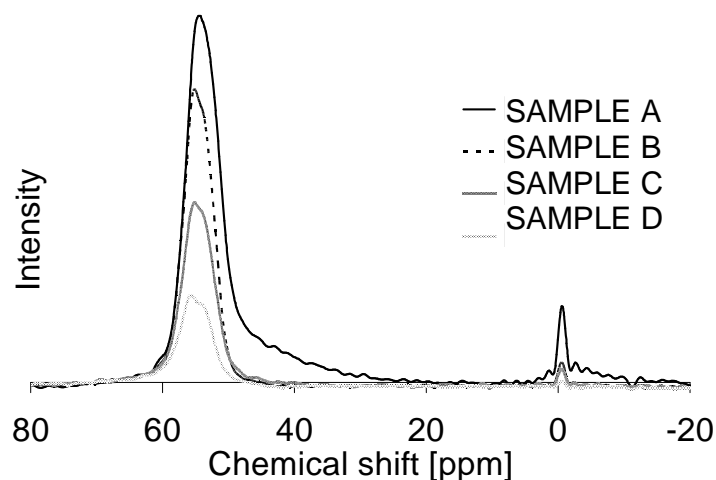
Figure 17. 1D ^{27}Al NMR spectra of HZSM-5 samples

2D MQMAS NMR was performed to distinguish the different tetrahedral coordinated species of aluminum (Figure 18). In an MQ MAS experiment, the quadrupolar interaction is refocused and an isotropic direction, free of anisotropic quadrupolar interactions, is present in the spectra. In this work, the spectra are sheared, so that the F1 axis is the isotropic dimension and the F2 axis contains the second-order quadrupolar line shape.

There are several contributing factors to shifts in peak position in ^{27}Al MAS NMR, because the peak position is a function of (1) the coordination number, (2) the Al-O-Si angle, (3) the mean Al-O distance and (4) the presence of quadrupolar interaction. In this work, any broadening visible in the F1 projection is attributed to isotropic shift distributions, i.e., the variations in Al-O-Si bond angle and/or Al-O bond lengths resulting in distributions in the quadrupolar couplings constant. Resonances that correspond to aluminum experiencing a large quadrupolar interaction are reflected in the spectra by a ridge parallel to the axis in the F2 dimension.

By overlaying the 2D MQMAS spectra of all the HZSM-5 samples (Figure 18 c), it is possible to see a single contour, which resonates close to the diagonal indicating small quadrupolar interaction for the higher silica SAMPLE B, C and D. The width of this contour is dominated by a distribution in isotropic shift, which can be due to a variation in bond angle.
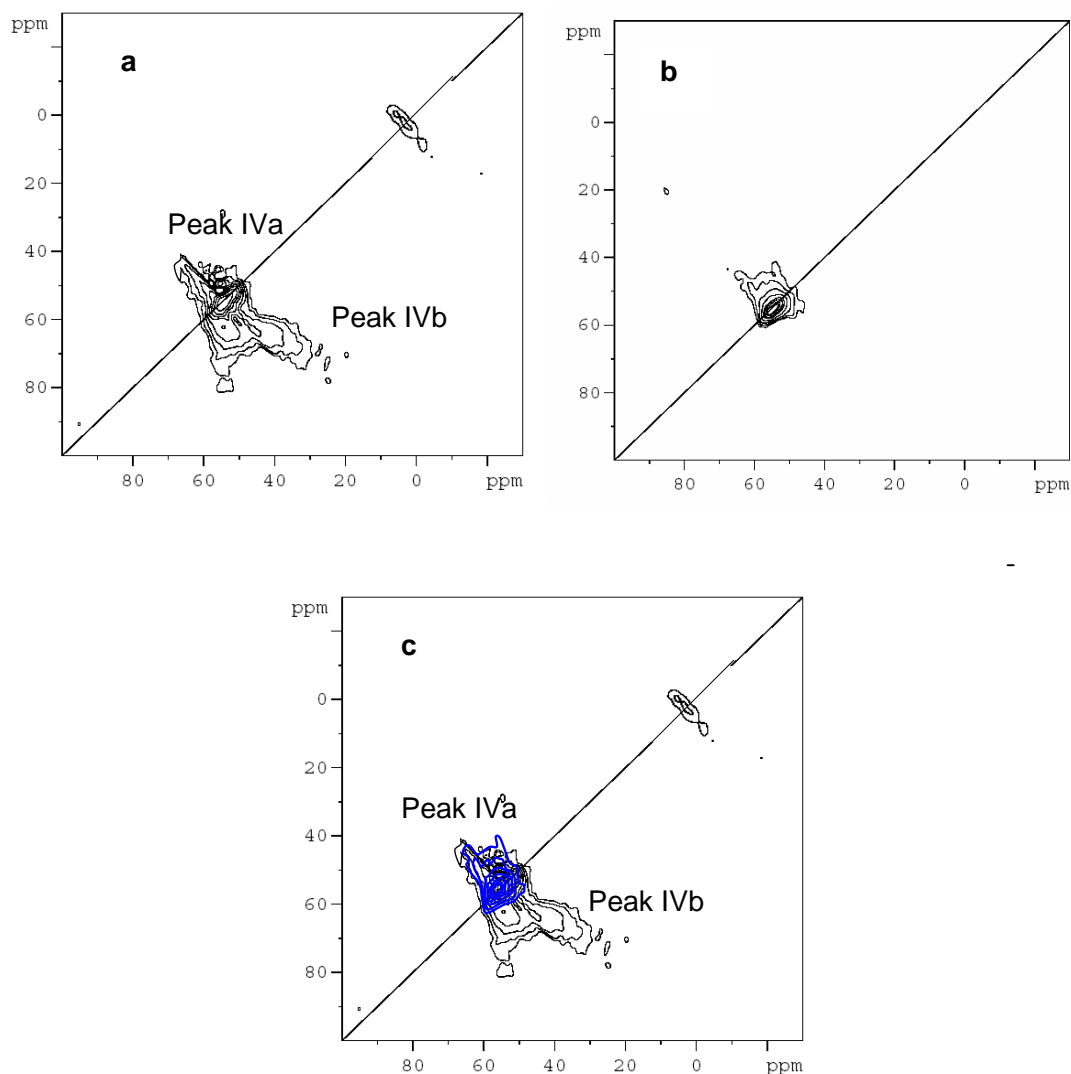
Figure 18. 2D ^{27}Al MQMAS of a) SAMPLE A, b) SAMPLE B, c) overlay of SAMPLE A, B, C and D

A second contour was observed in SAMPLE A (Figure 18a). The aluminum atoms represented by peak IVb experience a much larger quadrupolar interaction than the framework aluminum in peak IVa. Therefore, the aluminums represented by peak IVa have a fairly symmetric surrounding whereas the aluminum represented by peak IVb experiences a substantial electric field gradient. As mentioned above, distribution in isotropic shifts of the aluminum species in peak IVa is probably due to bond angle variations while that of peak IVb can be due to the polarization of highly charged extraframework octahedral aluminum on the framework aluminum inducing a

quadrupolar broadening of part of the framework aluminum in SAMPLE A. This effect is especially observed when the framework aluminum is in the vicinity of extraframework aluminum [33]. The polarization of the framework aluminum by the charged extraframework aluminum causes local distortion of the framework, which can result in the increase of the nearby Si-O-Al and Si-O-Si angles.

2.2.7. ^{29}Si MAS NMR spectroscopy

The concentration of aluminum in the framework of the HZSM-5 was determined through the deconvolution of ^{29}Si NMR measurements (Figure 19) and calculated using Equation 3. The results are in close correlation to the data obtained from AAS measurements except for SAMPLE A. This is due to the presence of extraframework aluminum as detected in the IR spectrum of the activated sample. Analysis for cationic impurities using AAS in the HZSM-5 samples was carried out to ensure that the observed differences in acid strength are not due to the electrostatic influence of different amounts of cationic impurities. A maximum of 600 wt ppm of cationic impurities was measured, which is too low for modifying significantly the acid strength of the Brønsted acid sites.
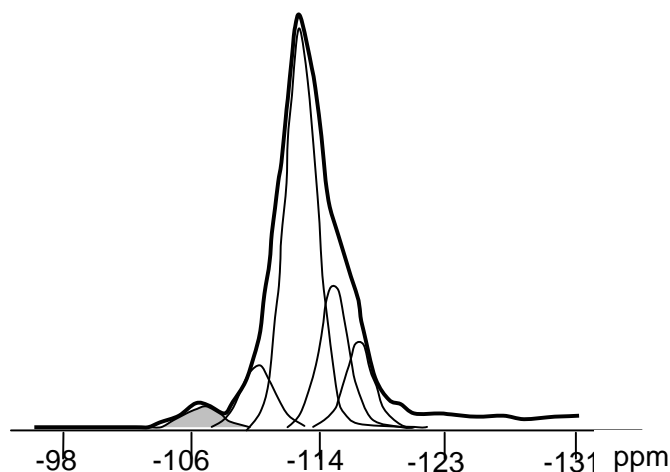
$$\frac{Si}{Al_{framework}} = \frac{\sum_{n=0}^{4} I_{Si(nAl)}}{\sum_{n=0}^{4} 0.25 n I_{Si(nAl)}} \qquad \text{Eq. 3}$$

where I = peak area

Figure 19. Deconvolution of ^{29}Si NMR spectrum of SAMPLE A

2.3.   Discussion

Generation of the acid sites

The three-dimensional microporous structure of an aluminosilicate zeolite consists of corner sharing of SiO_4 and AlO_4 tetrahedra. Replacing the Si atoms with Al by isomorphic substitution generates an excess negative charge in the silicate lattice. The compensation of the negative charges by protons leads to the generation of bridging hydroxyl groups per Al in the framework. It is, thus, evident that a linear increase in the concentration of Brønsted acid sites should be observed with the decrease of Si/Al ratio. This has been seen indeed from results of TPD of adsorbed ammonia, IR spectroscopy of adsorbed pyridine, [1] H NMR, and microgravimetry (Figure 16b) on the 4 investigated HZSM-5 samples with different concentrations of framework aluminum. The results indicate that none of the sites were blocked for the access of the probe molecules used.

Distribution of acid site strength

The concentration of Brønsted acid sites is frequently correlated with their respective strengths and it has been predicted that the acid strength increases with decreasing aluminum content until a sufficient degree of dilution of Al in the Si framework is reached [34]. However, this holds true only for homogenous sites that are well distributed within the framework structure. This is because the localization of aluminum charge density will increase protonic lability, when neighboring Brønsted sites are avoided.

In this work, minor heterogeneity in acid strength distribution within each investigated HZSM-5 sample was observed *via* IR spectra of basic probe molecules. This is somewhat surprising, as some of the HZSM-5 has low concentrations of aluminum. Differences of acid strengths were also observed between the investigated samples. SAMPLE A has the highest relative fraction of strong acid sites, whereas SAMPLE D possesses the highest relative fraction of weak acid sites. These weak sites constituted 40% of the total acid sites in SAMPLE D, leading to the impression of an overall lower acid strength. SAMPLE B and C show similar distribution of acid strength. The results show therefore that the subtle differences in the preparation procedures lead to markedly different distribution of Al atoms.

Acid sites strength and distribution as a function of aluminum

The results so far indicated that Al in the framework structure is not randomly distributed. This non random distribution causes surprisingly a similar number of weak Brønsted acid sites (which are restored at 250 °C outgassing temperature after adsorption of pyridine) in the four investigated HZSM-5. We speculate that these weak sites are localized at paired aluminum sites. Local Si-Al sequences described as ´aluminum pairs´ [Al-O-(Si-O)$_{1,2}$-Al] and ´single´ aluminum atoms [Al-O-(Si-O)$_{\geq 3}$-Al] that are far apart can be present in the lattice structure [35, 36]. ^{29}Si MAS NMR can distinguish only Al-O-Si-O-Al pairs which represent only small percentage of aluminum pairs in HZSM-5.

Other than the non random distribution of aluminum regardless of the concentration of framework Al observed in all the HZSM-5 samples, a significantly higher concentration of Lewis acid sites was observed in SAMPLE A. The Lewis acidity in protic zeolites is associated with aluminum species dislodged from the framework and their vicinity to the Brønsted acid sites may create a higher acid strength such as in the example of SAMPLE A.

Evidence for the role of the extra-lattice alumina stems from ^{27}Al NMR results, which indicates approximately 11% of the aluminum in SAMPLE A as extraframework with octahedral coordination while microcalorimetry yielded a value of around 15%. Comparing the TPD of ammonia in the IR study, 86% of the bridging OH group of SAMPLE A was restored after outgassing at 450 °C compared to the 98% restored in the other HZSM-5 samples. This suggests around 14% strong acid sites in SAMPLE A corresponding perfectly with the concentration of extra lattice aluminum.

Hence, this suggests that the higher Brønsted acid strength in the low Si/Al HZSM-5 is at least partially due to the participation of strong Lewis/Brønsted pair sites that could lead to enhancement of acid strength. The interaction would consist of a partial electron transfer from the OH bond to the (AlO)$^{+}_{p}$ species, which by decreasing the OH bond strength of the site would increase the proton lability and hence the acid strength of the site [37, 38]. These paired sites are most probably responsible for the generation of iminium ion which gives rise to a new band at 1462 cm^{-1} after desorption of pyridine at different temperatures

.

Trends in Al incorporation

The distribution of Al within the framework seems to be more influential than the overall concentration of framework Al in determining the overall observed acid strength. It exerts a critical influence on the observed acid strength in the high silica sample, especially when similar concentration of paired aluminum sites is present in all the HZSM-5 samples. This is tentatively explained by the use of organic templates in the synthesis causing a constant concentration of paired sites regardless of the concentration of Al in the HZSM-5 framework through a preference of incorporating aluminum in the very early stages of nucleation. It has been reported that the use of inorganic gels as templating agents does not give rise to such local gradients/zoning [39, 40].

There are other theoretical and experimental works that also supports the non random distribution of aluminum sites and this has been attributed to the influence of structure directing agent (SDA) used in the synthesis process [20]. The aluminum sites (a negative defect with respect to the silica framework) tend to locate near the positive charge introduced by the SDA used in the synthesis. The authors believed that the preferential location of aluminum at some specific T sites can result in a higher barrier towards the mobility of the acidic proton and hence, lower acid strength. This gives rise to differences in the chemical and structural embedding of the aluminum in the zeolites. When we consider the motion of acidic protons as constituting of small amplitude reorientation jumps between oxygen surrounding the aluminum atom in the Brønsted acid sites, then such preferential location of Al at certain T sites could influence the overall observed acid strength depending on the synthesis method employed.

Hence, the observed heterogeneity of acid strength within each sample and between the HZSM-5 samples can also be due to the differential location of aluminum in the 12 topologically different T sites and 26 different O-sites of the zeolite structure. This distribution of aluminum is evidenced by the distribution in isotropic shifts in the 2D ^{27}Al MQMAS for all the HZSM-5, especially that of SAMPLE A. Theoretical calculations indicate that the difference in the relative substitution energies of aluminum at the 12 different T sites of ZSM-5 can be up to 0.4 eV and scale with the charge difference between silicon and aluminum [17]. XRD studies of Olson et al found that the T-O-T bridge angle in the MFI structure varies from 143° to 175° and the T-O bond distances from 0.152 to 0.167 nm, which can influence the acidity of the zeolite [41].

Whether it is the preferential location of Al at specific T sites or the formation of local gradients resulting in paired aluminum sites, it is clear that a non random distribution of Al has been observed when the organic templates are used. Note also that it could be possible that specific T sites positions are required for the formation of paired aluminums. In any case, the results are in clear contrast to the general assumption of random T sites occupation giving rise to equal sites in HZSM-5 especially those with low aluminum concentrations.

The enrichment of Al at certain locations within the HZSM-5 crystals can have serious implications. First, the occurrence of such compositional gradients resulting in paired Al sites are not detected by bulk techniques such as ^{27}Al and ^{29}Si NMR. As the overall acid strength is strongly determined by the synthesis method, changes in the methodology can create a different number of such paired sites for samples of the same Si/Al ratio. This complicates the determination of the acidity in zeolites with strong aluminum zoning in which the extent of paired sites formation may differ even in individual crystals. Coupled with catalytic intra-particle diffusion limitation, different catalytic performance of the zeolite with the same overall chemical composition can result, depending on the synthesis methodology.

Hence, the acid strength of a zeolite is not only determined by the concentration of framework aluminum but also greatly influenced by the distribution and location of aluminum in the zeolite crystals. In addition, the presence of charged species (e.g. extraframework aluminum) near to the Brønsted acid sites can also induce changes in the charge localization of the framework aluminum.

2.4. Conclusions

The influence of Si/Al ratio on the acidity of HZSM-5 was investigated. TPD of ammonia, IR spectroscopy of adsorbed pyridine, microcalorimetry and ^{1}H NMR results indicate the linear decrease in the concentration of Brønsted acid sites with increase in Si/Al ratio. The polarizability of the SiOHAl sites measured via the molar extinction coefficient does not change throughout the lattice indicating that all sites appear to behave equal in the ground state.

IR studies at different outgassing temperatures indicate the highest concentration of strong acid sites in SAMPLE A, while SAMPLE D has the highest fraction of weak acid sites. This is in contrast to the expected equal statistical distribution of tetrahedral aluminum and strong Brønsted acid sites as concentration of aluminum varies, if

aluminum is randomly distributed throughout the lattice. As the concentrations of these weak Brønsted acid sites are identical for all four samples studied, we speculate that the unusual acid site distribution observed with the present zeolites is attributed to a preferred occurrence of paired sites at the early stages of crystallization. Thus, the paired occur preferentially in the inner of the zeolite crystals. Note that the difference in the acid strength must be related to the final state of the acid site in interaction with the base molecules, as the molar extinction coefficient did not show any variations between the four samples.

This difference in the aluminum distribution might not only have an influence on the acid site strength distribution. It might also have a profound impact on the stability of the tetrahedrally coordinated aluminum in the materials studied. As paired aluminum sites show a lower hydrothermal stability, a higher fraction of aluminum will be removed from the lattice in a steaming process.

2.5. References

1. Barthomeuf, D., J. Phys. Chem., **1979**, 83, 2, 249-256.
2. Mastikhin, V.M., Colloids Surf., A, **1993**, 78, 143-166.
3. Auroux, A., Top. Catal., **1997**, 4, 1-2, 71-89.
4. Lee, C., Parrillo, D. J., Gorte, R. J. and Farneth, W. E., J. Am. Chem. Soc., **1996**, 118, 13, 3262-3268.
5. Blumenfeld, A.L. and Fripiat, J.J., Magn. Reson. Chem., **1999**, 37, S118-S125.
6. Gorte, R.J., Catal. Lett., **1999**, 62, 1, 1-13.
7. Chen, D.T., Sharma, S. B., Filimonov, I. and Dumesic, J. A., Catal. Lett., **1992**, 12, 1-3, 201-212.
8. Gonzalez, M.R., Sharma, S. B., Chen, D. T. and Dumesic, J. A., Catal. Lett., **1993**, 18, 3, 183-192.
9. Janchen, J., Stach, H., Busio, M. and van Wolput, J. H. M. C., Thermochim. Acta, **1998**, 312, 1-2, 33-45.
10. Jozefowicz, L.C., Karge, H. G. and Coker, E. N., J. Phys. Chem., **1994**, 98, 33, 8053-8060.
11. Muscas, M., Dutel, J. F., Solinas, V., Auroux, A. and BenTaarit, Y., J. Mol. Catal. A: Chem., **1996**, 106, 1-2, 169-175.
12. Rakic, V., Dondur, V., Mioc, U. and Jovanovic, D., Top. Catal., **2002**, 19, 3-4, 241-247.

13. Solinas, V., and Ferino, I., Catal. Today, **1998**, 41, 1-3, 179-189.

14. Spiewak, B.E., Handy, B. E., Sharma, S. B. and Dumesic, J. A., Catal. Lett., **1994**, 23, 3-4, 207-213.

15. Parrillo, D. J. and Gorte, R., J. Phys. Chem., **1993**, 97, 34, 8786-8792.

16. Handbook of Heterogeneous Catalysis VCH, ed. G. Ertl, H.K., J. Weitkamp. 1997, Weinheim.

17. Kramer, G. J. and Vansanten, R. A., J. Am. Chem. Soc., **1993**, 115, 7, 2887-2897.

18. Corma, A., Chem. Rev., **1995**, 95, 3, 559-614.

19. Suib, S.L., Stucky, G.D., and Blattner, R.J., J. Catal., **1980**, 65, 1, 174-178.

20. Sastre, G., Fornes, V. and Corma, A., J. Phys. Chem. B, **2002**, 106, 3, 701-708.

21. Emeis, C.A., J. Catal., **1993**, 141, 2, 347-354.

22. Massiot, D., Fayon, F., Capron, M., King, I., Le Calve, S., Alonso, B., Durand, J. O., Bujoli, B., Gan, Z. H. and Hoatson, G., Magn. Reson. Chem., **2002**, 40, 1, 70-76.

23. Lercher, J.A., Ritter, G. and Vinek, H., J. Colloid Interface Sci, **1985**, 106, 1, 215-221.

24. Chiche, B.H., Fajula, F. and Garrone, E., J. Catal., **1994**, 146, 2, 460-467.

25. Karge, H. G. and Dondur, V., J. Phys. Chem., **1990**, 94, 2, 765-772.

26. Kim, J.H., Namba, S. and Yashima, T., Appl. Catal., A, **1993**, 100, 1, 27-36.

27. Farneth, W. E. and Gorte, R. J., Chem. Rev., **1995**, 95, 3, 615-635.

28. Katada, N., Igi, H., Kim, J. H. and Niwa, M., J. Phys. Chem. B, **1997**, 101, 31, 5969-5977.

29. Müller, M., Harvey, G. and Prins, R., Microporous and Mesoporous Mater., **2000**, 34, 3, 281-290.

30. Brunner, E., Ernst, H., Freude, D., Frohlich, T., Hunger, M. and Pfeifer, H., J. Catal., **1991**, 127, 1, 34-41.

31. Hunger, M., Solid State Nucl. Magn. Reson., **1996**, 6, 1, 1-29.

32. Freude, D., Hunger, M. and Pfeifer, H., Zeitschrift Fur Physikalische Chemie Neue Folge, **1987**, 152, 171-182.

33. van Bokhoven, J.A., Roest, A. L., Koningsberger, D. C., Miller, J. T., Nachtegaal, G. H. and Kentgens, A. P. M., J. Phys. Chem. B, **2000**, 104, 29, 6743-6754.

34. Barthomeuf, D., Mater. Chem. Phys., **1987**, 17, 1-2, 49-71.

35. Kaucký, D., Dědeček, J. I. and Wichterlová, B., Microporous and Mesoporous Mater., **1999**, 31, 1-2, 75-87.

36. Dědeček, J., Kaucký, D. and Wichterlová, B., Chem. Commun., **2001**, 11, 970-971.

37. Mirodatos, C. and Barthomeuf, D., J. Chem. Soc., Chem. Commun., **1981**, 2, 39-40.

38. Shigeishi, R.A., Chiche, B. H. and Fajula, F., Microporous and Mesoporous Mater., **2001**, 43, 2, 211-226.

39. Derouane, E.G., Gilson, J. P., Gabelica, Z., Moustydesbuquoit, C. and Verbist, J., J. Catal., **1981**, 71, 2, 447-448.

40. Lin, J. C. and Chao, K. J., J. Chem. Soc., Faraday Trans.I, **1986**, 82, 2645-&.

41. Olson, D.H., Kokotailo, G. T., Lawton, S. L. and Meier, W. M., J. Phys. Chem., **1981**, 85, 15, 2238-2243.

Chapter 3

Influence of alumina binder on

the acidity of HZSM-5

Abstract

HZSM-5 powders with Si/Al ratios between 20 and 250 were bound with 20 wt% γ-Al$_2$O$_3$ (25 wt% for SAMPLE B). Through addition of the alumina binder, the concentration of acid sites increased. The quantitative evaluation of ^{29}Si and ^{27}Al MAS-NMR indicates that the new sites are formed at the outside of crystals or with silica between crystals. It is suggested that these sites are constituted in part by tetrahedrally coordinated aluminum in an amorphous silica phase. Alternatively, these Brønsted acid sites may also form by coordinating alumina to external silanol groups. The decrease in the Brønsted acid site concentration of the bound zeolite with the highest alumina concentration is attributed to the partial compensation of charge of bridging oxygens by anionic alumina species near the pore entrance. This latter surface chemistry is also concluded to be the reason that the maximum acid strength of the extrudates is slightly lower than that of the parent materials.

3.0.   Introduction

Zeolite ZSM-5 is an important catalyst due to its high coke resistivity, high hydrothermal stability, and unique shape selectivity. The 10-membered ring channel structure imparts shape selective properties, which are important in industrial processes such as dewaxing of paraffins, conversion of methanol to gasoline (MTG), production of light alkenes from methanol (MTO), alkylation of benzene, xylene isomerization and toluene disproportionation [1-5]. ZSM-5 can be synthesized with a broad range of acidity which corresponds to different activities [6].

The macroscopic shape to which the zeolite is formed depends on the application. As additive in fluid catalytic cracking catalysts, ZSM-5 is formed to spherical 70 μm particles. For most fixed bed applications, tubular extrudates with a diameter of 1/16 or 1/8 of an inch are used. The extrudate form helps in reducing the pressure drop in fixed-bed reactors [7]. Because of the poor adhesion properties of pure zeolites, macroscopic shapes of catalyst particles are normally achieved by embedding the zeolite crystals in a matrix, usually a metal oxide such as alumina in order to increase the mechanical strength. This helps reducing high pressure drops

This matrix, or binder, is often considered to be essentially an inert component of the catalyst. However, several authors have shown that, even though the binder may not be active as a catalyst, it can change the overall acidic properties of formed catalyst. Several studies have been carried out to determine the influence of different binders on the catalytic performance of zeolites [8-10]. However, the effect of the binder on the overall acidity depends not only on the nature of the binder, but also on the procedure used to introduce it. The right combination of the two parameters can result in enhanced catalytic stability, whereby the bound catalysts undergo slower deactivation rate when the binder acts, e.g., a coke sink [11].

During the forming process, the binder can eventually block zeolite channels [12]. In addition, under certain conditions, the alumina binder can be inserted into the framework of high silica zeolites [13]. The neutralization of Brønsted acid sites by cationic species present in the binder was also reported to be one of the causes for the loss of Brønsted acid concentration in some preparation methods [14]. The study of the influence of the binder on zeolite is, thus, important to understand the role it plays in the overall physico-chemical and catalytic properties of the extrudates.

In order to address this, the present work explores the effect of alumina binder on the acidic properties of HZSM-5 zeolites. A wide variety of characterization methods

including TPD of ammonia, IR and NMR spectroscopy, and N_2 physisorption, was used to understand the changes occurring in the forming process.

3.1. Experimental

3.1.1. Materials and forming procedure

Dry HZSM-5 powders with Si/Al ratios between 20 and 250 were extruded by addition of 20 wt% γ-alumina binder using a home built single strand extruder with a constant pressure of not more than 10 bar. The extrudates were dried at 100°C in a flat bed for 24 hours and subsequently calcined to 550 °C. These formed HZSM-5 catalysts will be referred to as EXT A, EXT B, EXT C, and EXT D indicating the Si/Al ratio of the zeolite component. The parent material will be referred to as SAMPLE A, SAMPLE B, SAMPLE C and SAMPLE D.

3.1.2. IR spectroscopy of adsorbed pyridine

In situ IR spectra of the materials studied were measured with a *Perkin Elmer 2000* spectrometer. All spectra were recorded in the region between 4000 and 800 cm^{-1} at a resolution of 2 cm^{-1}. The spectra are reported as absorbance spectra with the activated parent EXT material subtracted as background spectrum in selected representations.

For IR spectroscopy of adsorbed pyridine the samples were pressed into self-supporting wafers (density 13-25 mg/cm^2). After activation in vacuum (10^{-6} mbar) for 1 h at 450 °C (heating rate 10 °C/min), the sample was cooled to 150 °C and pyridine was adsorbed in small doses until full saturation of the bridging OH group at 3606 cm^{-1}. The system was then equilibrated for 0.5 h. IR spectra were recorded at 150 °C before adsorption of pyridine, during the adsorption of pyridine and after outgassing (10^{-6} mbar) at 250, 350 and 450 °C. The concentration of Brønsted and Lewis acid sites was estimated from the areas of the bands at 1565 – 1515 cm^{-1} and 1470 – 1435 cm^{-1}, by applying Eq. 3.1. and 3.2., respectively [15]

$$c(BAS) = 4.32 \cdot 1000 \cdot r^2 \cdot \frac{IA(1565 - 1515 cm^{-1})}{m}$$ Eq. 3.1.

$$c(LAS) = 3.27 \cdot 1000 \cdot r^2 \cdot \frac{IA(1470 - 1435 cm^{-1})}{m}$$ Eq. 3.2.

where:

        c = concentration of acid sites [µmol/g]

        IA = integral of the respective peak [cm^{-1}]

        r = radius of the wafer [cm]

        m = mass of the wafer [mg]

3.1.3. Temperature programmed desorption (TPD)

For TPD of ammonia, 50-100 mg catalyst was pressed as wafers and loaded in the quartz tubes of a home-made 6 fold TPD set-up. After activation at 550 °C for 1 h (heating rate 10 °C/min) at a pressure of 10^{-3} mbar, 1 mbar of ammonia was adsorbed and equilibrated for 1 h at 100 °C. To remove gaseous and physisorbed ammonia, the pressure was reduced to 10^{-3} mbar for 2 h. The temperature was then increased at a rate of 10 °C/min to 750 °C. Desorbing molecules were analyzed by a *Balzers QMG 420* mass spectrometer. Mass 16 was used for ammonia. A HZSM-5 standard with known acid sites concentration (determined by microgravimetry) was used as a reference for quantification.

3.1.4. MAS NMR measurements

MAS NMR spectroscopy measurements of the zeolites were carried out using a *Bruker Avance AMX-500* NMR-spectrometer with a magnetic field of 11.75 T. The samples were packed in 4 mm ZrO_2 rotors and spun at 15 kHz.

For ^{27}Al-MAS and MQMAS NMR measurements, the samples were hydrated for at least two nights. The reference for the measurements was $Al(NO_3)_3 \cdot 9\,H_2O$ (δ = -0.543 ppm). An excitation pulse with power level of 7 dB and a length of 0.6 µs was applied for the 1D spectrum. The relaxation time was 250 ms. For all 1D spectra, 2400 scans were recorded. MQMAS spectra were recorded with a three pulse sequence. The power level was 7 dB for the first two pulses and 35 dB for the last one. The pulse lengths were p_1 = 8 µs, p_2 = 3.2 µs and p_3 = 52 µs. The evolution time t_1 was incremented in intervals of 1 µs and data were processed with XWINNMR. For quantification of the ^{27}Al-MAS NMR spectra, the chemical shift and the quadrupolar coupling constant (QCC) were obtained from the MQMAS spectrum and used to deconvolute the 1D spectra using dmWinfit2001 developed by Massiot [16].

The Larmor frequency for ^{29}Si was 99.36 MHz. The samples were packed in 4 mm ZrO_2-rotors and spun at 15 kHz. The reference for the measurements was solid

Si(OSi(CH$_3$)$_3$)$_4$ (δ = -9.843 ppm). For 1D spectrum, an excitation pulse with a power level of 7 dB and a length of 0.6 μs was applied. The relaxation time was 250 ms. For all 1D spectra 2400 scans were recorded. For determination of Si/Al framework ratio, the 1D spectra were simulated using dmWinfit2001.

3.1.5. X-ray diffraction

X-ray powder diffraction patterns of extrudates were measured using a *Philips X'Pert Pro System* operating with a CuKα1-radiation (0.154056 nm) at 40 kV / 40 mA. Measurements were performed on a spinner with a 1/4'' slit from 5° to 50° 2 θ (0.05°/min). All the extrudates showed similar crys tallinity.

3.1.6. Atomic absorption spectroscopy (AAS)

The silicon and aluminium contents of the materials were determined by AAS using a *UNICAM 939* spectrometer. Before measurement, 20-40 mg of each sample was dissolved in a mixture containing 0.5 mL of hydrofluoric acid (48%) and 0.1 mL of nitrohydrochloric acid and heated to the boiling point of the mixture. From the amounts of silicon and aluminium measured from AAS analysis, the overall Si/Al ratio was calculated.

3.1.7. Nitrogen physisorption

Surface area, pore volume and pore size distributions of the materials were obtained by nitrogen adsorption on a *PMI* automated BET sorptometer. *Brunauer, Emmet* and *Teller* (BET) and *Barrett, Joyner* and *Halenda* (BJH) methods were used for calculations. Micropore volume was determined using the t-plot method. Before adsorption, the sample (100 mg) was activated in vacuum at 400 °C for 2 h. After activation, the weight of the dried sample was determined. Finally, the sample was cooled to -196 °C and liquid nitrogen was adsorbed at increasing partial pressures.

3.2. Results
3.2.1. Characterization of binders and extrudates via TPD of ammonia

As all EXT materials contained approximately 20 wt% alumina binder, the TPD profile of the pure binder was used for the deconvolution of the TPD profiles of the extrudates, as indicated below. TPD of ammonia from the pure binder showed 173 μmol

Lewis acid sites/g binder (Figure 3.1) when integrating the full TPD peak between 100 and 600 °C.
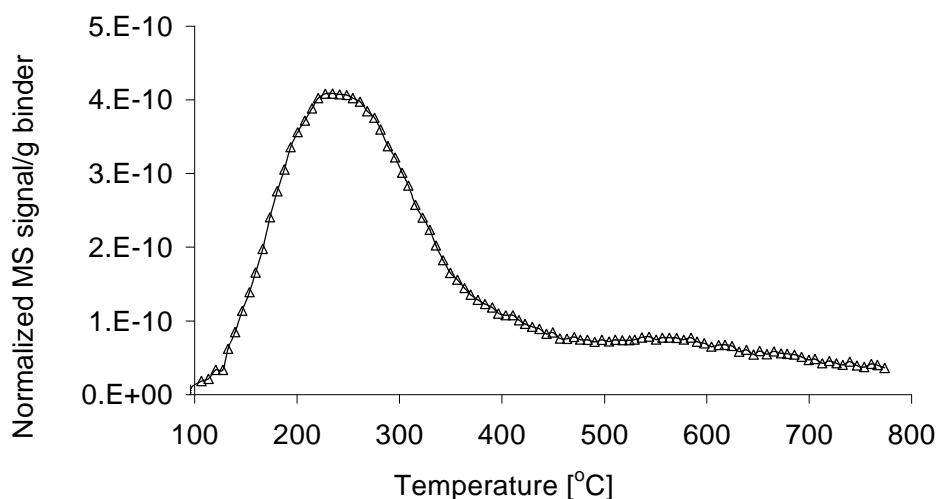

Figure 3.1. TPD of ammonia of alumina binder

The overall TPD profiles of the extrudates (Figure 3.2) show contributions of desorption from weak Lewis acid sites of the binder and from Brønsted acid sites of the powder HZSM-5.
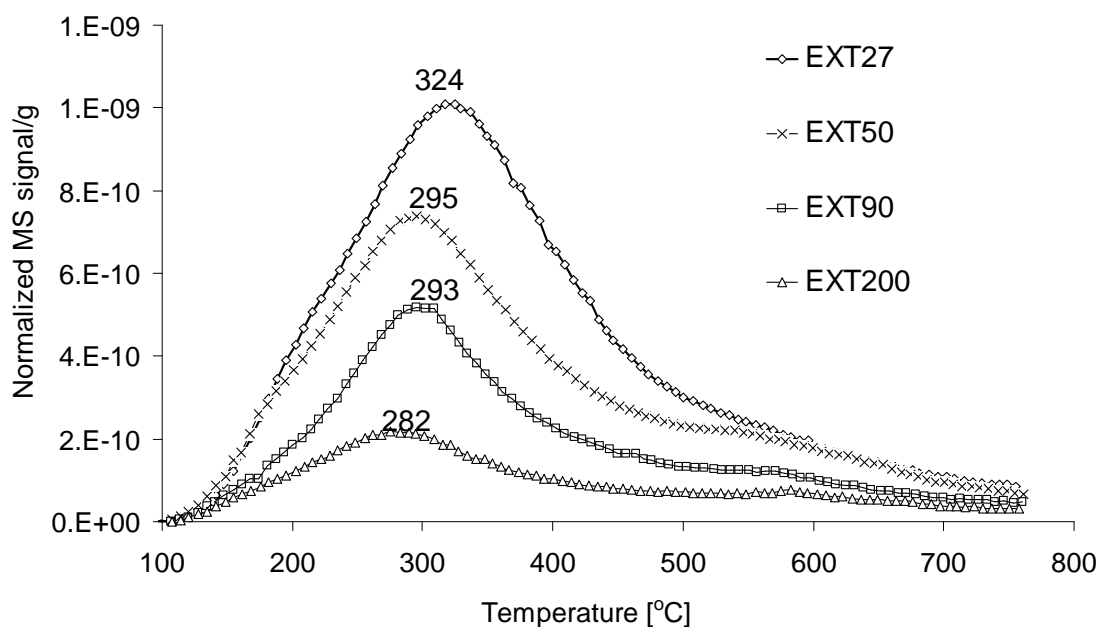
Figure 3.2. TPD of ammonia of EXT materials

Due to the complication that ammonia decomposes at temperatures above 600 °C, deconvolution of the TPD profiles of the extrudates was confined from 100 to 600 °C to compare the effect of binder on the concentration of Brønsted acid sites. The peak temperature of each deconvoluted peak was estimated from the peak temperature maxima of the pure binder (Figure 3.1) and powder HZSM-5 (shown in Chapter 2 of the thesis). The assignment of the different peaks is tabulated in Table 3.1 and an example of the deconvolution is shown in Figure 3.3.

Table 3.1. Assignment of the different peaks to type of acid sites of EXT A

	Peak temperature [°C]	Temperature range [°C]
Binder	230	100-400
BAS	325	150-500
BAS	450	300-600
LAS (with contributions from decomposition of NH_3)	550	400-700

Figure 3.3. Deconvolution of TPD profile of EXT A

Figure 3.4 compares the total concentration of acid sites measured on the extrudates and powders and the expected concentration in the extrudates by adding the contributions of 20 wt% binder to 80 wt% powder. Obviously, the acidit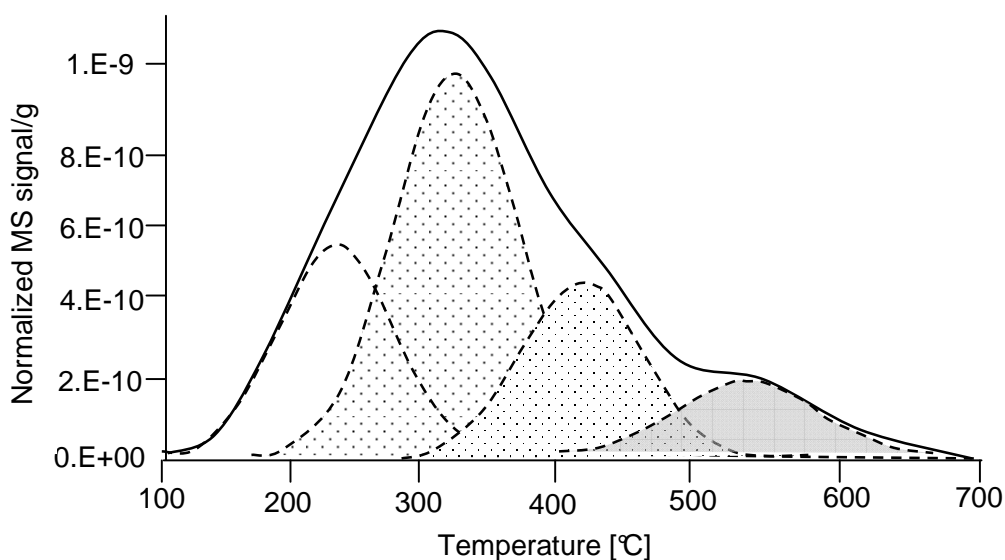y of the extrudate cannot be estimated as the sum of the acid sites of the zeolite and binder components. In order to determine the effect of forming on the Brønsted acid sites of HZSM-5, the Brønsted acid sites concentration of 1g of extrudate was compared with 0.8g of HZSM-5 powder so as to take into account the dilution effect of the binder (Figure 3.4).

In general, after forming HZSM-5 with alumina, the total acid sites concentration increased (with the exception of EXT A). This increase stems from the contributions of weak Lewis sites from the binder and the increase in Brønsted acid sites. The latter is most pronounced for EXT C and EXT D. Results from the deconvolution of TPD profiles indicate that the Brønsted acid sites concentrations of EXT C and EXT D increased by around 35% after binding with γ-Al$_2$O$_3$ while that of EXT A decreased by around 30%. The concentration of Brønsted acid sites of EXT B was only marginally lower by 3% than that of the parent zeolite.
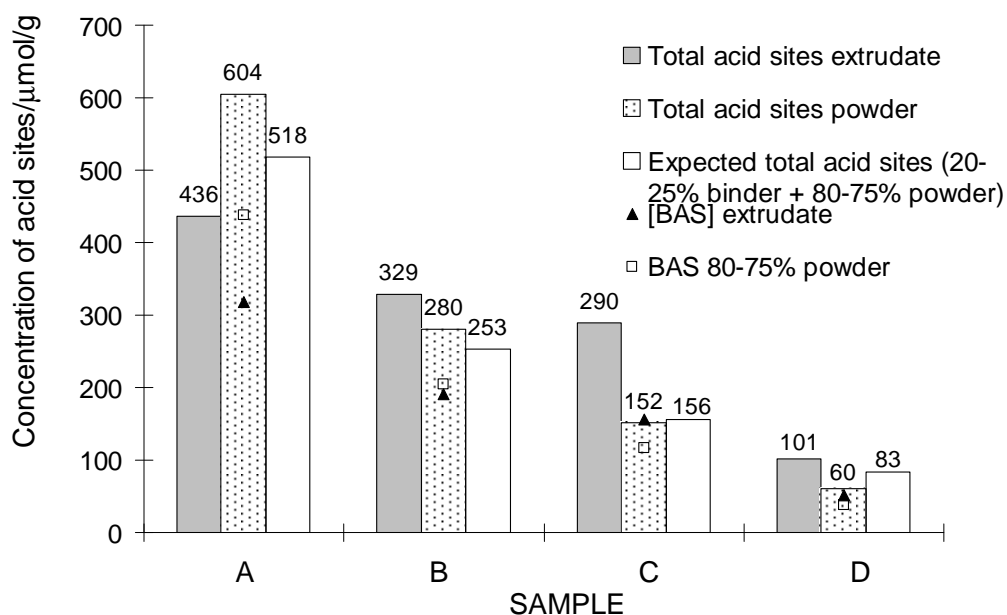

Figure 3.4. Comparison of the total and Brønsted acid sites concentration between extrudate and powder from deconvolution of TPD results

3.2.2. Characterization of binders and extrudates *via* IR spectroscopy of adsorbed pyridine

The IR spectrum of activated Al_2O_3 binder in the 3800-3400 cm^{-1} range (hydroxyl group region) is shown in Figure 3.5.
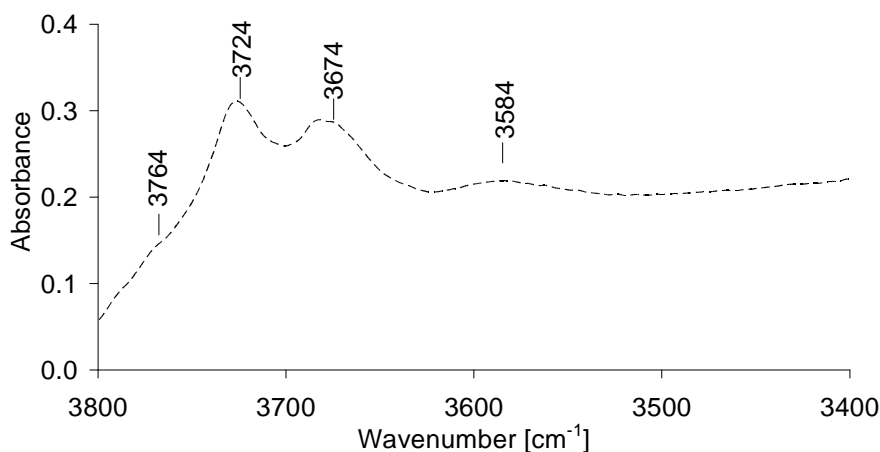
Figure 3.5. IR spectra of activated γ-Al_2O_3 binder

Several bands, characteristic of acid, neutral, or basic hydroxyl groups, were observed. The band at 3764 cm^{-1} is assigned to type I Al-OH basic hydroxyl groups. The band at 3724 cm^{-1} is assigned to type II neutral hydroxyl groups. The band at 3674 cm^{-1} is ascribed to type III Al^{VI}-OH acid hydroxyl groups. The broad and weak band at 3584 cm^{-1} is ascribed to hydrogen bond between hydroxyl groups [17].

In the IR spectra of Al_2O_3-bound ZSM-5 catalysts, the absorption bands of the alumina binder are superimposed to those of the zeolite powders (Figure 3.6). New band in the OH vibration range did not appear. When the normalized IR spectrum of the activated powder and EXT A are compared, bridging hydroxyl groups (Brønsted acid sites) at 3606 cm^{-1} and terminal silanol groups at 3743 cm^{-1} are observed. Note that the OH groups of zeolite dominate the IR spectrum of the activated extrudate.
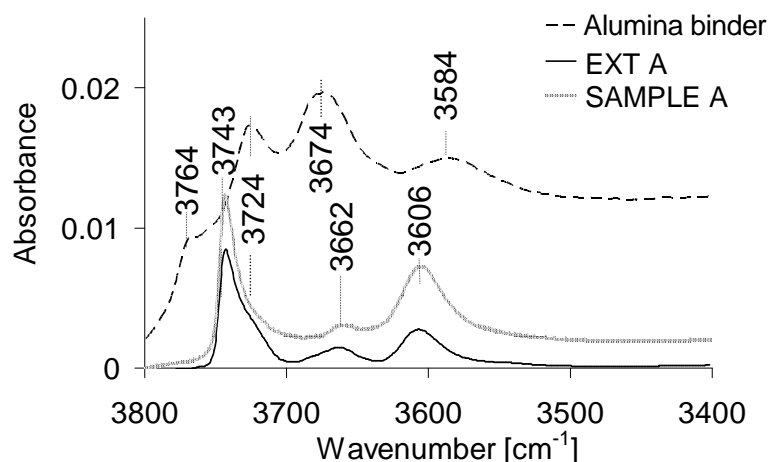
Figure 3.6. IR spectrum of activated binder, SAMPLE A and EXT A (IR spectra of activated extrudate and powder are normalized with respect to the overtone lattice vibrations. IR spectrum of alumina binder is magnified for comparison)

The shoulder on the terminal silanol group at around 3724 cm^{-1} in the IR spectra of the activated extrudate is due to the contribution of the Al_2O_3 binder. It was suggested that hydrogen bonding interaction between hydroxylated Al from the Al_2O_3 binder and terminal SiOH or defect sites at around 3743 cm^{-1} can also result in the formation of a shoulder appearing at 3724 cm^{-1} [18]. The broad peak between 3706 and 3640 cm^{-1} is due to hydroxylated Al from the Al_2O_3 binder, which also gives rise to weak Lewis acid sites [19]. In the example here, this broad band also contains contributions from AlOH groups of extraframework Al in HZSM-5. As shown in Figure 3.7, the IR bands described in Figure 3.6 for EXT A were also observed in all the investigated extrudates.
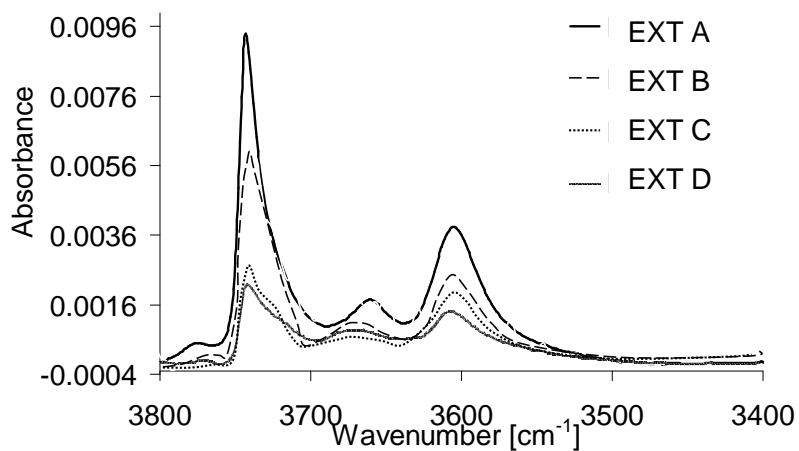
Figure 3.7. IR spectra of activated extrudates

Adsorption of pyridine on the extrudates reveals bands at 1545 cm^{-1} and 1455 cm^{-1} (Figure 3.8). As expected, the intensity of the band at 1544 cm^{-1}, which is due to pyridine adsorbed on Brønsted acid sites, increases with increase in framework Al of the extrudate.
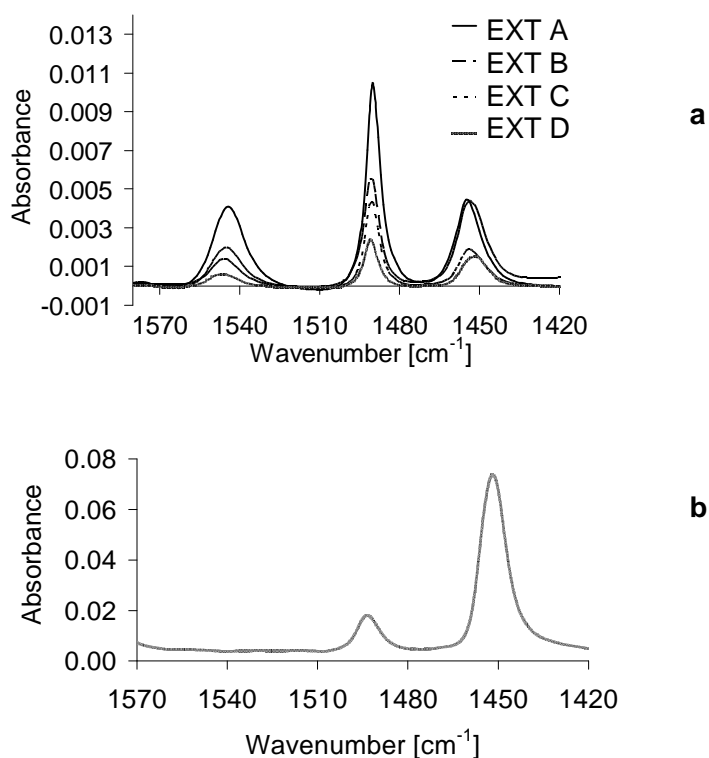
Figure 3.8. IR spectra of adsorbed pyridine on a) extrudates and b) alumina binder

The band at 1455 cm^{-1} is due to pyridine chemisorbed on Lewis acid sites of the Al$_2$O$_3$ binder. Figure 3.8b indicates only Lewis acid sites present in the alumina binder as evident from the band at 1452 cm^{-1} and quantification yields a total acid site concentration of 164 μmol/g. The presence of the Al$_2$O$_3$ binder resulted in the increase of Lewis acid sites concentration by at least a factor of two compared to the unbound powder HZSM-5 (Figure 3.9). A shift of this band from 1447 cm^{-1} in IR spectrum of the powder (due to adsorption on weak Lewis sites [20]) to 1455 cm^{-1} for the extrudate (due to pyridine coordinatively adsorbed on extraframework hexacoordinated Al from the catalyst and/or the binder) was observed.
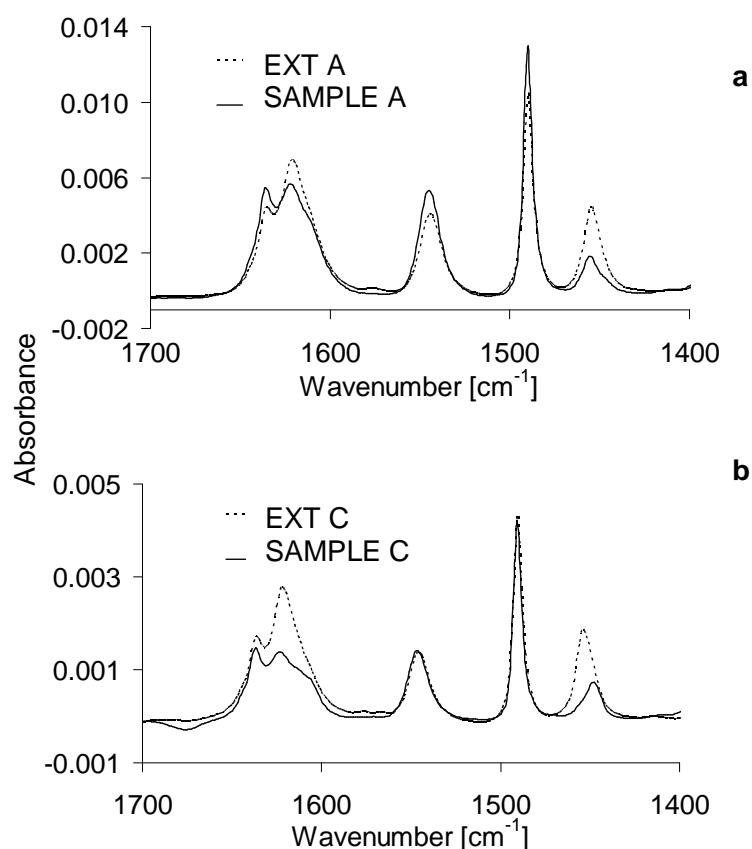
Figure 3.9. Comparison of IR spectra of a) EXT A and SAMPLE A and b) EXT C and SAMPLE C after pyridine adsorption and outgassing at 150 °C (normalized with respect to the lattice vibrations)

In general, the presence of the Al_2O_3 binder resulted in the overall increase in total acid sites concentration due to the increase in Lewis acid sites concentration from the alumina. As an exception, the total acid sites of EXT A decreased by approximately 8% (Figure 3.10). From Figure 10, the concentration of Brønsted acid sites of EXT C and EXT 200 was increased by around 25% while that of EXT A and EXT B was decreased by around 14 and 8%, respectively. This trend agrees with the trend obtained from TPD of ammonia (Figure 3.4).

The final properties of bound HZSM-5 vary for different Si/Al ratios. New acid sites are formed with high silica HZSM-5 while for the lowest silica HZSM-5, interaction with binder removed some Brønsted acid sites.
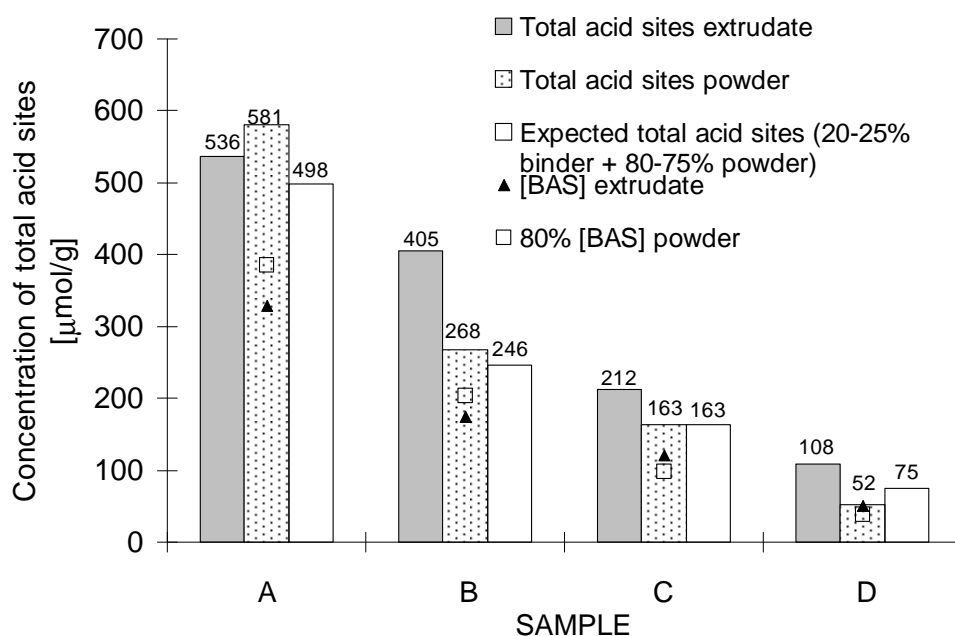
Figure 3.10. Comparison of total and Brønsted acid sites concentration of extrudate and powder from IR spectroscopy of adsorbed pyridine.

Upon adsorption of strong bases, reversible tetrahedral aluminum coordination has been observed. Such sites would re-convert to partially dealuminated sites upon desorption of that base. It can be speculated that such surface chemistry may occur also in the binding process resulting in flexible hydroxyl coordination occurring at the interface between the external of the zeolite crystals and the alumina matrix. Thus, if new Brønsted sites are formed that are not dependent on the presence of the base, the

78

intensity of the bridging OH groups at 3606 cm^{-1} should be more intense for the activated extrudate than for the corresponding HZSM-5 powder. The comparison of the normalized OH bands area (determined through the integration of the bridging OH band between 3644 cm^{-1} and 3560 cm^{-1}) is shown in Figure 3.11.
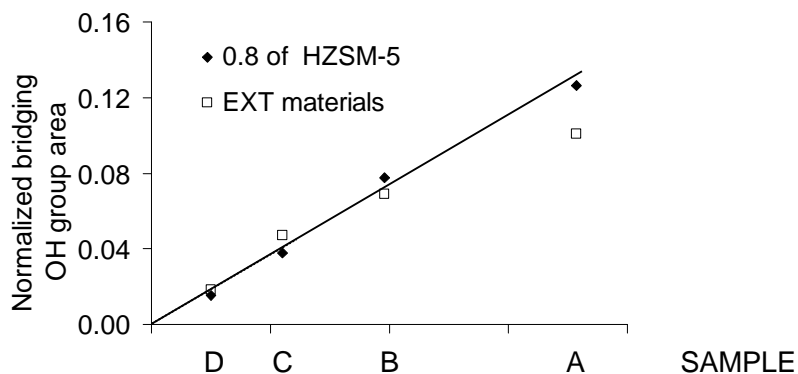
Figure 3.11. Comparison of integrated intensities of the IR band for bridging OH groups (normalized to overtone lattice band) between 0.8 g of HZSM-5 powder with 1 g of extrudates

The concentration of bridging OH groups decreased by 20% in EXT A, while the Brønsted acid site concentration measured by adsorption of pyridine decreased by around 14% compared to the corresponding powder. The difference suggests that, at least in part, the additional Brønsted sites result from the stabilization of tetrahedral sites formed in the presence of pyridine. The more pronounced perturbation of the terminal silanol group (which gives rise to apparent Brønsted acidity) could be due to the presence of Al$_2$O$_3$ in its vicinity. This is speculated to be a precursor in lateral interaction of the Si-OH groups with aluminum when pyridine is adsorbed. Evidence for this conclusion can be found by comparing the difference spectra [(spectrum after pyridine adsorption)-(spectrum of activated sample)] which indicate that more terminal silanol groups at 3743 cm^{-1} are perturbed by pyridine in EXT A compared to the parent HZSM-5 (Figure 3.12). It was observed with all extrudates. Note that apparent acidity of the terminal SiOH group was not observed for the parent unbound HZSM-5.
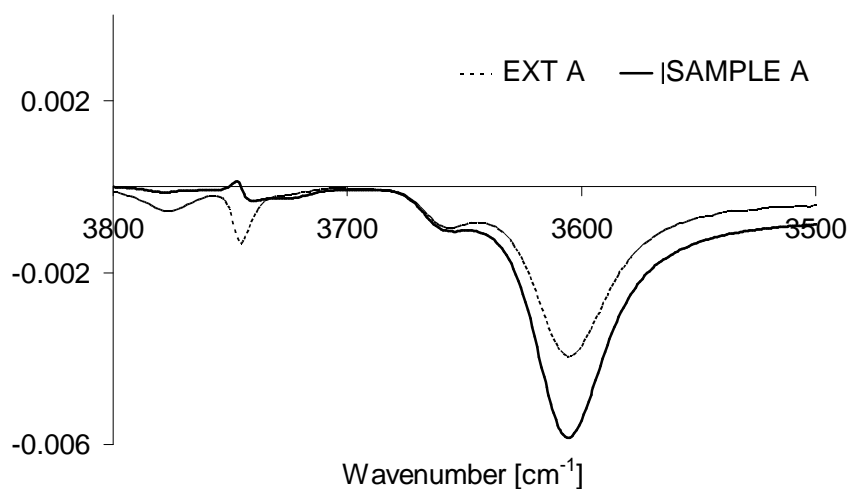
Figure 3.12. Comparison of difference spectra of SAMPLE A and EXT A after pyridine adsorption and outgassing at 150 ℃.

The 10% decrease in intensity of the bridging OH group of EXT B correlates with the 8% decrease in the concentration of Brønsted acid sites from pyridine quantification. Hence, no significant number of new sites is formed. On the other hand, approximately 20% more bridging hydroxyl groups are formed in high silica EXT C and EXT D as evident from the increase in the intensity of the 3606 cm^{-1} bridging OH band of these materials compared to the unbound parent HZSM-5. Note that the determination of the area of the bridging OH band has all been normalized to the weight contribution of the materials and integration was carried out in the same range between 3644 cm^{-1} and 3560 cm^{-1} on the normalized spectra.

Outgassing of pyridine adsorbed on the extrudate was carried out at 250, 350, and 450 ℃ to quantify the distribution of acid str ength in the extrudates. All the parent unbound HZSM-5 powders retained approximately 80% of the intensity of the 1544 cm^{-1} band after outgassing at 450 °C, indicating a significant number of strong Brønsted acid sites (see Figure 2.4b, Chapter 2 of thesis). However, binding with Al$_2$O$_3$ reduced the concentration of these strong sites to around 40-60% (Figure 3.13).
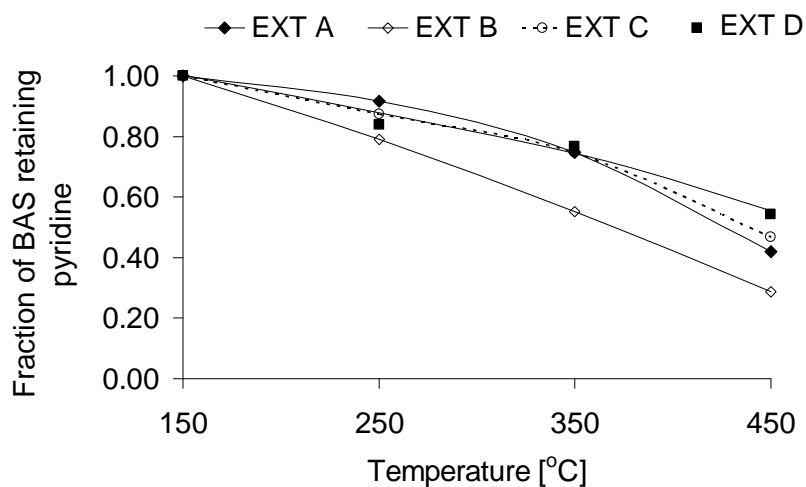
Figure 3.13. Fraction of Brønsted acid sites retaining pyridine as a function of the outgassing temperature.

3.2.3. ^{27}Al MAS NMR

MAS NMR measurements were performed to compare the bulk chemistry of extrudates and zeolite powders. The aluminum in the binder consists of both tetrahedrally and octahedrally coordinated aluminum species. The differentiation between framework and extraframework tetrahedral aluminum species was obtained through multiple quantum MAS NMR (MQMAS).

Figure 3.14a is the 2D MQMAS spectrum of powder SAMPLE A. The signal lying on the isotropic line at around 56 ppm indicates framework tetrahedral aluminum. The broadening of the contour below the isotropic line is an indication of the presence of distorted tetrahedral aluminum. The contour at around 0 ppm represents extraframework octahedral aluminum species of the powder samples.
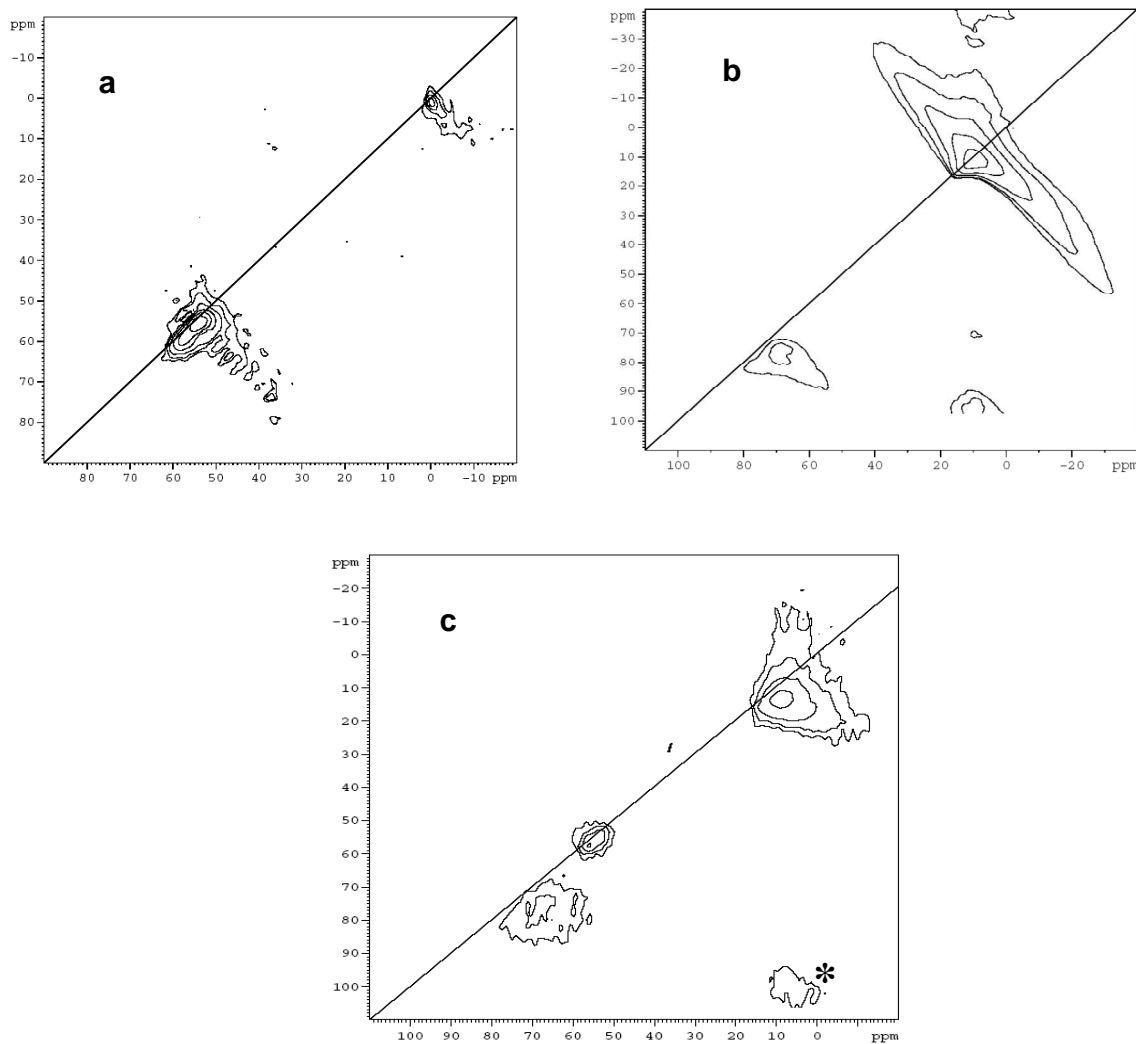
* spinning side bands

Figure 3.14. ^{27}Al MQMAS of a) SAMPLE A, b) Al$_2$O$_3$ binder and c) EXT A

Figure 3.14b shows the MQMAS spectrum of the pure Al$_2$O$_3$ binder. The amorphous nature of the Al$_2$O$_3$ binder resulted in highly distorted environment of the aluminum species with contours that lie away from the isotropic line. The low intensity of the contours with a wide distribution between 70 to 90 ppm which deviates from the isotropic line suggests the presence of several species of tetrahedrally coordinated aluminum in the binder. This holds also for the octahedral species of the aluminum spreading with a relatively broad distribution in the F1 (y axis) and F2 (x axis) dimension.

It should be emphasized at this point that the aluminum of the binder makes up to around 90% of the aluminum in the extrudate.

The 2D MQMAS of EXT A is shown in Figure 3.14c. The contours of the extrudate can be described as the superimposition of the contours of the powder (Figure 3.14a) and binder (Figure 3.14b). Similar features were also obtained for the other extrudates.

The chemical shift values derived from the F1 projections along the y axis are the true chemical shifts of the aluminum species in the 1D spectrum and are used to simulate the peaks of the respective species using dmWinfit2001. The chemical shifts and quadrupolar coupling constants are shown in Table 3.2. Thus, the contributions of aluminum from HZSM-5 and binder to the 1D ^{27}Al spectrum of the extrudate can be distinguished as presented in Figure 3.15.
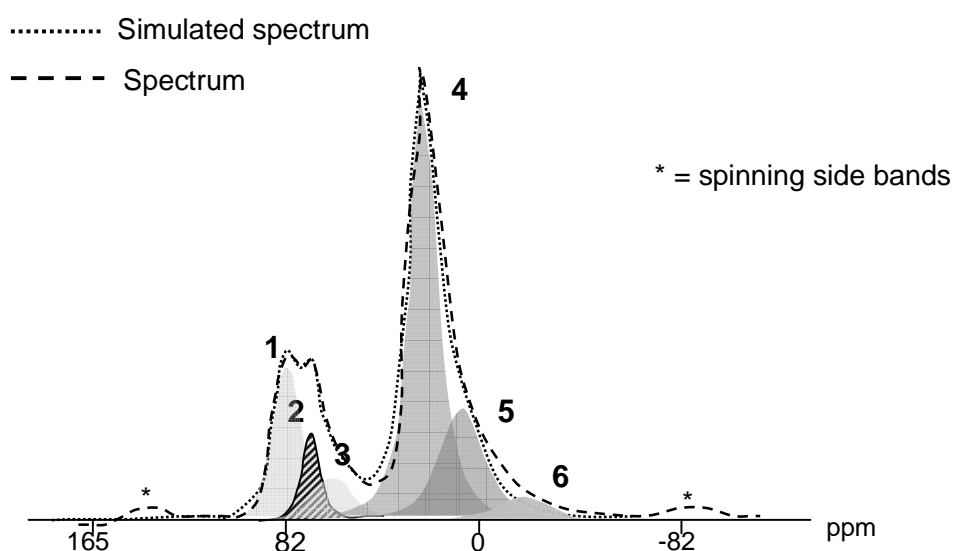
Figure 3.15. Deconvolution of 1D ^{27}Al MQMAS NMR of extrudate

Table 3.2. Chemical shifts and quadrupolar coupling constants (QCC) of EXT A

Peak number	Assignment of Al coordination	Chemical shift/ppm	QCC/kHz
1	Distorted tetrahedral from binder	75.3	4620
2	Framework tetrahedral from HZSM5	58.1	3498
3	Distorted tetrahedral from binder	54.4	5419
4	Distorted octahedral from binder	14.6	5288
5	Distorted octahedral from binder	8.5	5032
6	Distorted octahedral from binder	-9.6	5123

3.2.4 ^{29}Si MAS NMR

Framework Si in zeolites are tetrahedrally coordinated, and, thus, four different possible environments of a silicon atom denoted as Si (nA1) where n (n ≤4) exist and correlate with the number of aluminum atoms connected *via* oxygens to silicon. Information about the distribution of the aluminum among the T sites in next and next nearest neighbor shells may be inferred from line widths and intensities of the $Si(OAl)_n(OSi)_{4-n}$ peaks (n= 0-4) [21]. Thus, direct observation of silicon leads to an indirect determination of the framework aluminium (Figure 3.16) whereby the Si/Al$_{framework}$ ratio of the lattice can be calculated directly (Eq. 3.3). This enables us to determine if the new sites are formed at the external or within the HZSM-5 crystals.

$$\frac{Si}{Al_{framework}} = \frac{\sum_{n=0}^{4} I_{Si(nAl)}}{\sum_{n=0}^{4} 0.25 n I_{Si(nAl)}} \qquad \text{Eq. 3.3.}$$

where I = peak area.

-98   -106   -114   -123   -131 ppm
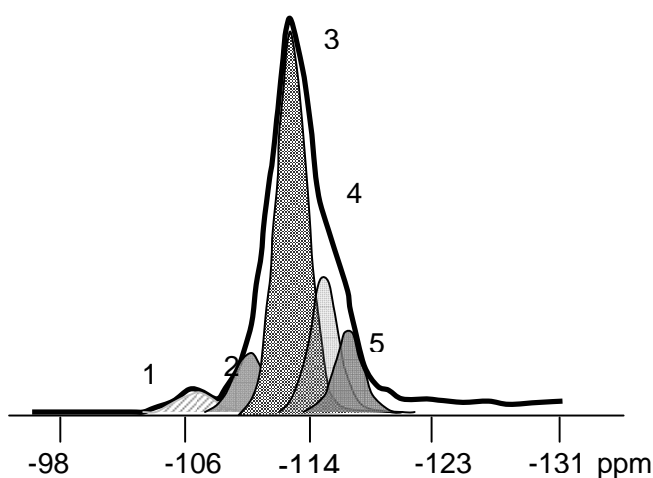
Table 3.3. Assignment of peaks in ^{29}Si NMR

Peak	Assignments
1	Si(1Al)
2 - 5	Si in different T sites

Figure 3.16. ^{29}Si MAS NMR spectrum of EXTA

The ^{29}Si NMR spectra for EXT B, EXT C, and EXT D with the corresponding powder were nearly identical. Thus, the Si/Al framework ratio of the extrudates determined by ^{29}Si NMR was close to that obtained for the corresponding powders for EXT B, EXT C and EXT D. This indicates that aluminum is retained in the framework position and that the forming process has not led to dealumination of the framework.

At this point, the very good agreement between the concentration of framework aluminum in the extrudate derived from ^{27}Al NMR and ^{29}Si NMR should be emphasized (Figure 3.17). The results show that within experimental error, binding with Al_2O_3 does not result in new intracrystalline bridging sites in all extrudates. At the same time, dealumination of the framework Al is insignificant.
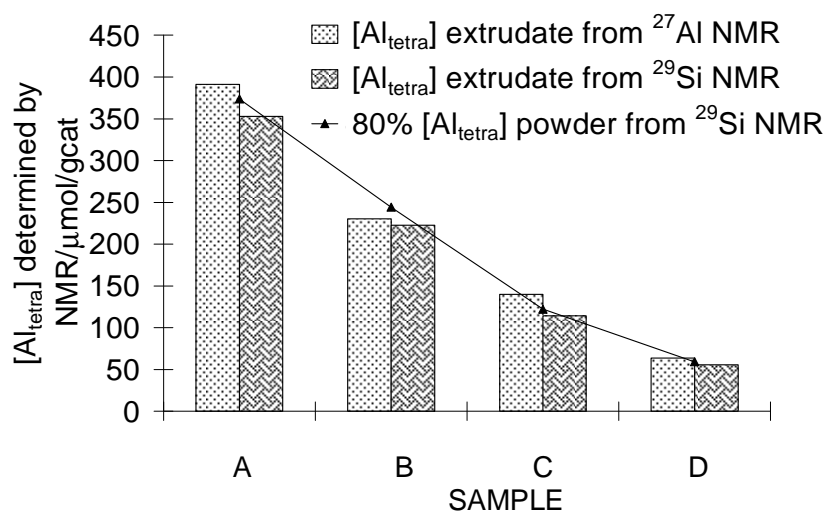
Figure 3.17. Comparison of aluminum concentration determined from ^{27}Al NMR and ^{29}Si NMR of powder and extrudate HZSM-5

3.2.5.   Atomic absorption spectroscopy (AAS)

The concentration of cationic impurities was analyzed to determine if the decrease of Brønsted acid sites concentration of EXT A and EXT B was due to neutralization by high concentration of cation impurities introduced with the binder.

Considering the dilution effect of the binder, the contribution of the binder to the Na and Fe impurities in the extrudate was calculated. The obtained values (Table 3.5) show the binder did not contribute significantly to the Na$^+$ content determined in the extrudate. Moreover, the contribution of the binder in EXT A and EXT B to the Fe content could not neutralize more than 5 µmol of BAS in the extrudate by assuming the Fe impurities to be trivalent. Thus, cationic impurities are not a significant factor causing the decrease in the concentration of the Brønsted acid sites in EXT A.

Table 3.5. Concentration of cationic impurities in powders and extrudates (in parenthesis is the cationic impurities in 0.8 g of extrudate in wt ppm)

Material	SAMPLE A	SAMPLE B	SAMPLE C	SAMPLE D
Na (wt ppm)	39 (31)	116 (87)	40 (32)	42 (34)
Fe (wt ppm)	300 (240)	425 (319)	310 (241)	469 (375)
Material	EXT A	EXT B	EXT C	EXT D
Na (wt ppm)	30	63	31	26
Fe (wt ppm)	321	435	556	492

3.2.6. Nitrogen physisorption

Surface area and pore volume of powders and extrudates are summarized in Table 3.6.

Table 3.6. Comparison of the micro and mesopore volume, and surface area of extrudates, powders and binders

	BET area [m^2/ g]	Mesopore volume [cm^3/g]	Micropore volume [cm^3/g]	Expected mesopore volume [cm^3/g]	Expected micropore volume [cm^3/g]
SAMPLE A	356	0.577	0.095		
EXT A	376	0.491	0.125	0.579	0.076
SAMPLE B	400	0.293	0.132		
EXT B	348	0.482	0.115	0.366	0.099
SAMPLE C	355	0.148	0.153		
EXT C	310	0.215	0.147	0.236	0.118
SAMPLE D	306	0.121	0.132		
EXT D	276	0.195	0.130	0.214	0.106
Binder	242	0.588	-		

The mesopore diameter distribution range in the extrudate was the same as for the binder. However, the mesopore volumes of the extrudate are smaller than the

predicted values for EXT A, EXT C and EXT D indicating that some blockage of the mesopores by aggregates with zeolite crystals has occurred.

Not much variation is observed in micropore volume between extrudate and corresponding powders. In fact, a marginal increase in micropore volume was observed when comparing 1g of extrudate with 0.8g of powder. The partial blockage of mesopore volume of the binder by the zeolite crystals could have generated micropore volume. In general, the micropore system of ZSM-5 is not affected by this binding method and binder type.

3.3.   Discussion

Overall, the forming process leads only to subtle changes of the parent zeolites. The specific changes vary with the concentration of aluminum in the lattice. In part, this is the result of very low concentrations of acid sites in some samples. So let us first address the effect of forming on the concentration of Brønsted acid sites.

The impact on the concentration of Brønsted acid sites varied with the Si/Al ratio of the zeolite taking the dilution effect of 20-25 wt% binder into account. For the low silica EXT A and EXT B, it decreased in average by around 14% and 5% respectively compared to the corresponding parent materials. In contrast, the concentration of Brønsted acid sites of high silica EXT C and D increased by 25-30%.

In order to rationalize the reason for the decrease of the Brønsted acid sites concentration in EXT A and EXT B, it is critical to address several issues when the zeolite is embedded into a matrix. The key issues for the loss of Brønsted acid sites are (i) solid state exchange of the cationic impurities introduced by the binder, (ii) pore blockage by the binder and (iii) localized interactions between binder fragments and HZSM-5 sites blocking acid sites locally.

Reasons for lower BAS concentration

As the concentration of cationic impurities other than cationic alumina species in EXT A and EXT B do not differ significantly from the corresponding parent zeolite, we conclude that the observed decrease in Brønsted acid sites concentration of EXT A cannot be due to the neutralization by cationic impurities. Note that it could however be compatible with the marginal decrease in Brønsted acid sites concentration of EXT B. In this respect, it is important to mention that binders of high purity have to be used in the forming process, because the concentration of acid sites can decrease significantly,

when solid-state ion exchange between Na^+ cations of the binder and the H^+ from the zeolite occurs [22, 23].

Poor accessibility to acid sites due to pore blockage is also ruled out, because all bridging OH groups of the extrudates disappeared in contact with pyridine. Hence, it is concluded that the pore channels are not blocked by alumina clusters. This is supported by nitrogen physisorption analysis, which indicates insignificant change in the micropore volume of the zeolites.

As one bridging OH group gives rise to one Brønsted acid site and estimations from the ^{27}Al and ^{29}Si NMR data indicated no significant loss of framework aluminum in EXT A, we conclude that a part of the aluminum maintains tetrahedral coordination in the framework, but does not form a bridging hydroxyl group. In EXT A, these Brønsted acid sites are neutralized by anionic hydroxylated aluminum species when the acidic proton is transferred to the OH group of the Al species from the binder, forming one coordinated water molecule. Such proton transfer is the result of the high basicity of the hydroxylated Al. This neutralization is postulated to take place during the extrusion process as shown schematically in Figure 3.18.

The migration of single Al as a hydroxylated soluble species during the extrusion process can happen during wet mulling of the extrudate. Acid sites near to the external surface of the zeolite crystals or near to pore entrance are preferentially neutralized in this way. This implies that the concentration of Al near to the pore mouth is higher in SAMPLE A compared to HZSM-5 with higher Si/Al ratios.
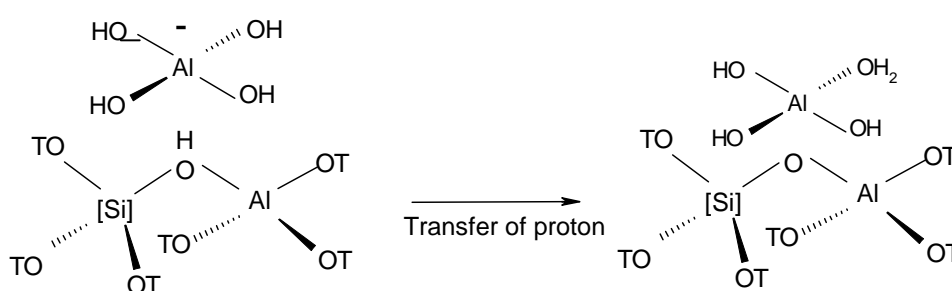

Figure 3.18. Neutralization of Brønsted acid sites by hydroxylated alumina species

Potential reasons for higher BAS concentrations

For EXT A, the decrease in the concentration of bridging OH groups (20%) was more pronounced than the decrease in the Brønsted acid site concentration measured

by adsorption of pyridine (14%). %). This implies that some acid sites are formed by protonation of pyridine on Brønsted acid sites formed at the interface between the binder and the zeolite crystals or in an amorphous silica alumina giving rise to acidic OH groups with bands at 3740 cm^{-1}. Acid sites formed in these cases are most likely as reversible bonding of Al^{3+} cations to SiOH groups. Such reversible coordination has been observed in alumino-silicate frameworks ranging from zeolites such as Beta, USY and HZSM-5 to amorphous alumina silica [24-26].

Evidence for such a process is drawn from ^{27}Al MQMASNMR and IR spectroscopy. Framework tetrahedrally coordinated aluminum associated with Brønsted acid sites are characterized by a band at 3650-3550 cm^{-1}. The IR spectrum of a dehydrated amorphous silica-alumina shows a single band at 3745 cm^{-1} in the hydroxyl region, due to terminal Si-OH groups. Bands of bridging hydroxyl groups at 3600 cm^{-1} are not observed. However, dosing ammonia onto dehydrated silica-alumina creates NH$_4^+$ species. The fact that this has been observed in amorphous silica alumina can be attributed to the interaction distance not exceeding the CID (critical interaction distance) and also a suitable degree of activation of the basic probe molecule, hence promoting the transfer of protons from surface OH groups adjacent to Lewis acid sites to a molecule chemisorbed on a Lewis site [27].

DFT calculations combined with thermodynamic evaluations enabled the establishment of detailed models of γAl$_2$O$_3$ surface under working conditions. The poorly hydroxylated (100) surface is favored under dehydration conditions with low water partial pressure, [28]. Figure 3.19 presenting a hydrated (100) alumina surface which forms apparent Brønsted acid sites in the vicinity of terminal silanol groups upon dehydration and pyridine adsorption in IR measurements. Trombetta et al. also observed the formation of pyH$^+$ species when pyridine was chemisorbed on dehydrated silica-alumina [31]. This reversible coordination of aluminum during pyridine adsorption can account for the smaller decrease in Brønsted acid sites concentration quantified from pyridine adsorption compared to the decrease in number of bridging OH group in EXT A.
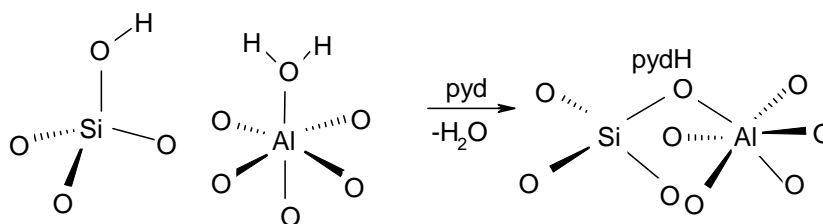
Figure 3.19.Apparent acidity of terminal SiOH group due to flexible hydroxyl coordination in alumino silicate systems observed in EXT A

Whatever the reasons for this discrepancy between the concentrations derived from IR spectroscopy of the bridging OH groups and from the adsorption of pyridine are, the concentrations of BAS in high silica samples increased as measured with both methods. It is in this critical to examine if these new sites are intracrystalline or intercrystalline. It has been observed that Al from the binder can substitute into the framework which increases the concentration of Brønsted acid sites of bound catalysts. Through catalytic reactions, it has been demonstrated that these new sites show Brønsted acidity. The authors have demonstrated through catalytic reactions that these new sites show Brønsted acidity [13].

In this work, the exhaustive use of MASNMR to determine the nature of these sites has been carried out. The conclusive evidence that the new Brønsted acid sites observed in EXT C and D are not intrazeolitic is derived from the ^{29}Si NMR spectra of these extrudates when compared to the parent unbound sample. No increase in the intensity of the band at -110ppm, associated to Si linked to one neighboring Al via oxygen atom in the bound HZSM-5, was observed. The spectra of the bound and unbound materials were identical when normalized to the same HZSM-5 weight contribution.

Another important indication stems from the ^{27}Al NMR spectra which yielded similar number of non distorted tetrahedral Al (peak at 56ppm). If these new Brønsted acid sites were truly intra-zeolitic, one would expect an increase in the peak intensity at 56ppm in the bound HZSM-5. This is because non framework Al would contribute to the peak intensity of distorted tetrahedral Al in the NMR spectra. (Note that to ensure the correct determination of the concentration of framework tetrahedral Al at 56ppm despite the low concentration, we have performed both the deconvolution of the peak and also the subtraction of the corresponding 20% contribution from the alumina binder from the extrudate spectra). Our results indicate that these new sites are not intrazeolithic and

hence are most likely associated with some new alumino-silicate phases formed at the grain boundaries.

The primary reason for the formations of these new sites in the high silica samples can be associated to the higher concentration of amorphous SiO_2 phases present during the preparation of HZSM-5 with low framework Al concentration. The reaction of Al_2O_3 from the binder with SiO_2 phase in the zeolite at high temperature during calcinations can result in the formation of new aluminosilicate phases, thence creating new intercrystalline acid sites in EXT C and EXT D.

Effect on acid strength

Beside the changes in the concentration of Brønsted acid sites upon forming with alumina, a decrease in the acid strength for all the investigated extrudates was observed. The amount of chemisorbed pyridine retained after sequential increase in outgassing temperatures during IR spectroscopic measurements gives a qualitative approximation of the acid strength distribution. We have observed that 40-70% of chemisorbed pyridine was retained (excluding contributions of the new acid sites) after the formed materials were outgassed at 450°C. This is in contrast with the 80% strong Brønsted acid sites which protonates pyridine as determined for the powder counterparts.

We attribute the decrease in the acid strength mainly to the preferential neutralization of the most acidic bridging hydroxyl groups in HZSM-5 when ion-exchanged by alumina species from the Al_2O_3 binder. This can take place during the mulling process when mobility of cationic impurities is enhanced at elevated temperatures and under hydrated conditions. An example has been illustrated for EXT A in Figure 3.18.

Effect on textural properties

The micropore volumes of the extrudates are slightly higher than the corresponding powder HZSM-5, indicating that pore blockage does not occur. The small increase in micropore volume is due to the reducing in size of some of the mesopores in the binder by zeolite crystals, inducing micropores formation. The overall contact feature of the extrudate and the powder is very similar, i.e., the binder does not modify the textural properties of the HZSM-5.

3.4. Conclusions

The introduction of Al_2O_3 as binder for HZSM-5 zeolite powders causes an overall increase in the concentration of acid sites concentration mainly as a result of the increase in Lewis acid sites concentration. Depending on the Si/Al ratio of the zeolite, the same binding conditions resulted in a preferential increase in the Brønsted acid sites in the high silica zeolites and an appreciable decrease in the Brønsted acid sites concentration in the lowest silica samples. The increase in the concentration of Brønsted acid sites is attributed to the generation of weak Brønsted acid sites (resembling in strength and labile nature to those in amorphous silica-alumina). In alumina rich zeolites, the binder causes partial neutralization of the acid sites by anionic alumina fragments. This preferential neutralization of acid sites in these materials occurs near to the external of the crystals, i.e., at pore mouths.

3.5. References

1.   Weitkamp, J., Acta Phys. Chim., **1985**, 31, 1-2, 271-290.

2.   Abdal Kareem, M. A., Chand, S. and Mishra, I. M., J. Sci. Ind. Res., **2001**, 60**,** 4, 319-327.

3.   Popova, Z., Yankov, M., Dimitrov, L. and Chervenkov, I., React. Kinet. Catal. Lett., **1994**, 52, 1, 51-58.

4.   Hochtl, M., Jentys, A. and Vinek, H, Appl. Catal., **2001**, 207, 1-2, 397-405.

5.   Haw, J. F., Nicholas, J. B., Song, W., Deng, F., Wang, Z., Xu, T. and Heneghan, C. S., J. Am. Chem. Soc., **2000**, 122, 19, 4763-4775.

6.   Puppe, L., Weitkamp, J. (Eds.), Catalysis and Zeolites (Fundamentals and Applications), **1999**, Berlin: Springer.

7.   Dorado, F., Romero R. and Canizares, P., Ind. Eng. Chem. Res., **2001**, 40**,** 16, 3428-3434.

8.   Rough, S.L., et al., Powder Technol., **2003,** 132, 2-3, 249-266.

9.   Wu, X., Alkhawaldeh, A., and Anthony R.G., Stud. Surf. Sci. Catal., **2002**, 143, 217-225.

10.   Chen, W.H., Huang, S. J., Lai, C. S., Tsai, T.C., Lee, H. K. and Liu, S.B.*,* Res. Chem. Intermed., **2003**, 29, 7-9, 761-772.

11. Misk, M., Joly, G., Magnoux, P., Guisnet, M. and Jullian, S., Microporous Mesoporous Mater., **2000**, 40, 1-3, 197-204.

12. Dorado, F., Romero, R., and Canizares, P., Appl. Catal., A, **2002**, 236, 1-2, 235-243.

13. Chang, C. D., Hellring, S. D., Miale, J. N., Schmitt, K. D., Brigandi, P. W. and Wu, E. L., J. Chem. Soc., Faraday Trans. 1, **1985**, 81**,** 2215-2224.

14. Uguina, M. A., Sotelo, J. L. and Serrano, D. P., Appl. Catal., **1991**, 76**,** 2, 183-198.

15. Emeis, C.A., J. Catal., **1993**, 141, 2, 347-354.

16. Massiot, D., Fayon, F., Capron, M., King, I., Le Calvé, S., Alonso, B., Durand, J-O., Bujoli, B., Gan, Z., Hoatson, G., Magn. Reson. Chem., **2002,** 40, 1, 70-76.

17. Knözinger, H. and Ratnasamy, P., Cat. Rev. - Sci. Eng., **1978**, 17, 1, 31-70.

18. Loeffler, E., Lohse, U., Peuker, C., Oehlmann, G., Kustov, L. M., Zholobenko, V. L. and Kazansky, V. B., Zeolites, **1990**, 10**,** 4, 266-271.

19. Loeffler, E., Peuker, Ch. and Jerschkewitz, H. G., Catal. Today, **1988**, 3, 415-420.

20. Lercher, J.A., Ritter, G., and Vinek, H., J. Colloid Interface Sci., **1985**, 106, 1, 215-221.

21. Lippmaa, E., Maegi, M., Samoson, A., Tarmak, M., and Engelhardt, G.*,* J. Am. Chem. Soc., **1981**, 103**,** 17, 4992-4996.

22. Jasra, R. V., Tyagi, B., Badheka, Y. M., Choudary, V. N., and Bhat, T. S. G., Ind. Eng. Chem. Res., **2003**, 42, 14, 3263-3272.

23. de Lucas, A., Valverde, J. L., Sánchez, P., Dorado, F. and Ramos, M. J., Appl. Catal., A, **2005**, 282, 1-2, 15-24.

24. Woolery, G. L., Kuehl, G. H., Timken, H. C., Chester, A. W. and Vartuli, J. C., Zeolites, **1997**, 19, 4, 288-296.

25. Wouters, B.H., Chen, T.H., and Grobet, P.J., J. Am. Chem. Soc., **1998**, 120, 44, 11419-11425.

26. Omegna, A., van Bokhoven, J. A., and Prins, R, J, Phys. Chem. B, **2003**, 107**,** 34, 8854-8860.

27. Basila, M. R. and Kantner, T. R., J. Phys. Chem., **1967**, 71, 3, 467-472

28. Digne, M., Sautet, P., Raybaud, P., Euzen, P., and Toulhoat, H., J. Catal., **2004**, 226, 54-68.

29.   Trombetta, M., Busca, G., Rossini, S., Piccoli, V., Cornaro, U., Guercio, A., Catani, R. and Willey, R. J., J. Catal., **1998**, 179, 2, 581-596.

Chapter 4

Dealumination model of

hydrothermally treated HZSM-5

Abstract

HZSM-5 steamed at 450 °C and 101.3 kPa water loses 60 % of Brønsted acid sites in the first 24 h of steaming because of the hydrolysis of labile Al mostly from zones of higher aluminum concentration. ^{27}Al MAS NMR indicates that these aluminum atoms have a lower T-O-T angle (150°) and a lower angle strain. Upon steaming, these Al atoms form tetracoordinated extraframework species, which neutralize neighboring Brønsted acid sites. Such neutralization leads to a more rapid decrease of the Brønsted acidity than of the concentration of aluminum in the lattice. Slow dealumination ensued after 24 h affecting aluminum atoms with higher hydrothermal stability possessing higher T-O-T angles and higher angle strain. The extraframework Al also contributes to the stabilization of Al in the framework. The preferential dealumination of Al from lower T-O-T angle shows that the inflexibility of local structures to accommodate distortion facilitates the hydrolysis of the weakest Al-O bond.

4.0.   Introduction

In general, the catalytic properties of a zeolite have a direct relation to its concentration of Brønsted acid sites, which is commonly associated with the concentration of framework aluminum. Hence, dealumination - a process in which framework aluminum is removed from the zeolite - adversely affects the rate of reactions catalyzed by protons. As steam is one of the most effective dealuminating agents, the presence of water, either in the feed or as a by-product in a catalytic reaction at high temperature, results in the loss of tetrahedral framework aluminum through the hydrolysis of Al-OH-Si and Al-O-Si bonds.

Several authors have investigated the kinetics of dealumination under hydrothermal conditions [1-4]. Fast and slow dealumination steps have been identified and several dealumination models based on different zeolites have been proposed. However, the rate determining step, which can potentially influence the stabilization of the remaining framework aluminum, is seldom discussed and experimental evidence for the elementary steps is scarce.

Some authors explain the extraction of aluminum from the framework via a pentacoordinated aluminum species identified by the signal at 30 ppm in the ^{27}Al MAS NMR spectrum [5]. Others suggest that the intermediate species are distorted tetrahedral aluminum species [6]. It is interesting to note, however, that also the nature of the resulting extra framework aluminum species is not unequivocally accepted. Up to three different kinds of octahedral aluminum species has been described according to data from ^{27}Al MAS NMR spectroscopy [7]. In addition, several proposals for reversible Al framework coordination have been discussed for zeolitic systems such as HZSM-5, HMOR, HBEA and HY [8-10].

When comparing the vast number of papers that propose dealumination models, it is important to keep in mind that the dealumination process is influenced by the zeolite structure, aluminum distribution and its inherent tendency towards defect formation. Often, the proposed models are based on low silica zeolites that are usually less stable against dealumination [11]. It is to be explored whether or not these models are applicable to high silica materials, which are hydrothermally more stable against hydrolysis.

Taking into account the complexity of the above issues, we chose to explore dealumination of HZSM-5 SAMPLE C under hydrothermal conditions and investigate the

gradual change of the framework Al and integrity of the zeolite structure with steaming duration. The choice for a high silica material with negligible extraframework Al was originally related to the ability to study the dealumination of acid sites, which are often assumed to be mostly isolated and non-interacting from the low silica containing materials in study. A second reason for the choice of material is related to the fact that high silica H-ZSM-5 is a frequently used zeolite when high steam stability is required for industrial applications.

4.1. Experimental

4.1.1 Materials and steaming procedure

The parent HZSM-5 zeolite was synthesized following the procedure described in Chapter 2. Before steaming, the zeolite was pressed and sieved into particles ranging from 355 to 500 µm. The scheme of the setup used for steaming and the packing of the corresponding reactor are illustrated in Figure 4.1.
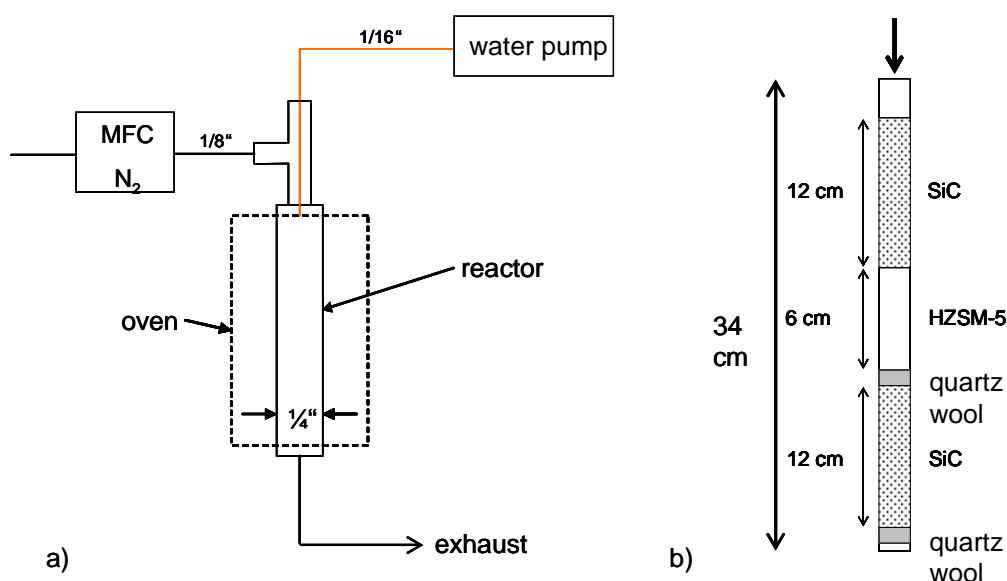
Figure 4.1. a) Setup for steaming experiment; b) packing of steaming reactor.

The zeolite (500 mg) was heated to 450 °C with rate of 10 °C/min under nitrogen flow. When 450 °C was reached, N_2 was switched to water which was pumped into the quartz tubular reactor by a *Gilson 307* HPLC pump. The total flow was kept constant at 0.333 mol/h. The layer of SiC on top of the catalyst allowed the constant vaporization of the injected water. The duration of the steaming experiment was varied from 2 to 48 h.

4.1.2. IR spectroscopy

IR spectra were measured with a *Perkin Elmer 2000* spectrometer. All spectra were recorded in the region between 4000 and 800 cm^{-1} at a resolution of 4 cm^{-1}. The background spectrum was subtracted from all spectra.

For IR spectroscopy of adsorbed pyridine, the samples were pressed into self-supporting wafers (density 13-25 mg/cm^2). After activation in vacuum (10^{-6} mbar) for 1 h at 450 °C (heating rate 10 °C/min), the sample was cooled to 150 °C and pyridine was adsorbed in small dosages until full saturation of the bridging OH group at 3606 cm^{-1} was observed. The system was then equilibrated for 0.5 h. All IR spectra were recorded at 150 °C before adsorption of pyridine, during the adsorption of pyridine and after outgassing (10^{-6} mbar) at 450 °C. The concentration of Brønsted and Lewis acid sites (referred to as BAS and LAS, respectively) was estimated from the areas of the bands at 1565 – 1515 cm^{-1} and 1470 – 1435 cm^{-1}, respectively, by applying Eq. 4.1 and Eq. 4.2 modified from reference [12]:

$$c(BAS) = 4.32 \cdot 1000 \cdot r^2 \cdot \frac{IA(1565-1515cm^{-1})}{m} \qquad \text{Eq. 4.1}$$

$$c(LAS) = 3.27 \cdot 1000 \cdot r^2 \cdot \frac{IA(1470-1435cm^{-1})}{m} \qquad \text{Eq. 4.2}$$

where:

c = concentration of acid sites [μmol/g]

IA = integral of the respective peak [cm^{-1}]

r = radius of the wafer [cm]

m = mass of the wafer [mg]

4.1.3. MAS NMR spectroscopy

All samples were packed in 4 mm ZrO$_2$-rotors and spun at 15 kHz. For ^{27}Al MAS and MQMAS NMR measurements, the samples were hydrated for at least 48 h. Al(NO$_3$)$_3$·9H$_2$O (δ= -0.543 ppm) was used as reference. An excitation pulse with power level of 7 dB and a length of 0.6 μs was applied for the 1D spectrum. The relaxation time was 250 ms. For 1D spectra, 2400 scans were recorded. MQMAS spectra were recorded with a three pulse sequence [13]. The power level was 7 dB for the first two pulses and 35 dB for the last one. The pulse lengths were p$_1$=8 μs, p$_2$=3.2 μs and p$_3$=52

µs. The evolution time t_1 was incremented in intervals of 1 µs and data were processed with Bruker Topspin. After Fourier transformation, the 2D spectra were sheared so that the orthogonal projection on the isotropic axis gives the 1D spectrum free of any anisotropic broadening [14]. For quantification of the ^{27}Al MAS NMR spectra, the chemical shift and the quadrupolar coupling constant (QCC) were obtained from the MQMAS spectrum and used to deconvolute the 1D spectra using dmWinfit2001 developed by Massiot [15].

For ^{1}H MAS NMR spectra, the samples were activated in vacuum at 400 °C for 14 h to eliminate adsorbed water. At the magnetic field of 11.75 T, the Larmor frequency for ^{1}H was 500 MHz. Adamantane $C_{10}H_{16}$ was used as reference material (δ=2.0 ppm). For spectra recording, an excitation pulse with a power level of 6.00 dB and a length of 1.60 µs was applied. The relaxation time was 2 ms. For all spectra, 100 scans were recorded. For quantification, the 1D spectra were simulated with Gaussian peaks using dmWinfit2001.

For ^{29}Si MAS NMR, the Larmor frequency was 99.36 MHz. The reference for the measurements was solid $Si(OSi(CH_3)_3)_4$ (δ= -9.843 ppm). An excitation pulse with a power level 7 dB and a length of 0.6 µs was applied. The relaxation time was 250 ms. For each spectrum, 2400 scans were recorded. The 1D spectra were simulated using dmWinfit2001 for the determination of Si/Al ratio.

4.1.4. X-ray diffraction (XRD)

X-ray powder diffraction patterns of the samples were measured using a *Philips X'Pert Pro System* operating with a CuKα1-radiation (0.154056 nm) at 40 kV/40 mA. Measurements were performed on a spinner with a 1/4'' slit from 5° to 50° 2 θ (0.05 °/min). The relative crystallinity of the steamed s amples was determined by measuring the intensity of the diffraction signal of the (051) peak and comparing it to that of the reference unsteamed sample.

4.1.5. Nitrogen physisorption

Surface area, pore volume and pore size distributions of the materials were obtained by nitrogen adsorption on a *PMI* automated BET sorptometer. *Brunauer, Emmet* and *Teller* (BET), *Barrett, Joyner* and *Halenda* (BJH; desorption branch), and t-plot methods were used for calculating specific surface area and meso- and micro-pore

volume. Before adsorption, the sample (100 mg) was activated in vacuum at 400 ℃ for 2 h. After activation, the weight of the dried sample was determined. Finally, the sample was cooled to –196 ℃ and liquid nitrogen was adsorbed at increasing partial pressures.

4.1.6. Transmission electron microscopy (TEM)

TEM micrographs were recorded with a *JEM-2010-JEOL* microscope with a resolution of 0.2 nm. The acceleration voltage was 120 keV (LaB$_6$ electron source). Before measurement, the samples were dispersed in ethanol using an ultrasonic bath. Drops of this dispersion were deposited on a copper grid-supported film.

4.2. Results

4.2.2. IR spectra of adsorbed pyridine

Figure 4.2 shows the effect of duration of steaming treatment on the IR spectra of the samples activated at 450 ℃.
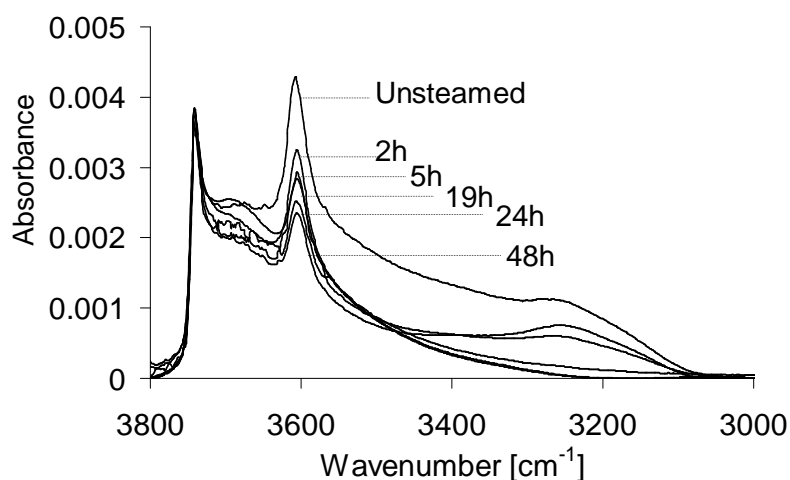
Figure 4.2. IR spectra of activated HZSM-5 as a function of steaming duration (450 ℃, 101.3 kPa water pressure).

The band at 3606 cm^{-1}, which is attributed to Brønsted acid sites, strongly decreased within 19 h steaming and attenuates slowly after this period. Visually, the band at 3743 cm^{-1}, attributed to terminal SiOH groups, did not change its intensity significantly with duration of steaming. An accurate qualitative determination of changes in the intensity of this band is difficult due to varying baselines with the evolvement of new species during steaming.

The band from 3726 to 3630 cm^{-1} is mainly attributed to OH groups on extraframework aluminum and/or on aluminum partially hydrolyzed from the framework [16]. This band was not observed for the unsteamed zeolite. It only appeared after 2 h steaming. Prolonging the steaming treatment decreased the intensity of this band and it was hardly detectable, when the steaming time exceeded 19 h. The width of this band suggests the presence of another band that may correspond to weakly hydrogen bonded Si-OH groups at defect sites as proposed by Jacobs and Uytterhoeven in the case of HY zeolites [17].

The rather intensive and broad band with the maximum at 3250 cm^{-1} is attributed to the formation of hydrogen bonding between bridged hydroxyl forming strained intramolecular hydrogen bond with neighboring lattice oxygen atom. This broad band cannot be clearly observed in the transmission spectrum on the background of a strong light scattering by the sample [18].

After adsorption of 0.1 mbar pyridine at 150 °C, th e band of the bridging OH group was completely eliminated while the band between 3726 and 3630 cm^{-1} remained unperturbed (Figure 4.3). This shows that, at the adsorption temperature used, the acidic strength of the corresponding hydroxyl groups was too low to allow interaction with pyridine.
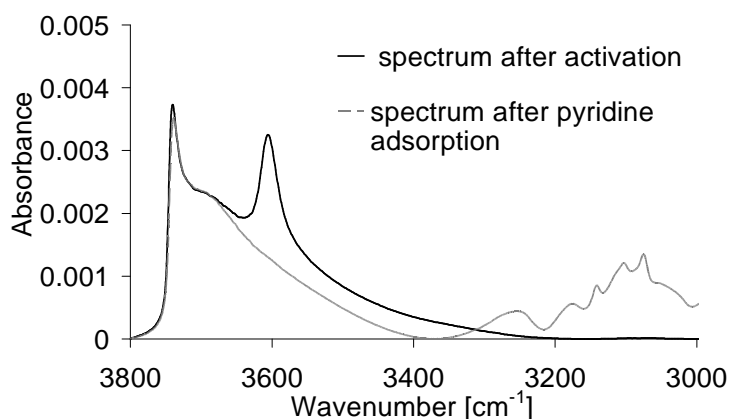

Figure 4.3. IR spectra of activated 2h-steamed HZSM-5, before and after pyridine adsorption at 150 °C.

The intensity of the band at 1545 cm^{-1}, which is attributed to pyridinium ions formed upon adsorption of pyridine on Brønsted acid sites, decreased with increasing

steaming duration (Figure 4.4). The band attributed to coordinatively adsorbed pyridine at 1455 -1442 cm^{-1} remained approximately constant in intensity, but shifted from an initial value of 1447 cm^{-1} in the unsteamed sample to 1455 cm^{-1} after 48 h steaming. This shift upon steaming is attributed to overlapping of bands corresponding to pyridine adsorbed on less accessible aluminum cations and on hydroxyl groups (band at 1447 cm^{-1}) already present in the parent material, and also on well-accessible Lewis-acidic aluminum cations at 1455 cm^{-1} (most likely in the form of extraframework aluminum species) [19].
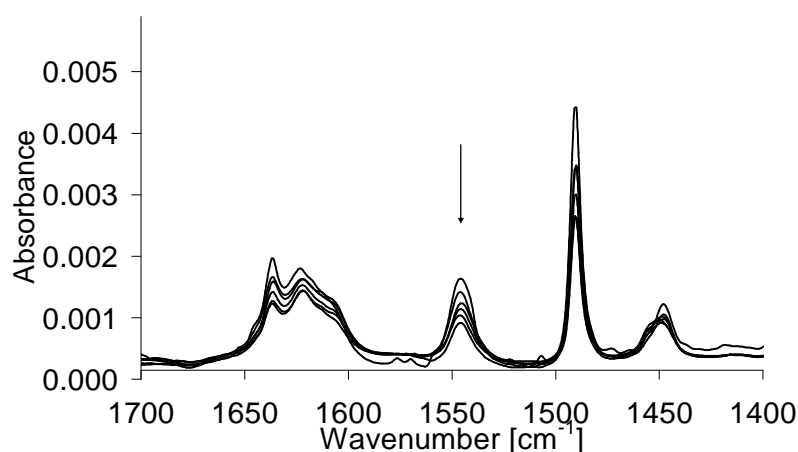

Figure 4.4. Difference IR spectra of pyridine on steamed HZSM-5 at different steaming times (arrow indicates intensity decrease with increasing steaming duration: 0, 2, 5, 19, 24 and 48h).

Figure 4.5 summarizes quantitatively the effect of steaming time on the concentration of Brønsted and Lewis acid sites. The intensity of the band of pyridinium ions strongly decreased with steaming duration until around 24 h. Then, the rate of decrease was considerably reduced. The concentration of Lewis acid sites showed a very small increase at the beginning of the steaming treatment and then remained almost constant. The initial increase is attributed to the formation of extraframework aluminum species. Thus, the overall decrease of the concentration of acid sites was mainly due to the decrease in the concentration of Brønsted acid sites.
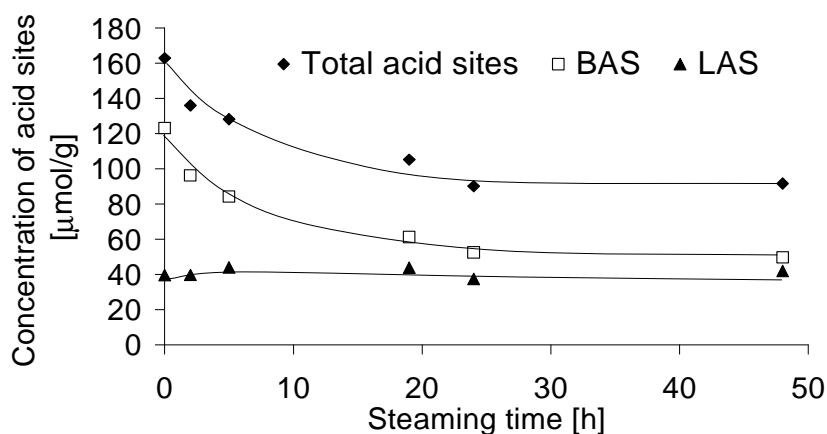
Figure 4.5. Change in acid sites concentration with steaming time (from IR spectroscopy of adsorbed pyridine).

4.2.2. ^{27}Al MAS NMR measurements

More than 99% of the Al adopts tetrahedral coordination in the unsteamed HZSM-5, as indicated by the NMR peak between 80 and 40 ppm chemical shift (Figure 4.6) [20]. In all the steamed HZSM-5 samples, most of aluminum also adopts tetrahedral coordination.

Figure 4.6. 1D ^{27}Al MAS NMR spectrum of parent and steamed HZSM-5 (arrow indicates intensity decrease with increasing steaming duration: 0, 2, 5, 19 and 24h).

As shown in figure 4.7, after 24 h steaming, the area of the NMR peak corresponding to framework tetrahedral Al was reduced to 80 % of that of the parent unsteamed sample, which is assumed to be proportional to the total Al content in this series of samples. The decrease of the peak corresponding to framework tetrahedral Al was not compensated by 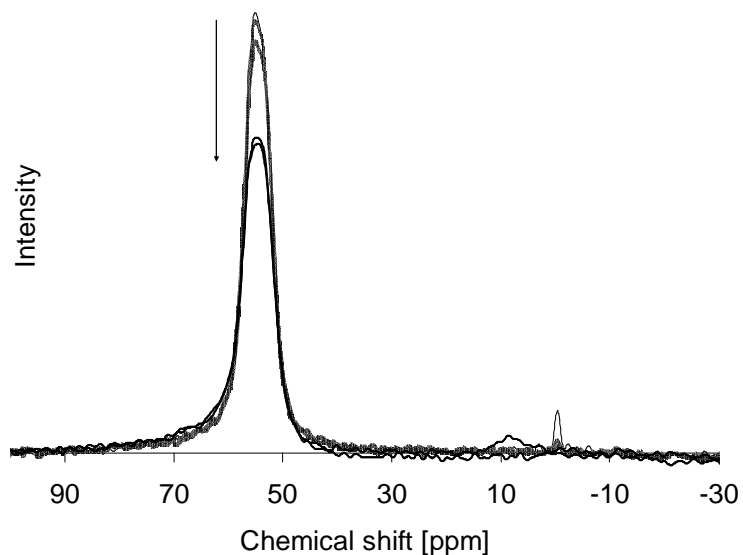a corresponding increase of the peak for Al in octahedral coordination. A mass balance suggests that approximately 15 % of the total aluminum was invisible to ^{27}Al MAS NMR spectroscopy in the 24 h steamed sample. This is determined by calculating the total intensity of the NMR spectrum between 80 and -15 ppm of the 24 h steamed HZSM-5 as a percentage of the total intensity of the NMR spectrum of the unsteamed parent material. These "NMR invisible" Al species are Al in highly distorted environment, resulting in high quadrupolar coupling constants which cause peak broadening beyond detection in the 1D spectrum. Despite the 15 % undetected Al, the relative decrease in Brønsted acid sites concentration derived from IR spectra of adsorbed pyridine was much more pronounced than that of tetrahedral Al in NMR spectra (Figure 4.7).
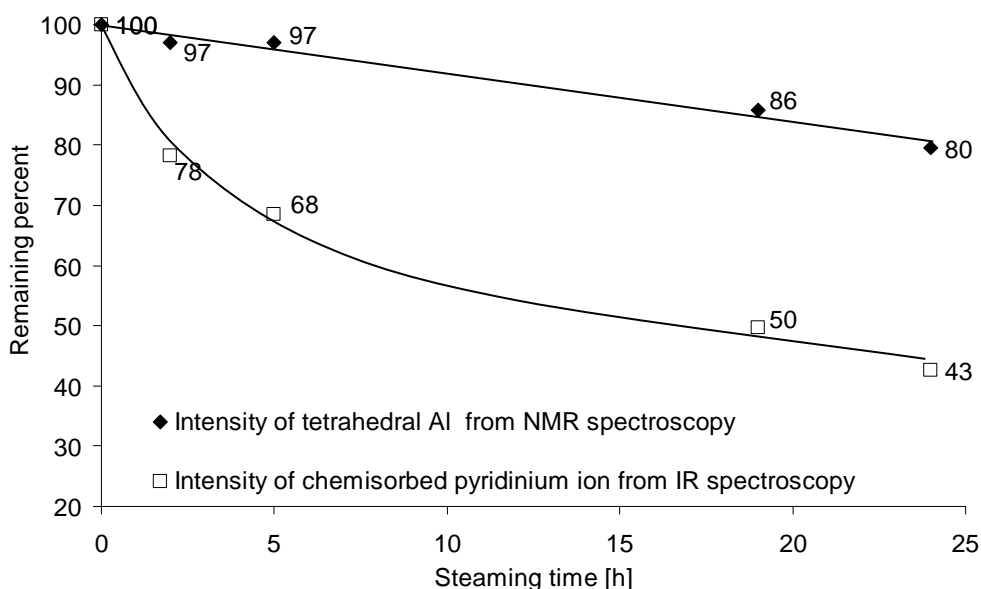

Figure 4.7. Correlation between the percent of the original intensity of Al$_{tetra}$ (80 to 40 ppm) from ^{27}Al MAS NMR and the percent of the original intensity of the IR spectroscopic band associated to chemisorbed pyridinium ions (1560-1520 cm^{-1}), as function of steaming time.

2D MQMAS NMR spectra were measured to verify the type of aluminum coordination in the steamed HZSM-5 samples (Figure 4.8).
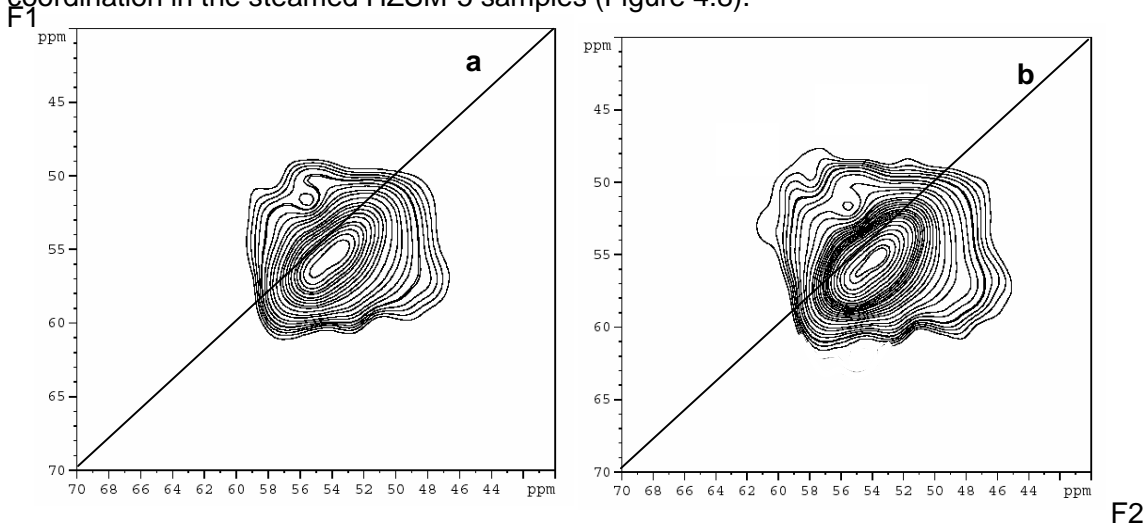

Figure 4.8. ^{27}Al MQMAS spectrum of a) 2h and b) 24h steamed HZSM-5

In the MQMAS spectra for all steamed samples, only tetra-coordinated aluminum, with isotropic distributions as a result of variations in Al-O-Si bond angle and/or Al-O bond length, was observed [21]. The presence of aluminum in distorted tetrahedral environment caused a non-symmetric interaction with the external magnetic field, resulting in a larger quadrupolar interaction. As a consequence, broadening of the contour below the isotropic line was observed. Samoson et al. reported similar features in spectra of dealuminated faujasites and ZSM-5 and suggested that the signal is related to non-framework tetrahedral aluminum species [6].

The isotropic projection in the F1 dimension gives a 1D high resolution spectrum of aluminum without quadrupolar second order broadening. A close examination reveals at least two types of aluminum species with tetrahedral coordination, as evident from the asymmetric shape of the peak (Figure 4.9a). This indicates two different types of aluminum sites in the steamed HZSM-5 [22]. They experience relatively small quadrupolar interactions and are comparable in concentration, since the contour of the Al in the 2D MQMAS spectra lies along the isotropic line (Figure 4.9b). Thus, we can assume that they have very similar MQ MAS efficiency.
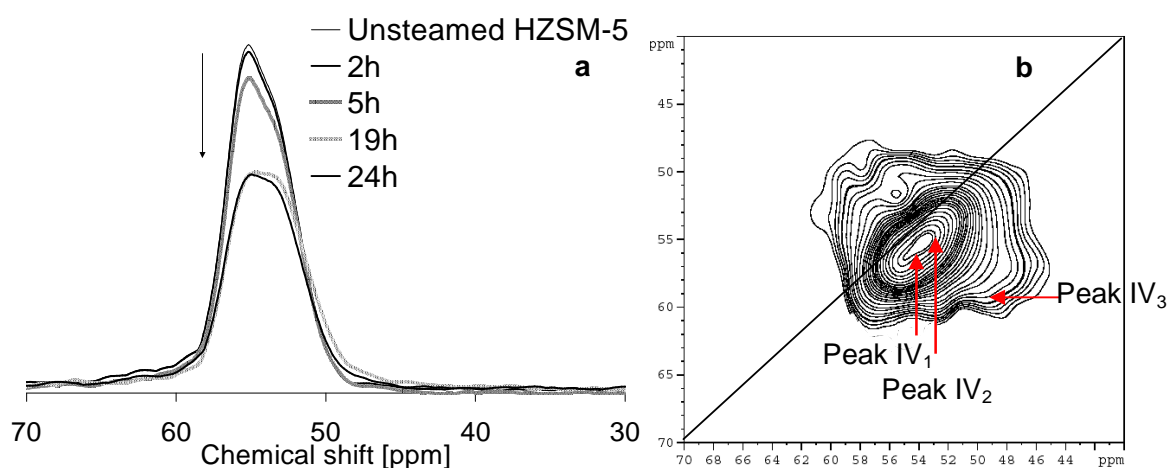
Figure 4.9.a) ^{27}Al MQMAS F1 projection of HZSM-5 at different steaming durations and b) aluminum in different T sites in the 2D MQMAS of 24 h steamed sample.

From the coordinates of the center of gravity of the different resonances in the 2D MQMAS spectrum, the quadrupolar coupling constants (C_{QCC}) as well as the isotropic chemical shifts δ_{iso} were calculated according to the following equations in which ν_L is the Larmor frequency, η is the asymmetry factor and P_Q is the "Second Order Quadrupole Effect" (SOQE)/quadrupolar interaction product:

$$\partial_{iso} = \frac{17\partial_{F1} + 10\partial_{F2}}{27} \qquad \text{Eq. 4.3.}$$

$$P_Q = C_{QCC}\sqrt{1+\frac{\eta^2}{3}} = \left(\frac{17}{162000}\nu_L^{\,2}(\partial_{F1} - \partial_{F2})\right)^{\frac{1}{2}} \qquad \text{Eq. 4.4.}$$

The excitation and conversion of MQMAS measurements depend on the ratio of ν_Q/ν_{rf} and so they are not quantitative [23]. Thus, quantification was done by fitting the corresponding F1 projection using the quadrupolar parameters determined in the MQ MAS experiment. The spectrum was deconvoluted into three peaks: peak IV$_1$ with chemical shift of 57.2 $\pm$ 0.5 ppm, peak IV$_2$ with chemical shift of 54.4 $\pm$ 0.5 ppm and peak IV$_3$ with a chemical shift of 60.5 $\pm$ 0.5 ppm (Figure 4.10 a and b). In the unsteamed sample, the average line width of the first two peaks was around 2.8 ppm with an

approximate intensity ratio of 2.7 (Figure 4.10 c). The relative intensity decreased to 1.4 after 24 h steaming duration indicating that Al represented by peak IV_1 was preferentially removed. Peak IV_3 at around 60 ppm linearly increased within 24 h steaming time. Therefore, it was attributed to extraframework tetrahedral aluminum or partially hydrolyzed distorted tetrahedral Al.
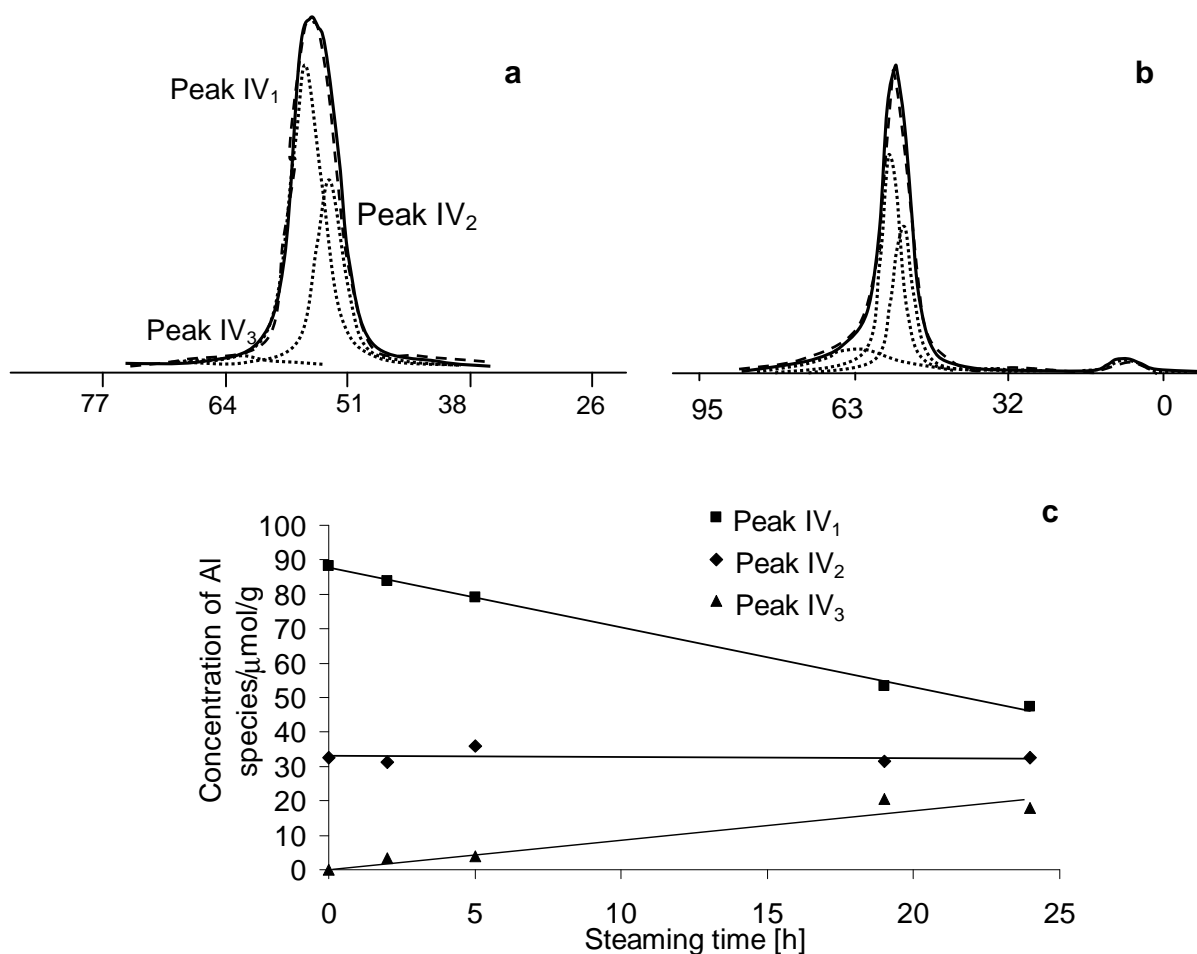
Figure 4.10. Deconvolution of ^{27}Al MAS NMR spectra of a) 5h and b) 24h steamed HZSM-5. Figure 4b has been magnified 1.2 times with respect to Figure 4a. Solid lines are actual spectra, sketched lines are simulated spectra and dotted lines are deconvoluted peaks; c) Change in concentration of Al species with steaming time.

Despite deconvolution of the ^{27}Al MAS NMR spectra, it was not possible to correlate NMR with IR data, when assigning the Al at the two groups of T-sites detected in NMR (sum of peak IV_1 and IV_2) to be directly related to Brønsted acid sites (Figure

4.11). 27µmol/g of Al_{tet} in the two T sites was found to be non Brønsted acidic after 24 h steaming.
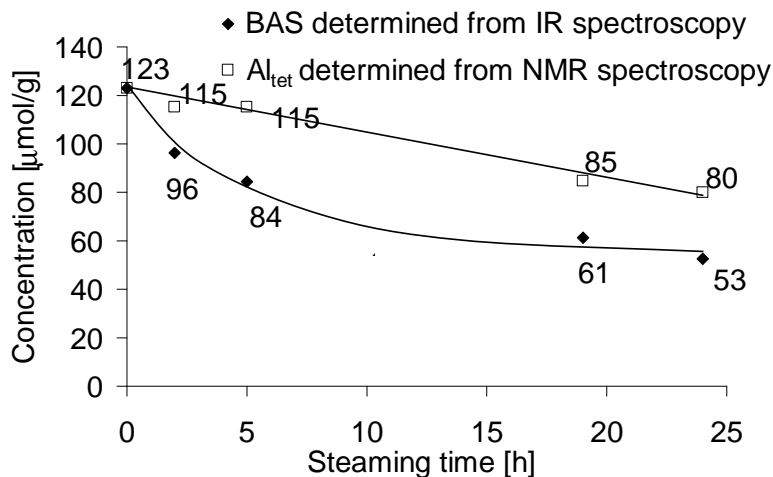
Figure 4.11. Concentration of BAS determined from IR of adsorbed pyridine and concentration of Al_{tet} (peak IV_1 + peak IV_2) determined from ^{27}Al MAS NMR vs. steaming time.

4.2.3 ^{29}Si MAS NMR

Lippmaa et al. have established an empirical relationship between the isotropic chemical shift δ and the average T-O-T angle α which is given by $^{Al}δ = -0.500α +132$ and $^{Si}δ = -0.5793α -25.44$ for ^{27}Al [24] and ^{29}Si [25], respectively. It is, thus, possible to relate the isotropic peaks in the ^{27}Al to those in the ^{29}Si MAS NMR spectra.

In the ^{29}Si MAS NMR spectrum of unsteamed HZSM-5, two peaks at -112.3 and -115.2 ppm were detected. They correspond to two groups of T sites at lower and at higher average bond angle, respectively. Using ref. [25] as guideline, we calculate these angles to be 150° and 155°. The concentration of th ese two groups, i.e., 69 % for the T-O-T sites giving a signal at -112.3 ppm and 26 % for the sites at -115.2 ppm, agrees well with the distribution of the two equivalent T sites derived from the ^{27}Al MAS NMR (peak IV_1 and IV_2 in Figure 4.10). No attempt was done to deconvolute the ^{29}Si MAS NMR spectra of the steamed HZSM-5 due to the overlapping of the peak of Si(1Al) at around -106 ppm with that of Si(nOH) corresponding to defect sites at around -110 ppm.

Peak #	Position (ppm)	Width (ppm)	Integral (rel)
1	-106.1	1.2	5
2	-112.3	2.9	69
3	-115.2	2.9	26

.... 24h steamed HZSM-5

—— Unsteamed HZSM-5

[ppm]   -90   -102   -114   -125   -137
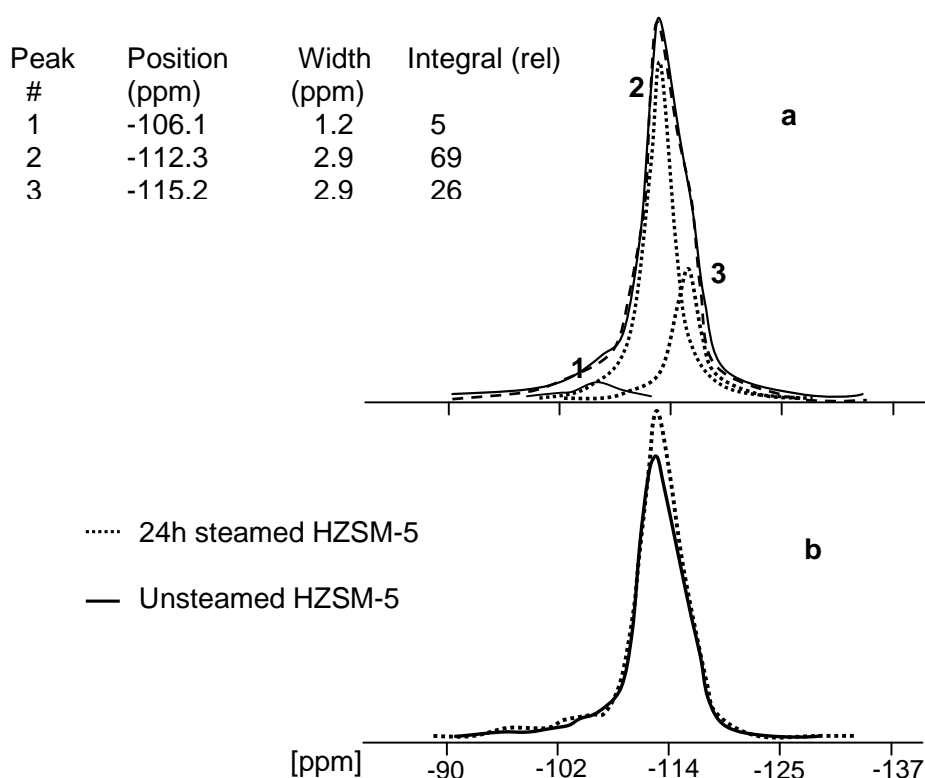
Figure 4.12. a) Deconvolution of the ^{29}Si MAS NMR spectrum for the unsteamed HZSM-5 (solid lines are actual spectra, sketched lines are simulated spectra and dotted lines are deconvoluted peaks); b) ^{29}Si NMR spectra for the unsteamed and 24h steamed HZSM-5.

4.2.4. ^{1}H MAS NMR

The change in the proton concentration of various hydroxyl groups was monitored via ^{1}H MAS NMR spectroscopy (Figure 4.13). The signal at 1.8 ppm is due to protons of terminal SiOH groups on the external of the crystal surface. The signal at 2.3 ppm is due to internal non acidic Si-OH groups, silanol nests, which are associated to defect sites present in the original material or formed upon dealumination [26, 27].

The change in intensity of the SiOH groups in terminal and defect sites observed in NMR is larger than the corresponding change in intensity from that observed in IR spectroscopic measurements. While it could be related to difficulties to defining the baseline of the SiOH groups from IR spectra shown in Figure 4.2, we would also point to the fact that the intensity of the bands could be obscured by changing molar extinction

coefficients. Thus in case of such a conflict, the concentrations derived from the NMR measurements are used for description of the changes. However, condensation of hydroxyl groups and healing of defect sites with steaming time would eventually contribute to the overall decrease in the intensity of the SiOH groups.

The non-acidic Al-OH group of extraframework/partially hydrolyzed Al should appear at around 0 ppm, when unperturbed. However, interaction with other OH or neighboring oxygen atoms results in a low field shift to 2.6-3.2 ppm [10]. This shift depends on the nature of the extra-framework cluster, distance of oxygen atoms around the species and pore shape of the zeolite. Thus, the peak centered at 3.1 ppm, which appeared already at short steaming time, was attributed to framework-related partially hydrolyzed Al-OH species, which are intermediates in the dealumination process [10]. Extended steaming treatment leads to full removal of such transient Al species which are finally converted into extraframework Al species. They also contribute to the peak at 3.1 ppm.

The intensity of the bridging OH groups at around 4.3 ppm decreases with increasing steaming time and stabilizes after steaming for 19 h.
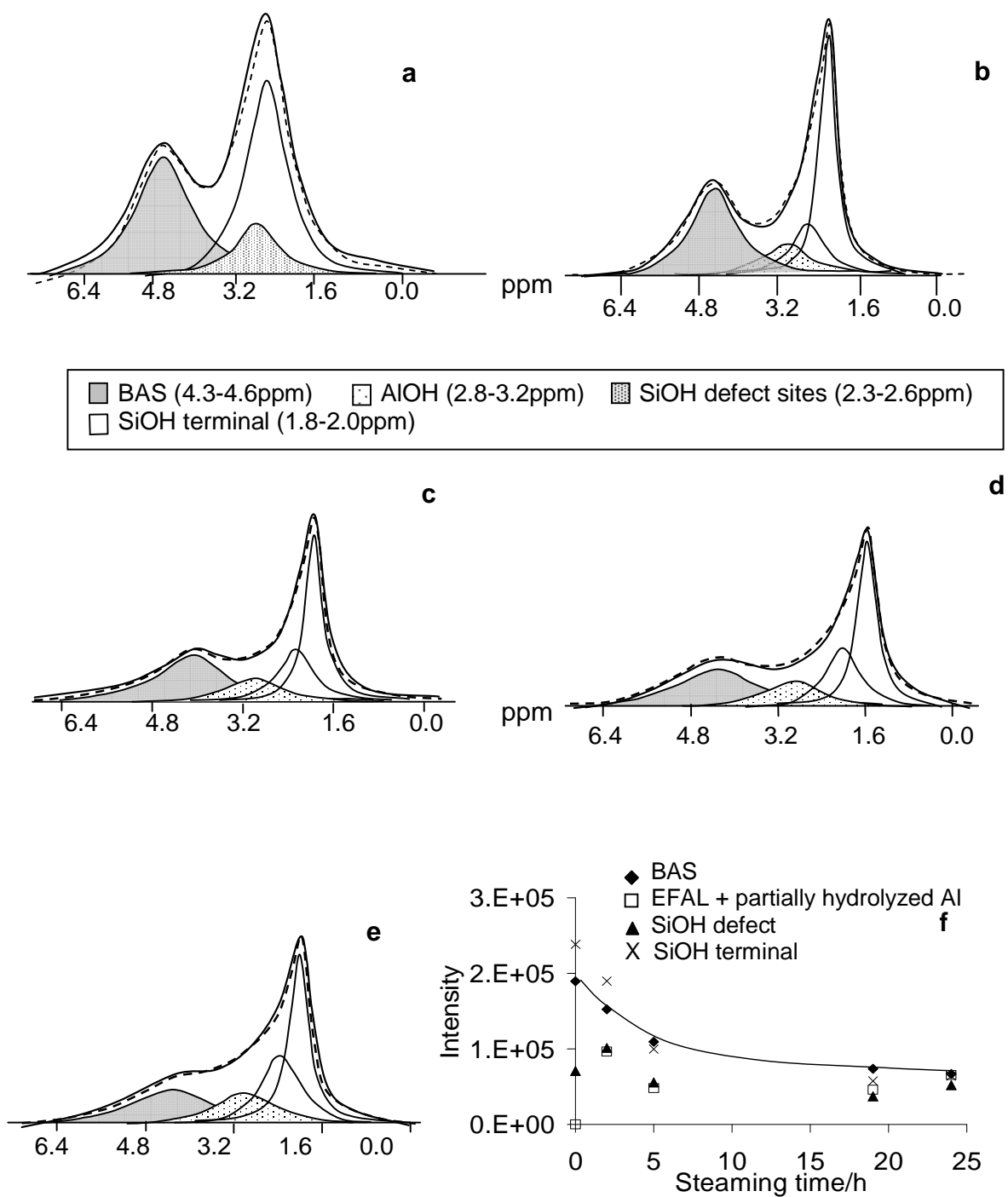
Figure 4.13. Deconvoluted ^{1}H MAS NMR spectrum of HZSM-5 after a) 0, b) 2, c) 5, d) 19 and e) 24 h steaming (solid lines are actual spectra and sketched lines are simulated spectra); f) Change in concentration of different hydroxyl species with steaming time from ^{1}H MAS NMR.

Good agreement was obtained between the Brønsted acid sites quantified from IR spectroscopy and bridging OH group determined from ^{1}H NMR (Figure 4.14).
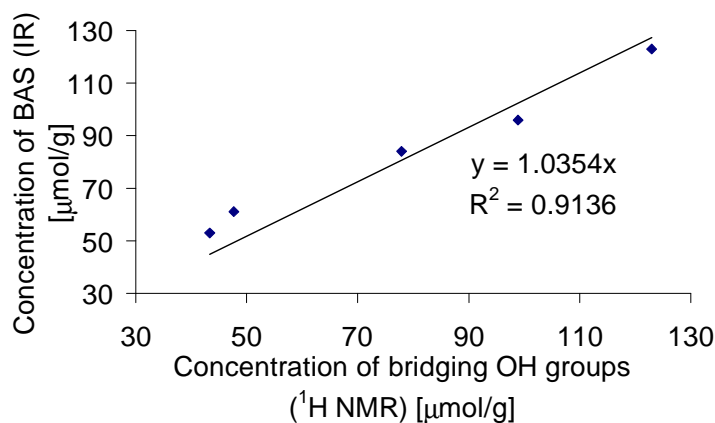
Figure 4.14. Concentration of Brønsted acid sites determined from IR spectroscopy of adsorbed Py vs. concentration of bridging OH groups from ^{1}H NMR.

4.2.5. X-ray diffraction

XRD was measured to determine the influence of steaming duration on the crystallinity of the zeolite. Figure 4.15 shows the XRD pattern of one steamed HZSM-5 sample, whereby spectra of steamed samples were almost indistinguishable. Only a slight loss in intensity of some reflexes was observed as a result of minor structural destruction of the crystallinity. This results in the formation of some amorphous phases in the steamed zeolites. Taking the unsteamed sample as reference, the crystallinity loss after 48 h steaming was calculated to be only 6 %. This shows that the zeolite structural integrity was largely maintained.
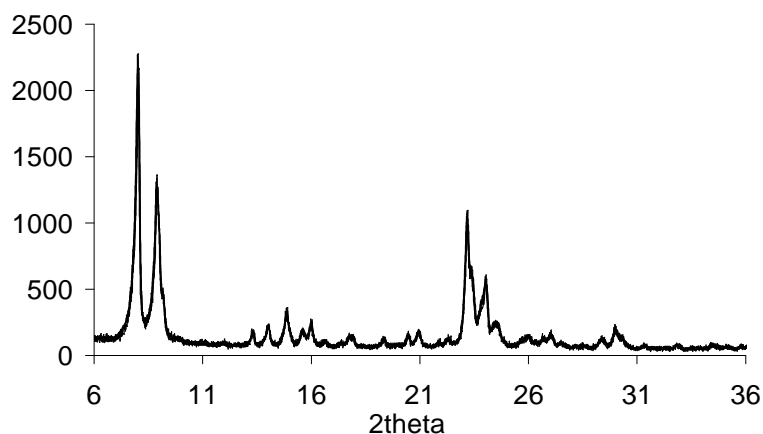
Figure 4.15. XRD patterns of HZSM-5 steamed at 450 ℃ and 101.3 kPa H $_2$O.

4.2.6. Nitrogen physisorption

N $_2$ adsorption measurements were carried out to explore changes in textural properties induced by steaming (Table 4.1). Direct correlation between the variation of specific surface area and steaming conditions was not observed. The micropore volume remained unchanged after steaming for 48 h meaning that extraframework aluminum did not block micropores. The mesopore volume slightly increased upon steaming. This is attributed to partial sintering of the amorphous components holding the primary particles together to small aggregates of secondary particles and eventually the formation of smaller entities, as suggested by TEM measurements (see infra)

Table 4.1. Textural properties of steamed HZSM-5 samples.

Steaming time	BET surface area	Micropore volume	Mesopore volume
[h]	m^2/g	cm^3/g	cm^3/g
0	335	0.15	0.15
2	372	0.15	0.20
19	341	0.15	0.16
48	349	0.16	0.18

4.2.7. Transmission electron microscopy

The effect of steaming on the morphology of the ZSM-5 zeolite was studied by transmission electron microscopy. Figure 4.16 shows an image of the unsteamed sample. The size distribution of the zeolite aggregates is around 250-550 nm.

Figure 4.16: TEM pictures of unsteamed HZSM-5 sample.

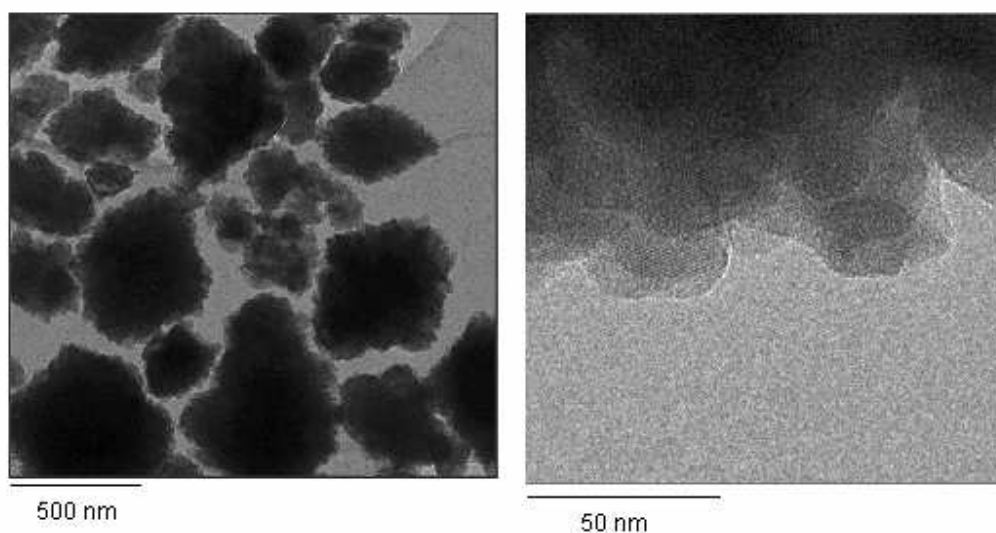Figure 4.17 compiles the TEM images of the powder after 48 h of steaming. The size distribution of the zeolite aggregates decreased from 250-550 nm to 320-400 nm. No obvious formation of mesoporous structure was observed from the TEM images. Only the edges of the steamed zeolite crystals seemed to be less defined compared to the unsteamed HZSM-5.

500 nm · 20 nm
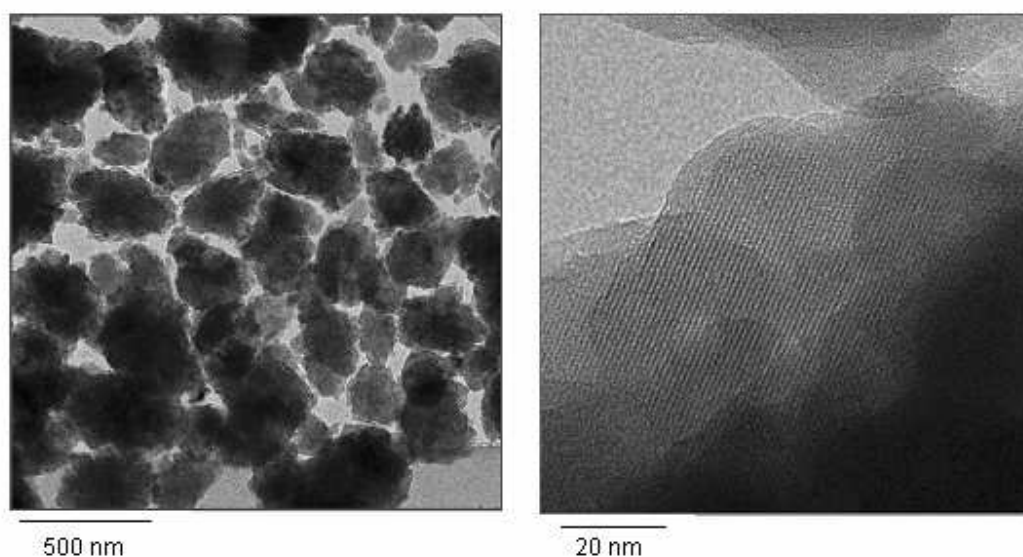
Figure 4.17: TEM pictures of steamed HZSM-5 sample.

4.3.   Discussion

The effect of steaming on the concentration, coordination, location and acidity of aluminum in high silica HZSM-5 was studied by IR and NMR spectroscopy. Mild steaming temperature conditions were applied in order to observe intermediate Al species and to monitor the steps involved in the dealumination process.

Coordination and acidity of aluminum

^{1}H MAS NMR and IR spectra of adsorbed pyridine indicate that only 53 µmol/g of the initial 123 µmol/g bridging OH groups was retained after 24 h steaming, while, on the same sample, 80 µmol/g of tetrahedrally coordinated framework aluminum was detected by ^{27}Al MAS NMR. This means that not all tetrahedral framework aluminum carry Brønsted acid sites in these dealuminated samples.

Two hypotheses can be formulated to account for the difference of 27 µmol/g Al_{tet} that do not lead to Brønsted acidity. First, part of the Al in the framework could be only partially hydrolyzed. These Al species no longer carry Brønsted acid sites with respect to pyridine but maintain tetrahedral coordination upon hydration with water. In the second hypothesis, the acidic hydroxyl group carried by some of the aluminum atoms in the framework could be neutralized by extraframework Al species. Hence, aluminum in

these sites would remain tetracoordinated, but the negative charge would not be balanced by a proton, but by an alumina cluster.

To explore the validity of the first hypothesis, we reviewed the possibility of formation of partially hydrolyzed aluminum in the form of framework Lewis acid sites. These sites were claimed to be formed during the calcination process of zeolites BEA and ZSM-5. The subsequent hydration of these sites generates partially hydrolyzed framework Al [28]. The adsorption of one water molecule on such a framework Lewis site can result in species a (Figure 4.18) which could account for the high proportion of tetra-coordinated Al in the ^{27}Al MAS NMR spectra with respect to the concentration of Brønsted acid sites determined by IR spectroscopy. However, the adsorption of pyridine on tri-coordinated Al should also lead to an increase in the number of Lewis acid sites (species b in Figure 4.18) corresponding to the decrease in Brønsted acid sites detected. As this was not observed, we conclude that the difference in the concentration of tetrahedrally coordinated aluminum and the concentration of Brønsted acid sites cannot be attributed to dehydroxylated aluminum species in the lattice. In addition, partially hydrolyzed aluminum, being connected to the framework by three or less bonds, are highly unstable in the lattice. Thus, such species would be rapidly removed by 24 h of steaming and partially hydrolyzed Al should account for only a small portion of the Al_{tet} not leading to Brønsted acid sites.
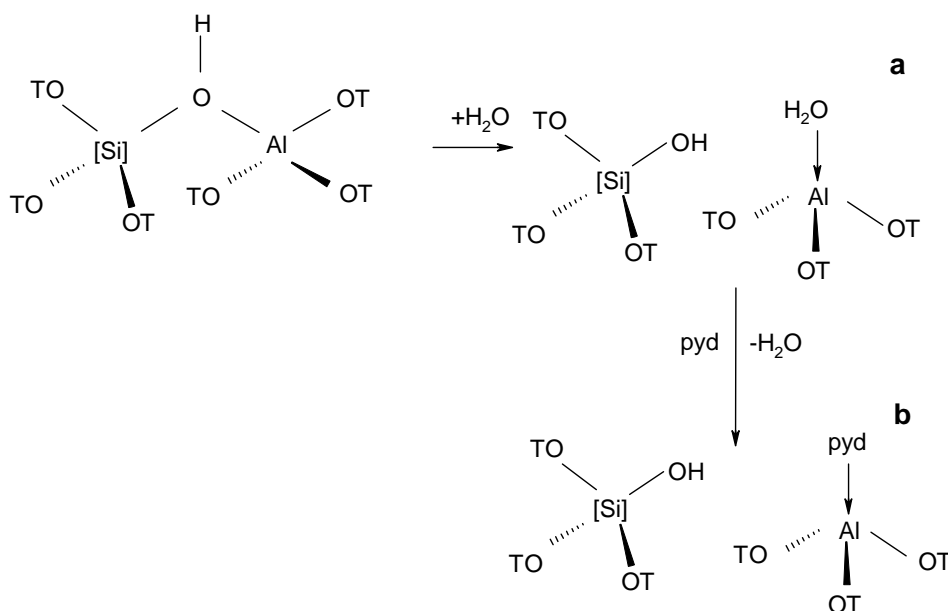
Figure 4.18. Proposed tricoordinated framework Lewis acid sites.

In this context, it should be noted that Jacobs et al. were also unable to experimentally detect tri-coordinated Al in dehydroxylated H-Y zeolite using X-ray fluorescence techniques [29]. In addition, Al K-edge XAS spectra measured at high temperatures clearly indicate that aluminum is mainly in the tetra-coordinated state even at temperatures up to 975 K. The exposure to air or water directly annihilates the tri-coordinated aluminum species, which are observed only in vacuum at temperatures above 675 K [30]. This is supported by the presence of the peak at 3.1 ppm in ^{1}H NMR spectra.

Overall, the combination of MAS NMR and IR spectroscopy allows concluding that tri-coordinated Al and partially hydrolyzed Al, if formed, can exist only as transient species. Such species are hardly present after 24 hours of steaming. Thus, the high proportion of tetra-coordinated Al detected in ^{27}Al MAS NMR is, in part, attributed to extraframework aluminum adopting four-fold coordination (peak IV_3) or to framework Al which do not carry Brønsted acidity due to the neutralization by EFAl species.

Let us now address the location and distribution of the labile aluminum species that are removed in the first 24 h steaming and the influence of these extraframework species on the remaining framework Al in steamed HZSM-5.

Fast dealumination: location and distribution of the labile Al species

In the initial 24 h steaming, ^{27}Al MAS NMR data indicated the preferential removal of Al from the HZSM-5 framework with T-O-T angle around 150°. Thereafter, the removal of the remaining Al populated at both T-O-T angles of 150° and 155° slowed down considerably. Similar results have been reported for steamed zeolite BEA [31].

It is interesting to note that adjacent, next nearest aluminum at tetrahedral positions hydrolyses preferentially and is usually only stabilized by exchanging the proton for a metal cation as observed in H-Beta [32]. Such Al paired sites have been detected in the parent unsteamed material despite its high silica/alumina ratio (see Chapter 2). Thus, it is concluded that Al present in next-nearest neighbor sites contributes mainly to the initial dealumination. Thus, the labile Al (peak IV_1 in ^{27}Al MAS NMR) are located in one of the aluminum atoms in the local Si-Al sequence of [Al-O-(Si-O)$_{1,2}$-Al] [33, 34]. Tentatively, we attribute the existence of such sites to the use of organic templates and the type of starting material in the synthesis process [35, 36, 37]. The formation of Si-O-Al bonds (as measured by the ΔG^orxn of condensation) is much

more favorable than the formation of Si-O-Si bonds [38]. In addition, alumina has an overall higher solubility than silica [39, 40]. Given the higher overall solubility of alumina in basic medium coupled with the more favourable formation of Si-O-Al bonds over Si-O-Si bonds, it is likely that these paired sites or local gradients are incorporated in the crystals during the initial nucleation process in the inner core, while the isolated single tetrahedral aluminum atoms are located near to the pore entrance

Theoretical calculations have shown that for such paired Al sites to be stable, both Al atoms have to be located in the same channel (or ring) in the Al-O-Si-O-Al sequence. The preference of this topological arrangement can be rationalized using the bond order conservation principle. The weaker Al-O bond makes the neighboring bonds relatively stronger [41]. The alternations of the bond weakening and strengthening make the second O-Al stronger which implies an attractive interaction between the neighboring Al (see Figure 4.19).
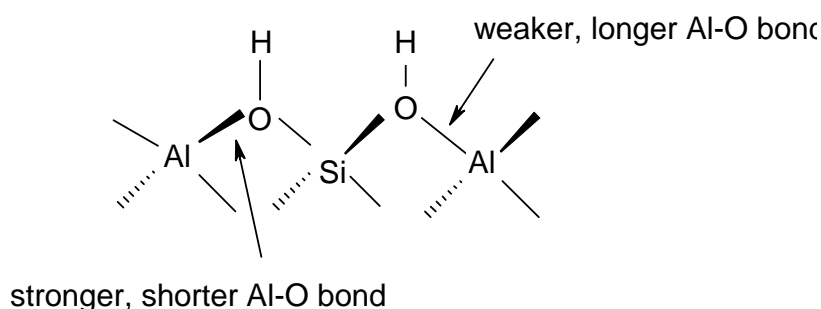
Figure 4.19. Alternation of bond strengthening and weakening at neighboring Brønsted acid sites.

The more pronounced lability of Al with a lower T-O-T angle is somewhat surprising as one would generally assume these species to be more stable against dealumination due to the higher symmetry around the Si-O-Al angel. However, the higher lability can be rationalized by taking into account that the flexibility is reduced for sites with more acute T-O-T angle, for which even protonation is less favorable [42]. Theoretical calculations have indicated the high capacity of larger inter-tetrahedral angle to accommodate geometrical distortion arising from Si $\rightarrow$ Al substitution and protonation. Thus, we propose the flexibility of the larger T-O-T angle, which allows distortion of the Al-O bond especially in terms of the resulting angle strain, without destabilization of the Al in the framework, to be the reason for their higher hydrothermal stability. They can

also accommodate distortions brought about by tetra-coordinated EFAL which helps to stabilize these framework Al against dealumination.

Moreover, the increase in the sp character of the oxygen over sp^2 hybridization of the oxygen with an increase in T-O-T angle could also account for the higher stability of the Al at these locations.

Overall, our results indicate that the dealumination process starts with the breaking of the weakest Al-O bond which occurs at lower T-O-T angle in Al paired sites.

Slow dealumination step: potential influence of extraframework Al

It has been shown that part of the Al located at sites of lower T-O-T angle of 150° is more labile and is removed preferentially. This implies that the remaining Al populated at T-O-T angle of 150° and 155° are more resistant against hydrolysis. As discussed above, this preferential removal of Al at T-O-T angle of 150° is most likely due to the removal of one of the Al at paired sites. The extraframework Al formed during this dealumination step also stabilizes the remaining Al against dealumination. EFAl adopt tetrahedral coordination, while being occluded in the pores.

As discussed above, to account for the difference of 27 µmol/g Al_{tet} that do not lead to Brønsted acid sites in the 24 h steamed sample, we propose that the Brønsted acid sites carried by Al_{tet} that remains in the framework are neutralized by extraframework Al that originated from paired Al sites. Tetra-coordinated EFAL, which gives rise to Peak IV_3 in the Al NMR spectra, has been quantified to correspond to a concentration of 18 µmol/g after 24 h steaming (Figure 4.10c), which is 9 µmol/g less than the difference between framework tetrahedral Al and BAS. Though the partially hydrolyzed aluminum are rather labile species, there still exists the possibility that the unaccounted 9 µmol/g of non acidic framework Al_{tet} is related to such entities.

The more labile Al from paired sites is hydrolyzed preferentially and once removed from the framework, may adopt many forms including cations like Al^{3+}, AlO^+, $Al(OH)_2^+$, $Al(OH)^{2+}$ or neutral forms like $AlO(OH)$, $Al(OH)_3$, $Al(OH)_3.H_2O$ [43-45]. Benco et al. have simulated the largest diameter of the relaxed $Al(OH)_3.H_2O$ to be approximately 0.5 nm, which can still fit within the HZSM-5 pore channels. These extraframework Al particles are most stable, when localized next to a Brønsted acid site [44]. In this process, the zeolite proton is permanently transferred to the basic extraframework aluminum oxide cluster [43]. The proposed mechanism of neutralization

of Brønsted acid sites by EFAl species is visualized in Figure 4.20 where EFAl species are exemplified as $Al(OH)_3$.
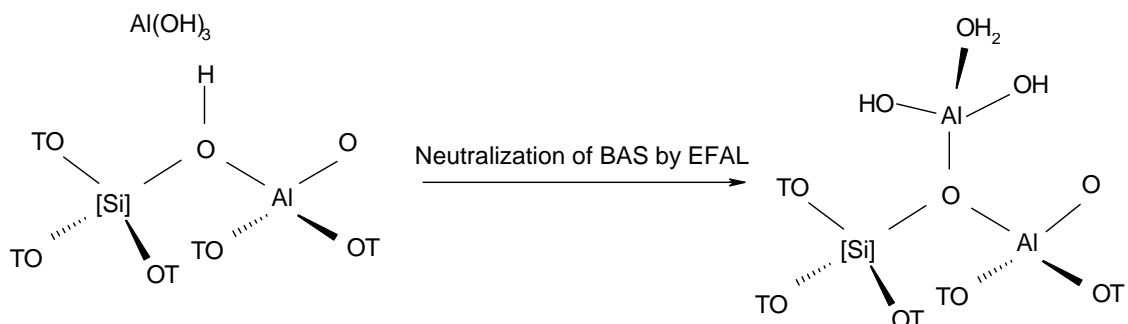
Figure 4.20. Proposed structure for stabilization of framework Al by extraframework species.

DFT calculations have also yield stable minima for cationic extraframework Al species such as $AlO^+/ Al(OH)^{2+}$ when coordinated to two Al in the framework as shown in Figure 4.21. This may also help to account for the addition 9 µmol/g of non acidic Al_{tetra} within the two T-sites as one extraframework Al neutralized two Brønsted acid sites when adopting such coordination.
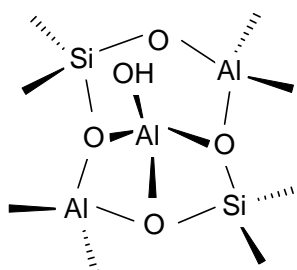
Figure 4.21. Extraframework Al species in the form $Al(OH)^{2+}$ coordinated to two framework Al.

Elementary reaction steps during dealumination

After the speciation of the aluminum atoms and acid sites in the zeolite structure, let us now discuss the sequence of the reaction steps involved in the dealumination process. The scheme is depicted in (Figure 4.22).

Dealumination starts with the breaking of the weakest Al-O bond rather than Si-O bond. This is due to the less electropositive nature of Al compared to Si, resulting in a weaker and longer Al-O bond (1.77-1.89 Å) compared to Si-O (1.67-1.72 Å) [46].

When the weakest Al-O bond is broken, the tri-coordinated Al is immediately coordinated by a water molecule forming an Al-OH group. The additional proton formed from hydrolysis of water attaches to the remaining Al-O-Si but the rapid breaking of the remaining Al-O bonds results in its final state as part of the hydroxyl group attached to Si in the form of Si-OH. This process results in the formation of new hydroxyl groups found in silanol nests (peak at 2.3 ppm in ^{1}H MAS NMR spectrum) and also on partially hydrolyzed framework/extraframework Al (peak at 3.1 ppm in ^{1}H MAS NMR spectrum). These partially hydrolyzed Al groups do not possess Brønsted acidity, because all involved OH groups are terminal hydroxyl groups. For silica-alumina mixed oxides, these are known to have only very weak Brønsted acid strength.

The complete removal of one Al should result in the formation of four Si-OH groups, but the relatively modest increase in silanol nest formation represented by the peak at 2.3 ppm in the ^{1}H MAS NMR spectra, indicates the healing of defect sites. This can occur through the migration of hydrolyzed silicic acid species formed from framework destruction or from the amorphous part of the zeolite to fill the defect sites formed from Al eliminated from the framework. Since XRD points out to an almost unaffected crystallinity even after 24 h steaming, this healing of sites should be mainly attributed to the migration of silicic species from amorphous silica phase of the zeolite left from the synthesis process (Figure 4.23).
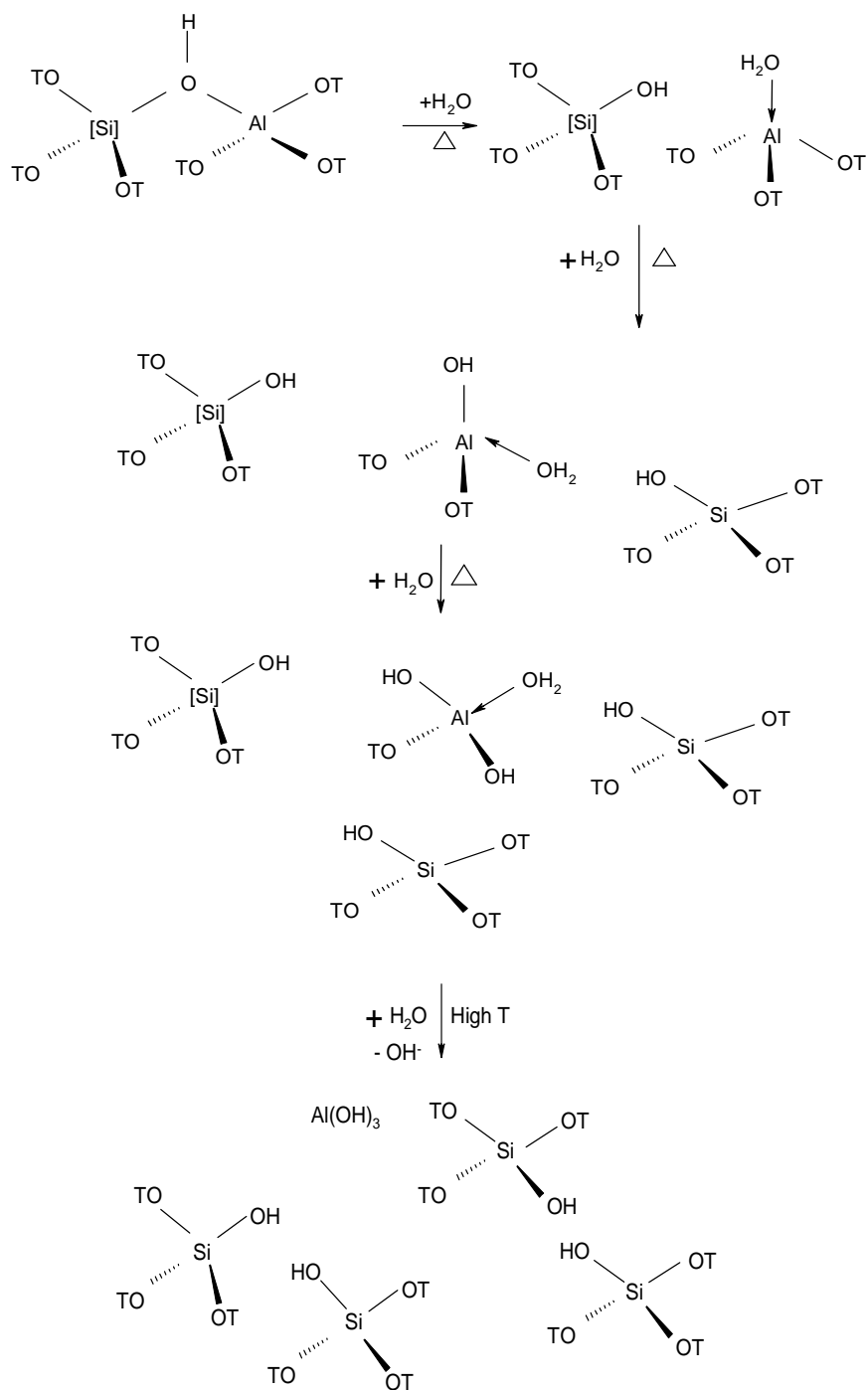
Figure 4.22. Proposed scheme for dealumination of framework Al
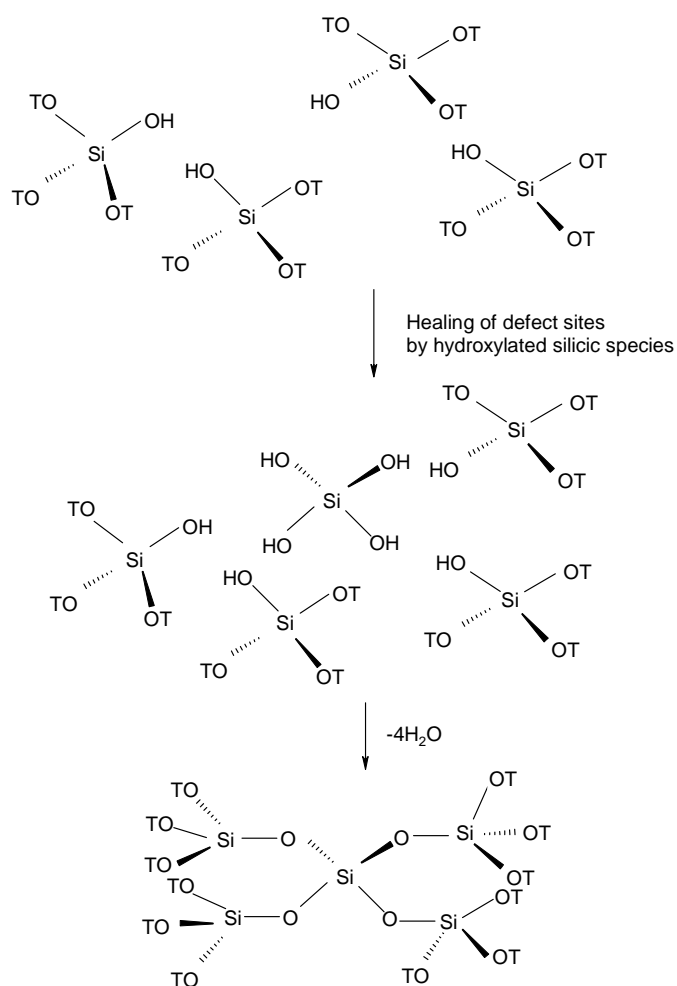
Figure 4.23. Scheme for the healing of defect sites.

The Al speciation during dealumination of the HZSM-5 framework is shown in Figure 4.24. The proposed structures of the different Al species are represented in Table 4.2.
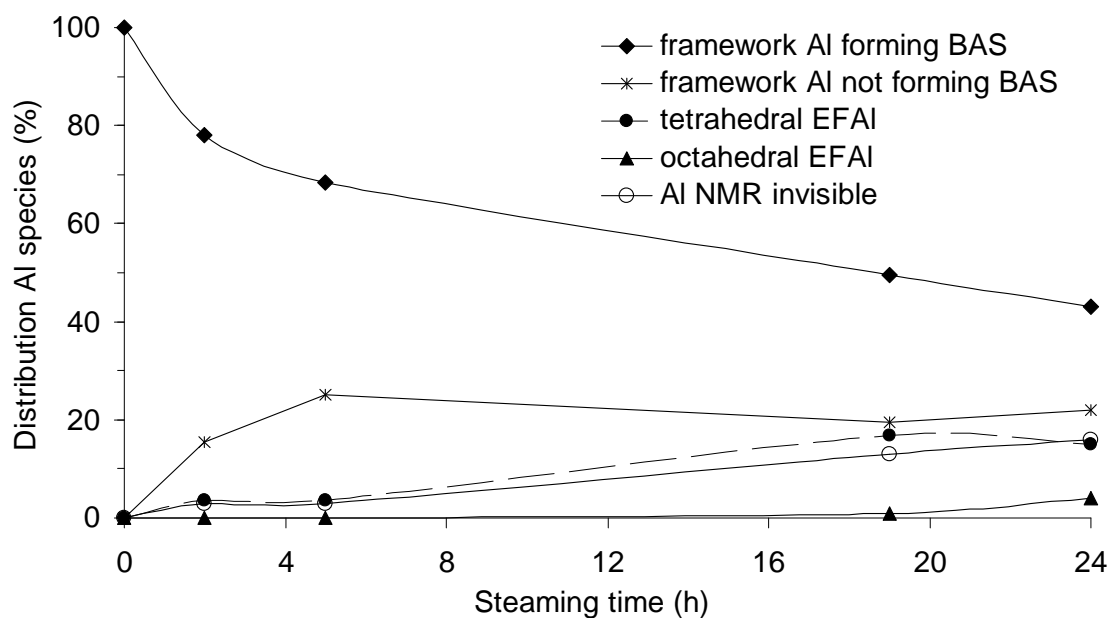
Figure 4.24. Graphical representation of the distribution of Al species during dealumination of the HZSM-5 framework. "Framework Al forming BAS" was obtained from IR spectroscopy of adsorbed Py; "framework Al not forming BAS" was calculated as difference of framework tetrahedral Al (sum of peak IV_1 and peak IV_2 in Al NMR spectra) and "framework Al imparting BAS"; "tetrahedral EFAl" corresponds to peak IV_3 in Al NMR spectra; "octahedral EFAL" was calculated from Al NMR spectra; "Al NMR invisible" was obtained as difference between the total amount of Al in the parent material and the sum of all above mentioned Al species.

Table 4.2. Proposed structures for intermediate and final Al species in the sequential dealumination of HZSM-5

Al species (chemical shifts in ^{27}Al MAS NMR spectra)	Proposed structure of Al species
Acidic Al in tetrahedral coordination (80-40ppm)	
Partially hydrolyzed Al species (NMR visible)	
Neutralized sites (single neighboring BAS) (60.5 $\pm$ 0.5 ppm - tetracoordinated EFAL)	
Neutralized Al at high density pockets (NMR visible) (60.5 $\pm$ 0.5 ppm - tetracoordinated EFAL)	
Dealuminated Al from paired sites[1]	Al^{3+}, AlO^+, $Al(OH)_2^+$, $Al(OH)^{2+}$, $AlO(OH)$, $Al(OH)_3$, $Al(OH)_3.H_2O$
Partially hydrolyzed Al species (nmr invisible)[2]	Probably in the form of highly distorted Al attached to the framework with less than 3 bonds with highly elongated Al-O bonds
Octahedral Al species (10ppm to -5ppm)	

[1]As proposed in refs. [43-45]
[2]Deduced from the large quadrupolar coupling constant of these species which made them NMR invisible. Such species is in a much distorted environment with highly non-symmetric coordination.

4.4. Conclusions

The mild steaming of high silica SAMPLE C at 450 ℃ has been performed at different durations and transient/extraframework Al species were observed, giving rise to Al-OH groups at 3.1 ppm in ^{1}H MAS NMR spectra and also contributing to the broad peak from 3726 to 3630 cm^{-1} in the IR spectra. The removal of partially hydrolyzed transient Al species is very rapid due to the non stabilized location in the framework. The labile Al originated from local gradients or paired Al sites situated at T-sites with lower T-O-T angle. This facilitates the neutralization of neighboring Brønsted acid sites, resulting in the rapid loss of Brønsted acidity in the first 24 h.

Once the unstable Al from paired sites is removed and exchanged onto the nearby Brønsted acid sites, the hydrolysis of the remaining Al in the framework becomes very slow. This is a direct consequence of the greater structural stability mainly contributed by Al located at larger T-O-T angle of around 155° in the lattice and the stabilization effect against dealumination of the remaining framework Al by the extraframework Al. The tetra-coordinated extraframework Al and the remaining framework Al in the lattice (both neutralized and non-neutralized) account for the high concentration of Al in the 80-40 ppm chemical shift range as detected in ^{27}Al MAS NMR.

Because paired Al sites (eventually induced by strong zoning) in the HZSM-5 are responsible for the rapid loss of Brønsted acidity, it is important to minimize the formation of such paired sites, when the zeolite is used in the presence of water. This will ensure the high activity of the catalysts with respect to reactions catalyzed by Brønsted acid sites under severe operating conditions.

4.5 References

1. Guisnet, M., Wang, Q. L. and Giannetto, G., Catal. Lett., **1990**, 4, 4-6, 299-302.
2. Sano, T., Ikeya, H., Kasuno, T., Wang, Z. B., Kawakami, Y. and Soga, K., Zeolites, **1997**, 19, 1, 80-86.
3. Sano, T., Yamashita, N., Iwami, Y., Takeda, K. and Kawakami, Y., Zeolites, **1996**, 16, 4, 258-264.
4. Suzuki, K., Sano, T., Kiyozumi, Y., Hagiwara, H., Shin, S. and Takaya, H., Nippon Kagaku Kaishi, **1989**, 11, 1818-1823.
5. Gilson, J. P., Edwards, G. C., Peters, A. W., Rajagopalan, K., Wormsbecher, R. F., Roberie, T. G. and Shatlock, M. P., J. Chem. Soc., Chem. Commun., **1987**, 2, 91-92.

6.   Samoson, A., Lippmaa, E., Engelhardt, G., Lohse, U. and Jerschkewitz, H. G., Chem. Phys. Lett., **1987**, 134, 6, 589-592.

7.   L. Yingcai, J.M., S. Yaojun, W. Tailiu, W. Liping and F. Lun, J. Chem. Soc., Faraday Trans. 1, **1996**, 92, 1647.

8.   Wouters, B.H., Chen, T. H. and Grobet, P. J., J. Phys. Chem. B, **2001**, 105, 6, 1135-1139.

9.   Chen, T.H., Wouters, B. H. and Grobet, P. J., Eur. J. Inorg. Chem., **2000**, 2, 281-285.

10.   Wouters, B.H., Chen, T. H. and Grobet, P. J., J. Am. Chem. Soc., **1998**, 120, 44, 11419-11425.

11.   Wang, Q.L., Giannetto, G., Torrealba, M., Perot, G., Kappenstein, C. and Guisnet, M., J. Catal., **1991**, 130, 2, 459-470.

12.   Emeis, C.A., J. Catal., **1993**, 141, 2, 347-354.

13.   Amoureux, J.P., Fernandez, C. and Steuernagel, S., J. Magn. Reson. Ser. A, **1996**, 123, 116.

14.   Ernst, R., Bodenhausen, G. and Wokaun, A., Principles of Nuclear Magnetic Resonance in One and Two Dimensions, **1987**, New York: Oxford University Press.

.15.   Massiot, D., Fayon, F., Capron, M., King, I., Le Calve, S., Alonso, B., Durand, J. O., Bujoli, B., Gan, Z. H. and Hoatson, G., Magn. Reson. Chem., **2002**, 40, 1, 70-76.

16.   Loeffler, E., Peuker, CH. and Jerschkewitz, H.G., Catal. Today, **1988**, 3, 415-420.

17.   Jacobs, P. A. and Uytterhoeven, J. B., J. Chem. Soc., Faraday Trans. I, **1973**, 69, 2, 373-386.

18.   Zholobenko, V.L., Kustov, L. M., Borovkov, V. Y. and Kazansky, V. B., Zeolites, **1988**, 8, 3, 175-178.

19.   Lercher, J.A., Ritter, G. and Vinek, H., J. Colloid Interface Sci., **1985**, 106, 1, 215-221.

20.   Müller, D., Gessner, W., Behrens, H. J. and Scheler, G., Chem. Phys. Lett., **1981**, 79, 1, 59-62.

21.   Alemany, L.B., Appl. Magn. Reson., **1993**, 4, 1-2, 179-201.

22.   Sarv, P., Fernandez, C., Amoureux, J. P. and Keskinen, K., J. Phys. Chem., **1996**, 100, 50, 19223-19226.

23.   Kentgens, A. P. M., Geoderma, **1997**, 80, 3-4, 271-306.

24.   Lippmaa, E., Samoson, A. and Magi, M., J. Am. Chem. Soc., **1986**, 108, 8, 1730-1735.

25.   Thomas, J. M., Klinowski, J., Ramdas, S., Hunter, B. K. and Tennakoon, D. T. B., Chem. Phys. Lett., **1983**, 102, 2-3, 158-162.

26.   Hunger, M., Freude, D., Frohlich, T., Pfeifer, H. and Schwieger, W., Zeolites, **1987**, 7, 2, 108-110.

27.   Hunger, M., Solid State Nucl. Magn. Reson., **1996**, 6, 1, 1-29.

28.   Woolery, G.L., Kuehl, G. H., Timken, H. C., Chester, A. W. and Vartuli, J. C., Zeolites, **1997**, 19, 4, 288-296.

29.   Jacobs, P. A. and Hermann K. B., J. Phys. Chem., **1979**, 83, 9, 1174-1177.

30.   van Bokhoven, J.A., van der Eerden, A. M. J. and Koningsberger, D. C., J. Am. Chem. Soc., **2003**, 125, 24, 7435-7442.

31.   van Bokhoven, J.A., Koningsberger, D.C., Kunkeler, P., van Bekkum, H., and Kentgens, A. P. M., J. Am. Chem. Soc., **2000**, 122, 51, 12842-12847.

32.   Penzien, J., Abraham, A., van Bokhoven, J. A., Jentys, A., Müller, T., Sievers, C. and Lercher, J.A., J. Phys. Chem. B, **2004**, 108, 4116-4126.

33.   Dědeček, J., Kaucký, D. and Wichterlová, B., Chem. Comm., **2001**, 11, 970-971.

34.   Kaucký, D., Dědeček, J. I. and Wichterlová, B., Microporous Mesoporous Mater., **1999**, 31, 1-2, 75-87.

35.   Corma, A., Melo, F. V. and Rawlence, D., Zeolites, **1992**, 12, 3, 261-264.

36.   Corma, A., Melo, F. V. and Rawlence, D. J., Zeolites, **1990**, 10, 7, 690-694.

37.   Sklenak, S., Dědeček, J., Li, C., Wichterlová, B., Gábová, V., Sierka, M., and Sauer, J., Angew. Chem. Int. Ed., **2007**, 46, 7286 –7289

38.   Fedeyko, J.M., Egolf-Fox, H., Fickel, D.W., Vlachos, D.G., and Lobo, R.F., Langmuir, **2007**, 23, 8, 4532-4540.

39.   Dezelic, N., Bilinski, H., Wolf, R. H. H., J. Inorg. Nucl. Chem. **1971**, 33, 791-798.

40.   Iler, R. K. The Chemistry of Silica: Solubility, Polymerization, Colloid and Surface Properties and Biochemistry, **1979**, New York:Wiley, 866.

41.   Barbosa, L.A.M.M., van Santen, R.A., and Hafner, J., J. Am. Chem. Soc., **2001**, 123, 19, 4530-4540.

42.   Demuth, T., Hafner, J., Benco, L., and Toulhoat, H., J. Phys. Chem. B, **2000**, 104, 19, 4593-4607.

43.   Benco, L., Demuth, T., Hafner, J., Hutschka, F., and Toulhoat, H., J. Catal., **2002**, 209, 2, 480-488.

44.   Bhering, D.L., Ramirez-Solis, A. and Mota, C. J. A., J. Phys. Chem. B, **2003**, 107, 18, 4342-4347.

45.   Scherzer, J., Catalytic Materials: relationship Between Structure and Activity. A.C.S. Symp. Ser. 248, ed. White, T. E., Della Betta, R.A., Derouane, E. G., Baker, R.T.K., **1984**, Washington, D. C: American Chemical Society, 157.

46.   Redondo, A. and Hay, P.J., J. Phys. Chem., **1993**, 97, 45, 11754-11761.

Chapter 5

Impact of steaming conditions on the acidity of parent and formed HZSM-5

Abstract

The effect of water partial pressure and steaming temperature on the concentration of Brønsted acid sites of powder and extrudate HZSM-5 (SAMPLE C and EXT C, respectively) was investigated. The marked initial decrease in concentration of Brønsted acid sites during steaming of HZSM-5 extrudates is attributed to the rapid removal of intercrystalline acid sites formed during the extrusion process. The rate of decrease had a reaction order of two with respect to Brønsted acid site concentration for parent and formed HZSM-5 and indicates the higher lability of aluminum at paired sites. [27]Al MQMAS shows that those Al are located at sites with relatively low T-O-T angles of around 150°. Embedding the zeolite crystals into a matrix leads to higher hydrothermal stability. The segregation of vacancies/defect sites formed in the steamed HZSM-5 to the surface of the zeolitic crystals is concluded to be followed by the realumination of these vacancies by hydroxylated Al species from the binder.

5.0. Introduction

HZSM-5 is a highly important catalyst in a number of commercial processes because of its shape selective properties and its high resistance to deactivation by coke deposition [1]. The latter property has been related to the absence of large cavities in the pore structure and low concentration of acid sites [2-4].

Industrial processes use water co-feeds to further limit coking [5-7], control the exothermicity of the reaction, and reduce the partial pressure of the reactant. Hence, the influence of steaming conditions on the properties of the zeolites is particularly interesting. It is known that steaming leads to the dealumination of the zeolite structure and, therefore, to the decrease in Brønsted acid site (BAS) concentrations. However, if the zeolitic catalyst is pretreated under optimized steaming conditions, the resulting material can show higher stability under reaction conditions. In fact, the careful control of the hydrothermal conditions can lead to fine tuning of the concentration of framework aluminum, of the strength and distribution of Brønsted and Lewis acid sites (LAS), and of the sorption capacity [8-12]. It has been reported that rates of alkane cracking [13] and isomerization [14, 15] were often greatly enhanced after steaming treatment.

Temperature, duration and water partial pressure are the most important parameters affecting the modification of the zeolite during hydrothermal treatment. Hence, the systematic investigation and understanding of the effects of these three factors on the zeolite properties is needed for a knowledge based development of an appropriate methodology to produce thermally stable zeolites for specific catalytic applications. In consequence, the current manuscript addresses the changes in powder and formed (bound with 20 wt% alumina binder) zeolite HZSM-5 (SAMPLE C and EXT C, respectively) in two sections

In the first part, the kinetics of the change in BAS concentration under hydrothermal conditions of HZSM-5 in the pure powder form and extrudate form is investigated. In this respect, it is useful to mention that some authors have observed an influence of the binder under steaming conditions for processes such as fluid catalytic cracking [16, 17]. Hence, it is important to compare the behavior of the zeolite in powder and extrudate form before one can infer the physicochemical properties of the steamed extrudate from the corresponding steamed HZSM-5. The second part deals with the effect of the steaming temperature on the acid sites concentration of extrudate and powder.

5.1. Experimental

5.1.1. Preparation of samples and apparatus used for hydrothermal treatment

The parent HZSM-5 was synthesized according to the procedure described in Chapter 2, section 2.2.1. The extrudate counterparts are synthesized according to Chapter 3, section 3.1.1. For the first part of this work, the samples were steamed according to the procedure described in Chapter 4 to derive rate expressions on the change in BAS concentration with steaming time.

For the second part of this work, steaming treatments at different temperatures were performed in the setup represented in Figure 5.1.
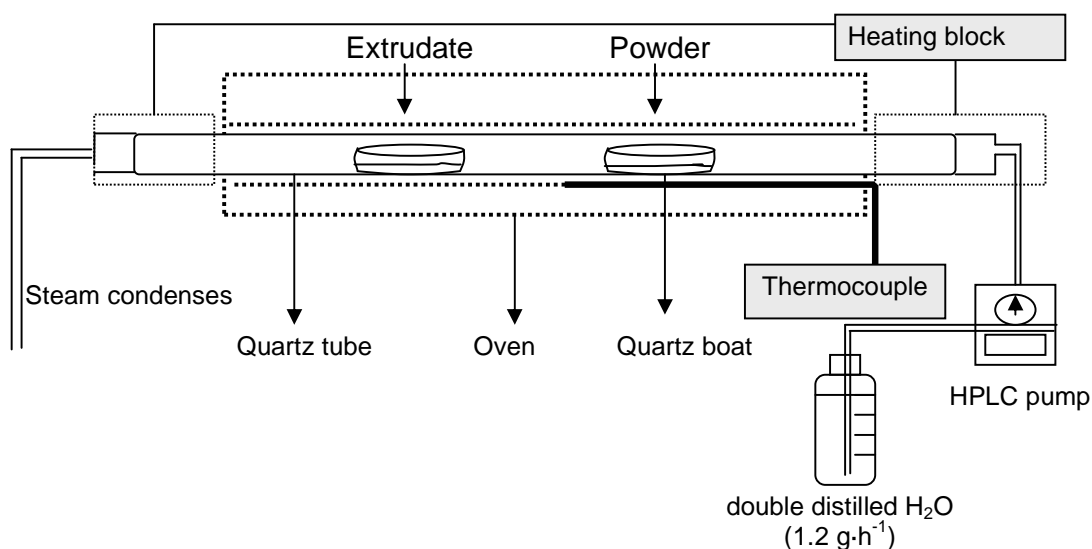
Figure 5.1. Setup for the variation of steaming temperature and duration.

Powder and extrudate samples (1 g each) were put into two quartz boats positioned in a quartz tube inside a horizontal oven. Water was pumped into the system with a *Gilson 307* HPLC pump at a constant flow rate of 1.2 g/h. To prevent condensation of water vapour at the outlet of the reactor, this area was heated to 150 °C. This steaming procedure was carried out at five different temperatures (450, 480, 530, 580 and 630 °C) for three different durations (24, 48 and 72 h).

5.1.2. IR spectroscopy of adsorbed pyridine

IR spectra were measured with a *Perkin Elmer 2000* spectrometer. All spectra were recorded in the region between 4000 and 800 cm^{-1} at a resolution of 2 cm^{-1}. The background spectrum was subtracted from all spectra.

For IR spectroscopy the samples were pressed into self-supporting wafers (density 13-25 mg/cm^2). After activation in vacuum (10^{-6} mbar) for 1 h at 450 °C (heating rate 10 °C/min), the sample was cooled to 150 °C an d pyridine was adsorbed in small doses until complete disappearance of the bridging OH group at 3606 cm^{-1}. The system was then equilibrated for 0.5 h. IR spectra were recorded at 150 °C before adsorption of pyridine, during the adsorption of pyridine and after outgassing (10^{-6} mbar) at temperature of 250, 350 and 450 °C. The concentrati ons of BAS and LAS were estimated from the areas of the bands at 1565 – 1515 cm^{-1} and 1470 – 1435 cm^{-1}, by applying Eq. 5.1. and 5.2. modified from reference [18]:

$$c(BAS) = 4.32 \cdot 1000 \cdot r^2 \cdot \frac{IA(1565 - 1515 cm^{-1})}{m} \qquad \text{Eq. 5.1.}$$

$$c(LAS) = 3.27 \cdot 1000 \cdot r^2 \cdot \frac{IA(1470 - 1435 cm^{-1})}{m} \qquad \text{Eq. 5.2.}$$

where:

c = concentration of acid sites [μmol/g]

IA = integral of the respective peak [cm^{-1}]

r = radius of the wafer [cm]

m = mass of the wafer [mg]

5.1.3. MAS NMR measurements

MAS NMR spectroscopy measurements of the zeolites were carried out using a *Bruker Avance AMX-500* NMR-spectrometer with a magnetic field of 11.75 T. The samples were packed in 4 mm ZrO$_2$ rotors and spun at 15 kHz.

For ^{27}Al MAS and MQMAS NMR measurements, the samples were hydrated for at least 48 h. The reference for the measurements was Al(NO$_3$)$_3$·9 H$_2$O (δ = -0.543 ppm). An excitation pulse with power level of 7 dB and a length of 0.6 μs was applied for the 1D spectrum. The relaxation time was 250 ms. For all 1D spectra, 2400 scans were recorded. MQMAS spectra were recorded with a three pulse sequence. The power level

was 7 dB for the first two pulses and 35 dB for the last one. The pulse lengths were $p_1 = 8$ μs, $p_2 = 3.2$ μs and $p_3 = 52$ μs. The evolution time t_1 was incremented in intervals of 1 μs and data were processed with Bruker Topspin. For quantification of the ^{27}Al MAS NMR spectra, the chemical shift and the quadrupolar coupling constant (QCC) were obtained from the MQMAS spectrum and used to deconvolute the 1D spectra using the program dmWinfit2001 developed by Massiot [19].

5.1.4. X-ray diffraction

X-ray powder diffraction patterns of powder and extrudates were measured using a *Philips X'Pert Pro System* operating with a CuKα1-radiation (0.154056 nm) at 40 kV / 40 mA. Measurements were performed on a spinner with a 1/4'' slit from 5° to 50°, 2 θ (0.05°/min)..

The relative crystallinity of the steamed samples was determined by measuring the intensity of the diffraction signal of the (051) peak and comparing it to that of the reference unsteamed sample.

5.1.5. Nitrogen physisorption

Surface area, pore volume and pore size distributions of the materials were obtained by nitrogen adsorption on a *PMI* automated BET sorptometer. *Brunauer, Emmet* and *Teller* (BET), *Barrett, Joyner* and *Halenda* (BJH; desorption branch), and t-plot methods were used for calculating specific surface area and meso- and micro-pore volume. Before adsorption, the sample (100 mg) was activated in vacuum at 400 °C for 2 h. After activation, the weight of the dried sample was determined. Finally, the sample was cooled to –196 °C and liquid nitrogen was adsorbed at increasing partial pressures.

5.2.   Results

5.2.1.   Kinetic studies on the effect of the water partial pressure on the BAS concentration of powder and extrudate HZSM-5

Figure 5.2 shows the IR spectra of activated powder HZSM-5 after different steaming durations at 450 °C and water partial pres sure of 67.5 kPa. As a reference, the spectrum of the corresponding unsteamed sample is also shown.

Bridging hydroxyl groups give rise to a band at 3606 cm^{-1}. Visually, there appeared to be no evident relationship between the steaming duration and the intensity of the 3606 cm^{-1} band associated to bridging hydroxyl groups. This is due to varying baselines in the different steamed HZSM-5. Integration using a straight baseline of the bridging OH groups from 3642 to 3565 cm^{-1} indicates an initial continuous decrease in intensity of the bridging hydroxyl band with steaming duration, while the intensity hardly changed beyond 24 h steaming time. Quantification of the bridging hydroxyl groups was not carried out as their molar extinction coefficient was not determined.
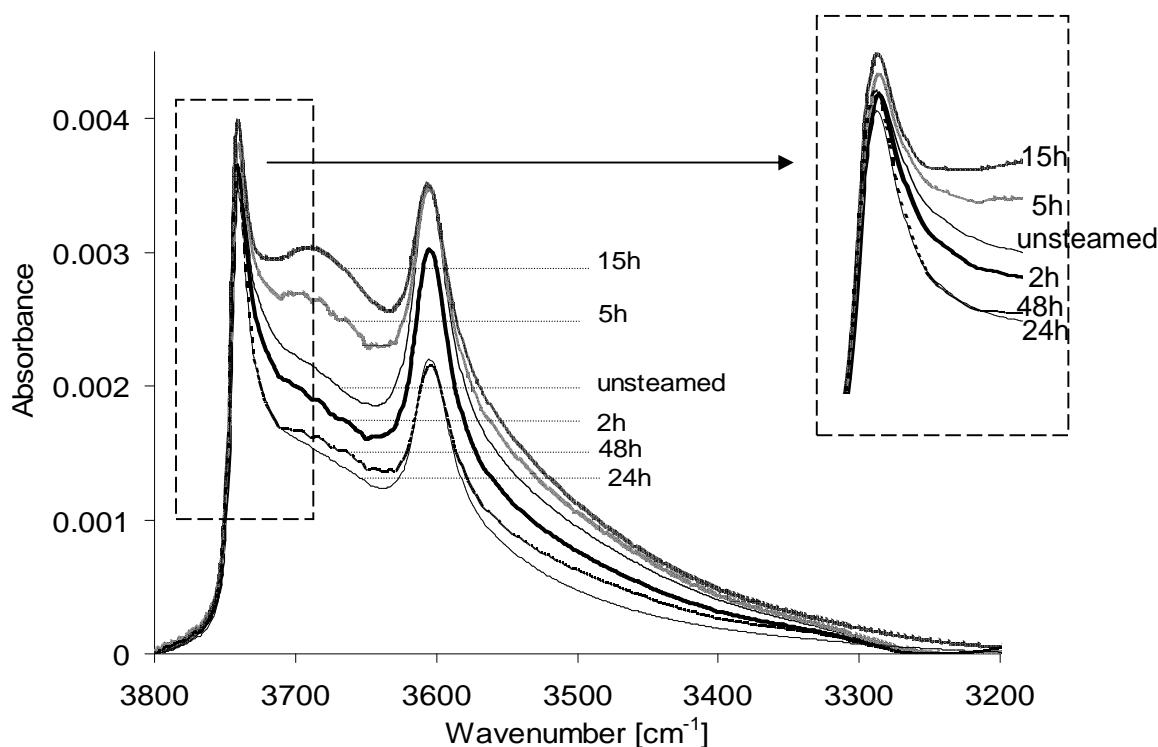
Figure 5.2. IR spectra of activated powder HZSM-5 as a function of steaming duration (450 °C, p (H$_2$O) = 67.5 kPa).

The broad band between 3706 and 3642 cm^{-1} developed upon 5 to 15 h steaming and is attributed to the AlOH group of partially hydrolyzed aluminum in the framework and/or to extraframework aluminum [20, 21]. This band was not clearly observable for steaming time exceeding 15 h and was absent in the IR spectrum of the unsteamed activated powder HZSM-5.

The band at 3743 cm^{-1} is attributed to terminal SiOH groups. The width at half height of this band narrowed after 24 h steaming. This is tentatively attributed to freeing of the terminal silanol groups from hydrogen bonding interaction with silanol groups at defect sites or with hydroxyl groups present on extraframework Al or transient Al species.

Figure 5.3 shows the IR spectra of activated extrudate HZSM-5 steamed for different durations at 450 °C and 67.5 kPa water partial pressure. As observed for the powder sample, the intensity of the band at 3606 cm^{-1} decreased with increasing steaming time. The band at 3743 cm^{-1}, which is attributed to terminal SiOH, became sharper with steaming time, which is attributed to the reduction of the interaction between the terminal SiOH groups and the alumina binder upon steaming.

The shoulder at 3725 cm^{-1} was observed in the IR spectrum of every steamed extrudate HZSM-5. This band (also present in the IR spectrum of the unsteamed extrudate) is attributed to hydrogen bonding interaction between OH groups, with the so called silanol nests in the steamed materials. The intensity of this shoulder reached its maximum at 2 h steaming time. Then, it decreased gradually with a concomitant increase in the intensity of the terminal silanol group, and finally stabilized at 15 h steaming time. This indicates that at first silanol nests are formed, as alumina is eliminated from the tetrahedral position. With increasing steaming duration a significant fraction of these hydroxy groups condensed.

The broad band between 3706 and 3642 cm^{-1} is due to the AlOH groups of the alumina binder and extraframework species [22]. Due to the severe overlapping of bands, it is difficult to comment on the effect of steaming duration on the intensity of each contributing species.
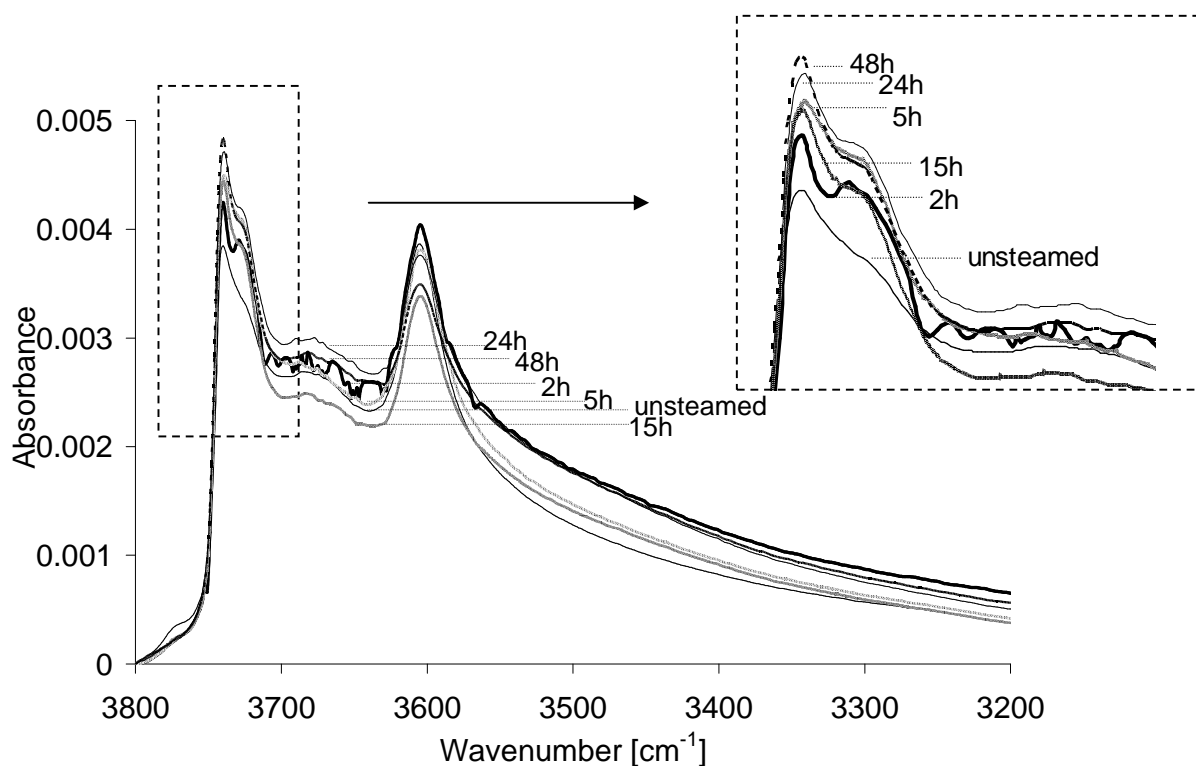
Figure 5.3. IR spectra of activated extrudate HZSM-5 as a function of steaming duration (at 450 °C, p (H$_2$O) = 67.5 kPa).

The concentration of Brønsted and Lewis acid sites was quantified by IR spectroscopy of adsorbed pyridine. Figure 5.4a shows a series of subtracted spectra of powder samples steamed for different durations at 450 °C and 67.5 kPa water partial pressure. The spectrum of the unsteamed sample is also shown as a reference. The spectrum of the activated sample was always subtracted from the spectrum with adsorbed pyridine.
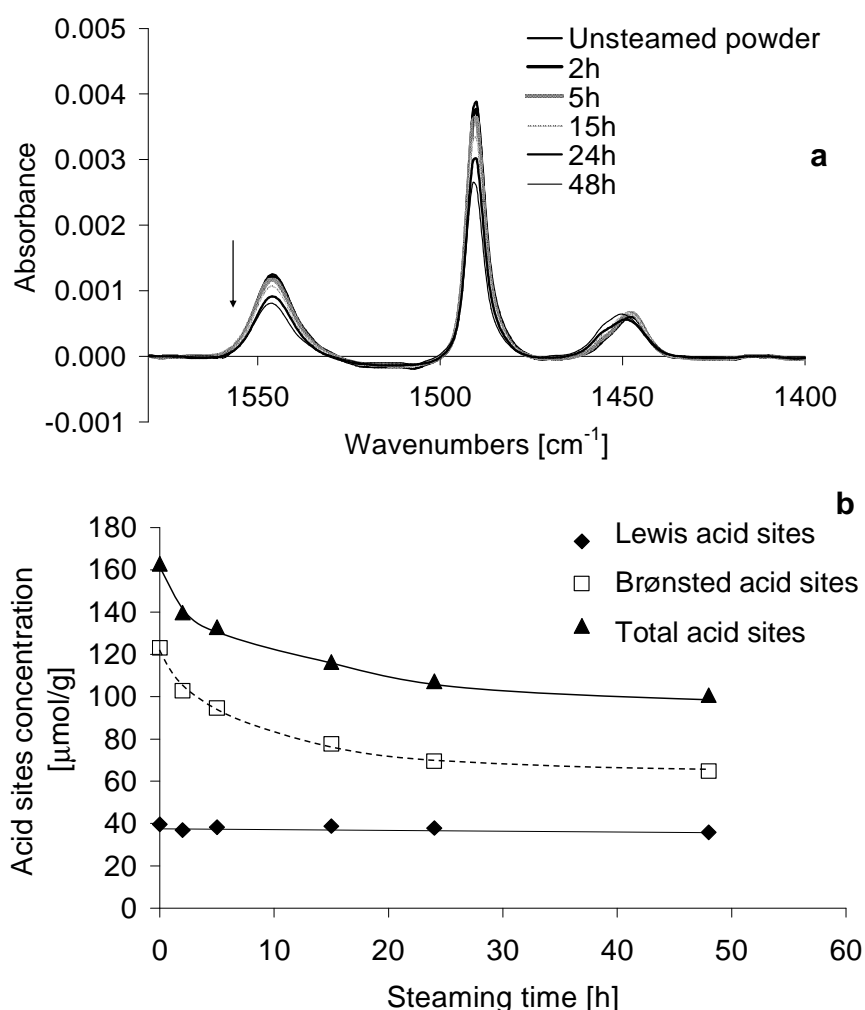
Figure 5.4. a) Difference IR spectra of pyridine adsorbed on steamed powder HZSM-5 and b) Concentration of acid sites in steamed powder HZSM-5 (T = 450 ℃, p (H₂O) = 67.5 kPa).

The BAS band at 1545 cm^{-1} decreased with steaming duration as indicated by the arrow (Figure 5.4a). The LAS band remained approximately constant, but the position was shifted from an initial value of 1447 cm^{-1} to 1455 cm^{-1} after 48 h of steaming. This shift is most likely due to the overlapping of bands corresponding to pyridine adsorbed on cationic impurities (1447 cm^{-1}) and on extraframework aluminium species (1455 cm^{-1}) [23].

The effect of steaming duration under 67.5 kPa steam partial pressure on the concentration of BAS and LAS is quantitatively summarized in Figure 5.4b. Similar trends were also observed for the other two series of powder samples steamed at water partial pressures of 101.3 kPa and 50.7 kPa. The decrease in BAS concentration is attributed to the increasing degree of dealumination with prolonged steaming treatment. We have shown in Chapter 4 that the complete removal of 1 framework Al (termed as dealumination) may result in the loss of more than one BAS. Therefore, the rate of dealumination and the rate of decrease of BAS are not numerically equivalent. However, we monitor the change in BAS concentration under hydrothermal conditions because of its importance for catalytic reactions.

Figure 5.5 shows the BAS concentration versus steaming time as a function of the three water partial pressures used for the powder sample. The rates of decrease of BAS are given by the slopes of these curves. The decrease in BAS seems to occur in two steps whereby the fast step occurs at steaming times below 24 h, and the slow step after 24 h. It has been discussed in Chapter 4 that the rapid dealumination within the first 24 h is due to the preferential removal of Al located at lower T-O-T angle. These Al are probably positioned at local gradients in the HZSM-5 crystals or as ´aluminum pairs´ with local Si-O-Al sequences of $[Al-O-(Si-O)_{1,2}-Al]$ [24, 25]. The hydrolysis of the remaining more stable Al required harsher steaming conditions to hydrolyze the Al-O bond.
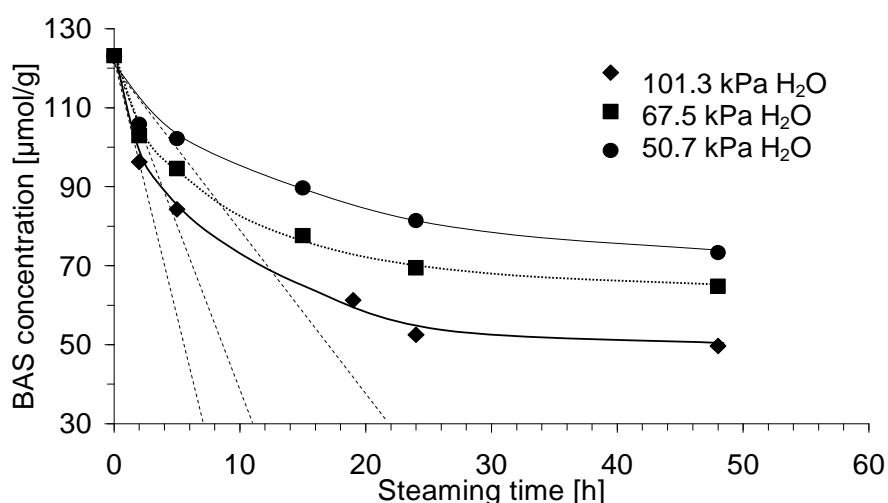

Figure 5.5. Determination of the initial rate of decrease of BAS of powder HZSM-5 steamed at 450 °C.

The initial rate was considered for our kinetic studies (Table 5.1).

Table 5.1. Initial rate of decrease of BAS of powder HZSM-5 at different water partial pressures.

Water partial pressure	Initial rate of decrease of BAS concentration
[kPa]	[µmol/g/h]
101.3	18
67.5	11
50.7	6

The general rate equation (Eq 5.3) for the loss of BAS can be written as follows:

$$\frac{d[BAS]}{dt} = r = -k \cdot [BAS]^x \cdot p(H_2O)^y \qquad \text{Eq. 5.3}$$

with   r = rate of BAS decrease

      k = rate constant

      [BAS] = concentration of Brønsted acid sites

      p (H_2O) = partial pressure of water.

To determine the rate order dependence, the rate equation was used in the natural logarithmic form (Eq 5.4):

$$\ln(-r) = \ln k + x \cdot \ln[BAS] + y \cdot \ln p(H_2O) \qquad \text{(Eq. 5.4)}$$

If the concentration of BAS is constant, the slope of the straight line ln (-r) vs. ln p (H_2O) gives the reaction order with respect to water. In the initial time on stream, the BAS concentration can be assumed as constant (differential conditions) and thus, the logarithm of the initial reaction rate (from Table 5.1) can be plotted vs. ln p (H_2O) (Figure 5.6).
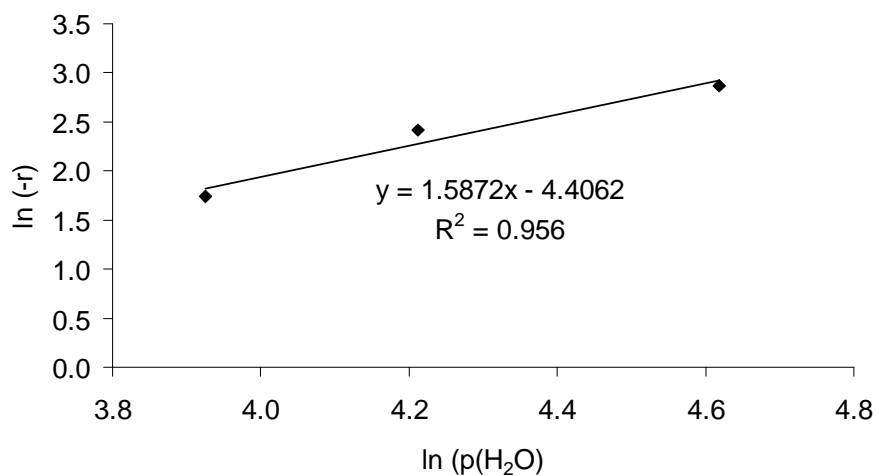
Figure 5.6. Determination of the reaction order of water partial pressure on powder HZSM-5.

The obtained reaction order y with respect to water is 1.6, indicating a complex reaction. Note that the order in water would be expected to be one, if the rate determining step would be the initial interaction of the water molecule to break the Al-O bond.

For the determination of the reaction order x with respect to the concentration of BAS, the integral method was applied to the three sets of data represented in Figure 5.5. Figure 5.7 shows the fit of the experiment data by assuming a second order reaction.

Figure 5.7. Fit of experimental data by assuming reaction order 2 with respect to BAS concentration of powder HZSM-5.

Finally, the kinetic constant k was obtained from Eq. 5.3. with y = 1.6, x = 2, r = initial rate and [BAS] = concentration of BAS for the unsteamed powder HZSM-5 (123 µmol/g).

$$k_{powder} = 7.64 \cdot 10^{-7} \frac{g}{\mu mol \cdot kPa^{1.6} \cdot h}$$ (Eq. 5.4)

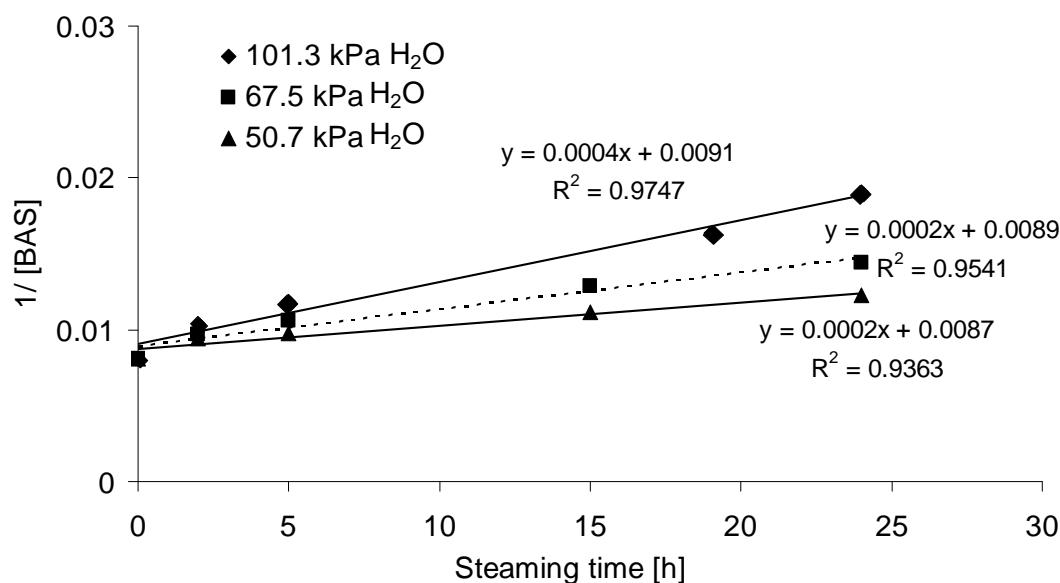Summarizing all these results, the rate equation for the removal of BAS in powder zeolite under hydrothermal conditions can be written as indicated in Eq. 5.5 :

$$r_{powder} = 7.64 \cdot 10^{-7} \frac{g}{\mu mol \cdot kPa^{1.6} \cdot h} \cdot [BAS]^2 \cdot p(H_2O)^{1.6}$$ (Eq. 5.5)

It has to be noted at this point that the dealumination has been treated in this equation as the lump between the sites that dealuminate with a faster and the sites that dealuminate with a slower rate and in consequence two rate constants should be observed. However, as the contribution of the slower dealumination is much smaller, the approach is permissable. The same procedure described above for the powder sample was applied for the determination of the rate of decrease of BAS of extrudate HZSM-5 under similar hydrothermal conditions.

Figure 5.8a shows the subtracted spectra of the extrudate HZSM-5 steamed at 450°C with p (H$_2$O) = 67.5 kPa. In general, both the Brønsted acid site band at 1545 cm$^-$^{1} and the Lewis acid site band at 1450 cm^{-1} decreased with increasing steaming time. This is due to the progression of dealumination with longer steaming duration. The decrease in Lewis acid sites may be explained by the dehydroxylation and agglomeration of the extraframework Al species and alumina binder [26]. The same trend was observed for the other two series with water partial pressures of 101.3 kPa and 50.7 kPa.
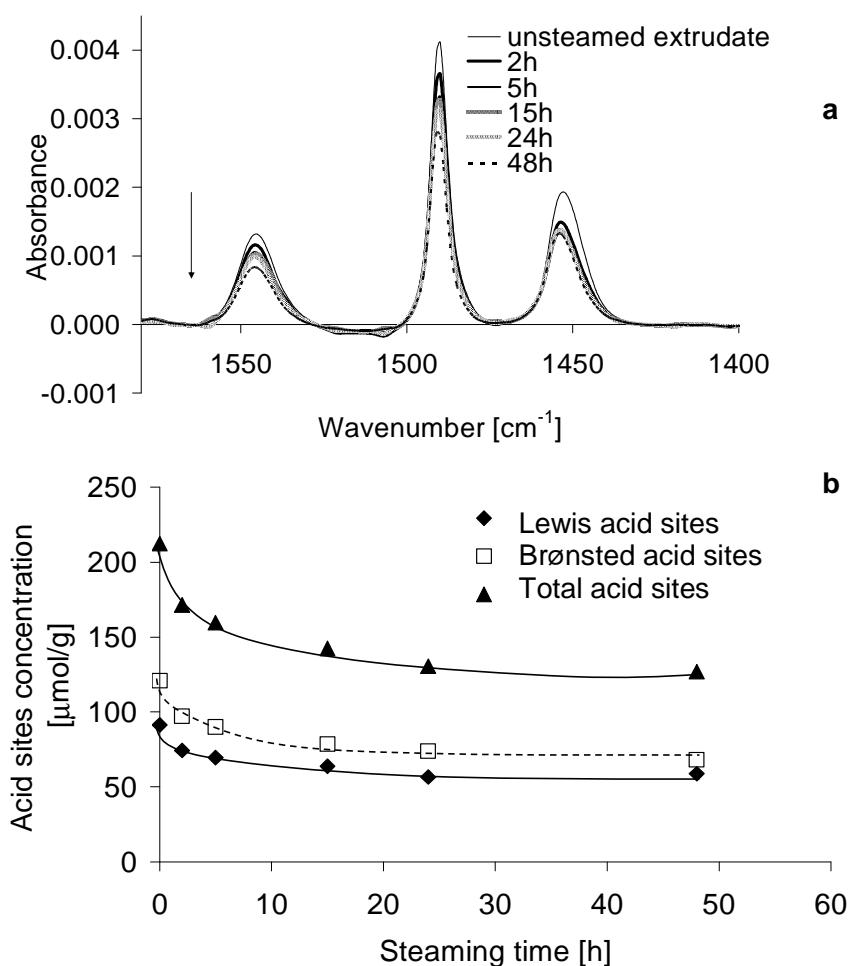

Figure 5.8 a) Subtracted IR spectra of pyridine adsorbed on steamed extrudate and b) Concentrations of acid sites in steamed extrudate (T = 450 °C, p (H$_2$O) = 67.5 kPa).

Figure 5.8b summarizes the decrease of acid sites with steaming duration for extrudate HZSM-5 steamed at 450 ℃ and 67.5 kPa wat er partial pressure. As in the case of the powder HZSM-5, the concentration of the Brønsted acid sites decreases with increasing steaming duration. The Lewis acid sites concentration remained nearly constant after the initial agglomeration with 5 h steaming duration.

The decrease of the Brønsted acid sites concentration with steaming time under different water partial pressures was taken into account for the following kinetic study (Figure 5.9). The initial rate of decrease of BAS of extrudate HZSM-5 was determined as the slope of the curve [BAS] vs. time for $t = 0$. The initial rate increases in proportion to the water partial pressure (Table 5.2). The rapid initial loss of BAS primarily involves the removal of intercrystalline Brønsted acid sites (formed during the extrusion process) and in part, to the more labile Al located at the crystalline part of the zeolite where local gradients are present. They are located at lower T-O-T angle of around 150 °[27, 28]. At the same water partial pressure, the initial dealumination rate is higher for extrudate than for powder HZSM-5.
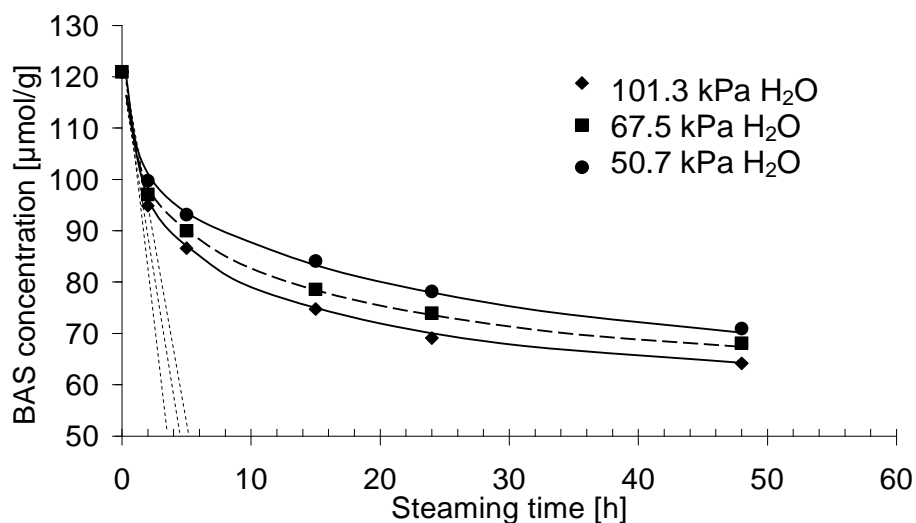
Figure 5.9. Determination of the initial rate of decrease of BAS for extrudate steamed at 450℃.

Table 5.2. Initial rate of decrease of BAS of extrudate HZSM-5 at different water partial pressures.

Water partial pressure	Initial rate of decrease of BAS concentration
[kPa]	[µmol/g/h]
101.3	61
67.5	30
50.7	24
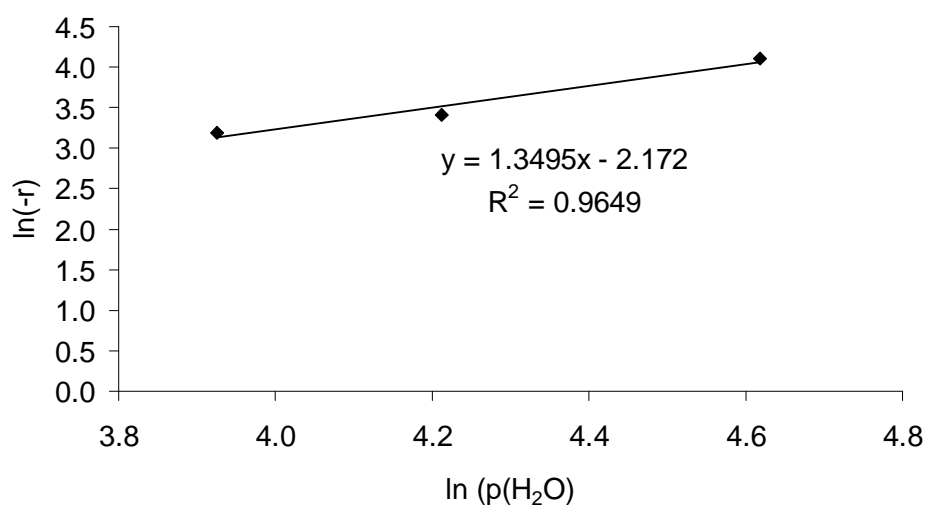
Figure 5.10. Determination of the reaction order of water partial pressure of extrudate HZSM-5.

To obtain the reaction order with respect to water from the initial rate of decrease of BAS (Table 5.2), the general rate equation for the decrease in BAS defined for the powder sample (Eq. 5.3) was also used for the extrudate. Reaction orders of 1.4 for water and of 2 for the Brønsted acid site concentrations were determined from Figure 5.10 and Figure 5.11.
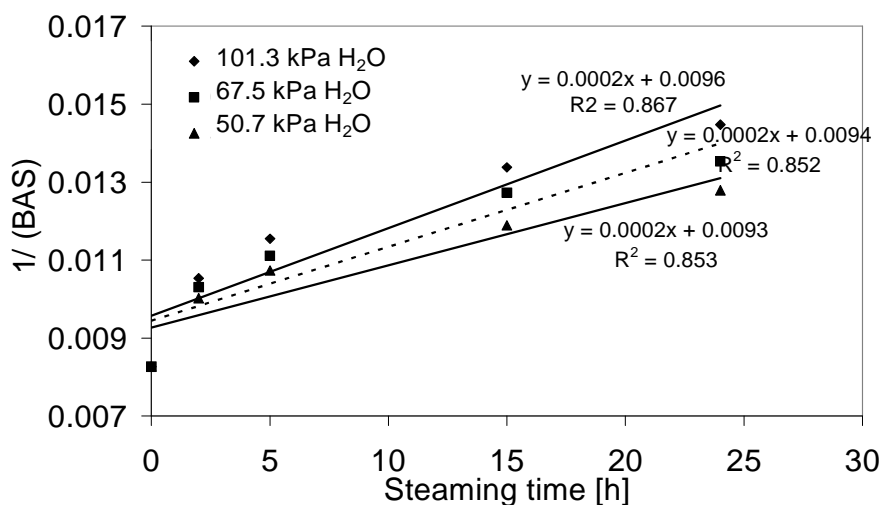
Figure 5.11. Fit of experimental data by assuming reaction order 2 with respect to BAS concentration.

From the concentration of Brønsted acid sites of the unsteamed extrudate HZSM-5 (121 µmol/g), the following value for k was obtained:

$$k_{extrudate} = 6.30 \cdot 10^{-6} \; \frac{g}{\mu mol \; \cdot kPa^{1.4} \cdot h}$$

Summarizing all these results, the rate equation for the removal of BAS of the extrudate zeolite can be written as in Eq. 5.6:

$$r_{extrudate} = 6.30 \cdot 10^{-6} \; \frac{g}{\mu mol \; \cdot kPa^{1.4} \cdot h} \cdot [BAS]^2 \cdot p(H_2O)^{1.4} \qquad \text{Eq. 5.6}$$

Eq. 5.6. Rate equation for the removal of BAS in extrudates under hydrothermal conditions.

5.2.1.1. Comparison of steamed powder and extrudate samples

The concentrations of BAS remaining in the powder and extrudate were compared to examine the relative stability of the zeolite under hydrothermal conditions.
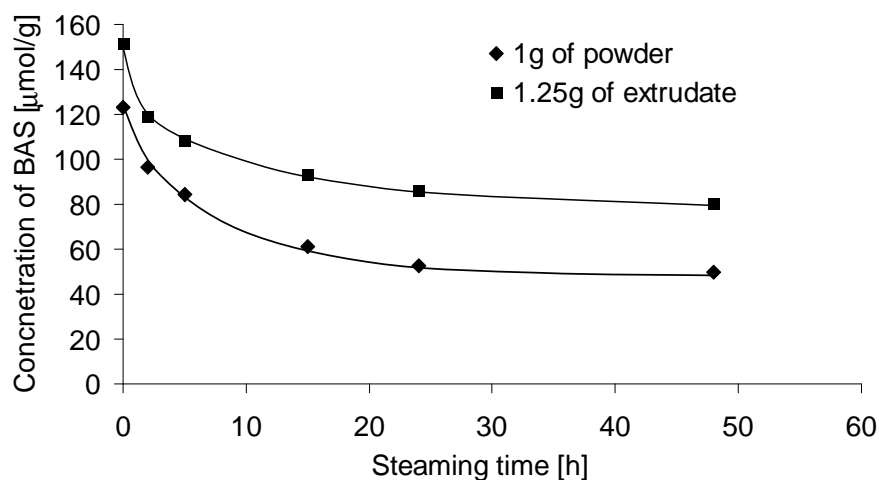
Figure 5.12. Comparison of BAS concentration of 1 g of powder with 1.25 g of extrudate after steaming (450 °C; 50.7 kPa H_2O).

Figure 5.12 compares the decrease of the Brønsted acid sites of the powder and extrudate HZSM-5 after steaming at T = 450 °C with p (H_2O) = 50.7 kPa. The initial rate of decrease of BAS of the extrudate is higher than that of powder. Previous work described in Chapter 3 suggests 20% of the total Brønsted acid sites are intercrystalline and are created during the binding process between the alumina binder and the silica phase of the zeolite crystal. These intercrystalline sites are removed in the initial stage of steaming, as they are not as stable as the Al within the zeolite lattice structure.

The initial loss of LAS as a result of agglomeration of alumina binder changes the contact between binder and zeolite resulting in the destabilization of the weak BAS formed at the interface. To have an accurate comparison of the hydrothermal stability of the zeolite catalysts, it is vital to separate the contributions from the alumina binder from that of the zeolite. Hence, the concentration of remaining acid sites of 1g of powder HZSM-5 is compared with 1.25g of extrudate (1.25g of extrudate = 1g of powder HZSM-5 + 0.25g of alumina binder (20 wt%)). The results show that up to 50% more $Al_{zeolite}$ remained in the extrudate after 48 h steaming at 450 °C and 101.3 kPa H_2O.

5.2.2. Effect of steaming temperature on powder and extrudate HZSM-5

The effect of steaming temperature and duration on the decrease of Brønsted acid sites was also investigated. The complete set of the corresponding steaming experiments was performed at 101.3 kPa water partial pressure. Figure 5.13 shows the

IR spectra of activated powder HZSM-5 steamed for 48 h at different temperatures. As the steaming temperature increased, the intensity of the bridging hydroxyl groups at 3606 cm^{-1} decreased. This decrease was very drastic after steaming at 630 °C, as almost no bridging hydroxyl groups were detected. Clearly, the decrease in the concentration of BAS is more pronounced with higher steaming temperatures. The concentration of terminal (isolated) silanol groups was hardly affected.
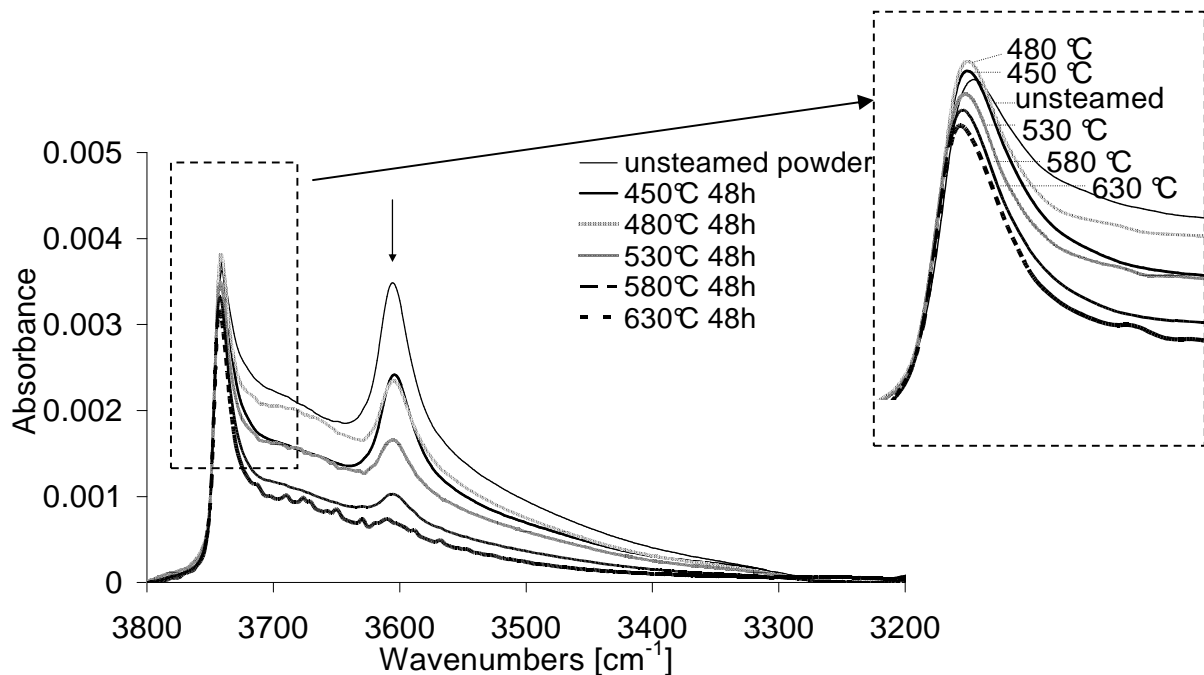
Figure 5.13. Normalized IR spectra of activated powder HZSM-5 steamed at different temperatures for 48 h and 101.3 kPa H$_2$O pressure.

The narrowing of the terminal SiOH group of powder steamed at harsher conditions seemed to indicate the freeing of the silanol groups from hydrogen bonding interaction with hydroxyl groups from extra-framework Al or from interactions with silanol nests at defect sites. This suggests the agglomeration of extraframework Al into alumina clusters or the healing of the defect sites through the migration of hydroxylated silicic species from the amorphous part of the zeolite, thus removing the hydroxyl group from the silanol nests in the process [29, 30].

After steaming at 480 °C, a broad band between 3730 and 3630 cm^{-1} due to the hydroxyl group of the extraframework Al was observed. This peak was not observed in the fresh powder catalyst. As the steaming temperature increased, this broad peak

disappeared, most probably due to the agglomeration of Lewis acid sites at high temperatures.

Figure 5.14a shows the concentration of acid sites remaining in powder HZSM-5 upon steaming at different temperatures for 24 h. While the Lewis acid sites remained relatively constant, the decrease in Brønsted acid sites with increase in steaming temperatures resulted in the overall decrease in the total acid sites concentration.

As shown in Figure 5.14b, the concentration of Brønsted acid sites remained more or less constant regardless of the steaming duration at mild and severe steaming conditions (450, 480 and 630 °C). However, at inter mediate steaming temperature (530 and 580 °C), a further decrease in the concentratio n of Brønsted acid sites was observed from 72 h steaming time.

Figure 5.14. a) Acid sites concentration of powder HZSM-5 after 24 h steaming at different temperatures and 101.5 kPa H_2O pressure b) Effect of steaming duration at different steaming temperatures on powder HZSM-5.

150

Figure 5.15 shows the IR spectra of the activated extrudate steamed at different temperatures. The observed decrease of the intensity of IR band at 3606 cm^{-1} corresponding to bridging OH groups during the dealumination indicates that tetrahedrally coordinated Al is hydrolyzed from the framework. The complete expulsion can result in octahedrally coordinated extra-framework Al, which should increase the broad band between 3706 and 3640 cm^{-1}. While we want to note that hydroxylated Al of the extraframework Al species and the hydroxylated Al from the alumina binder show the same spectral characteristics, the intensity of the IR band characteristic of Al-OH groups decreased with increasing steaming temperature. This trend can be attributed to the agglomeration of alumina nanoparticles in the zeolite pores, which leads to the reduction of the concentration of AlOH group and, thus, to a decrease in the number of Lewis acid sites per atom of extraframework Al.
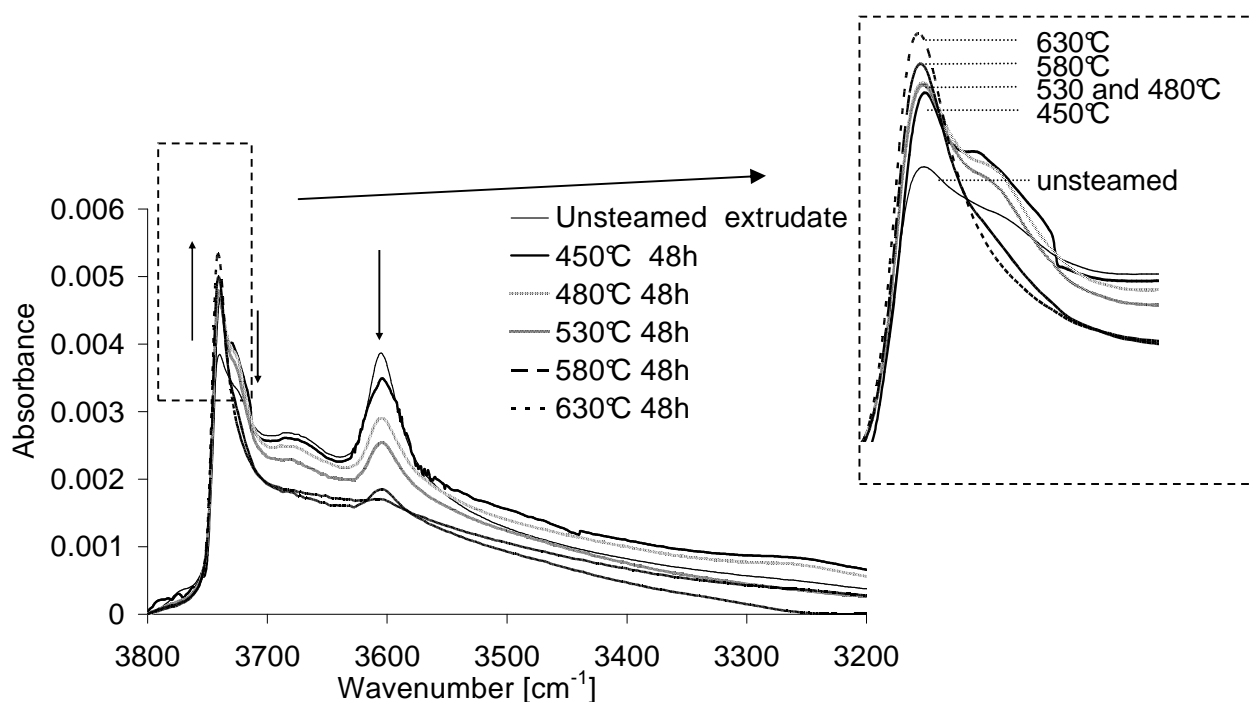
Figure 5.15. Normalized IR spectra of extrudate HZSM-5 steamed at different temperatures for 48 h and 101.5 kPa H$_2$O pressure.

As dealumination progresses, more defect sites are formed due to the loss of Al from the lattice. The silanol nests generated in this process contribute partly to the shoulder at 3725 cm^{-1} [31]. As steaming temperature increased up to 530 °C, the intensity of the shoulder increased due to hydrogen bonding interaction between

terminal silanol groups (3743 cm^{-1}) and that of silanol nests (3725 cm^{-1}) or with the alumina binder. This increase may also be due to the interaction of terminal silanol groups with new amorphous silica/alumina phase formed during the steaming process.

As the steaming temperature increased further (530 to 630 °C), the intensity of the shoulder at 3725 cm^{-1} decreased. This is accompanied by a small increase in the intensity of the terminal silanol group. The decrease of the band at 3725 cm^{-1} after steaming at 580 °C indicates further healing of str uctural defects at silanol nests.

Figure 5.16a shows the concentration of acid sites remaining in extrudates HZSM-5 upon steaming at different temperatures for 24 h. While the Lewis acid sites decreased marginally as a result of agglomeration of alumina particles upon steaming, the Brønsted acid sites decreased markedly with increasing steaming temperature.
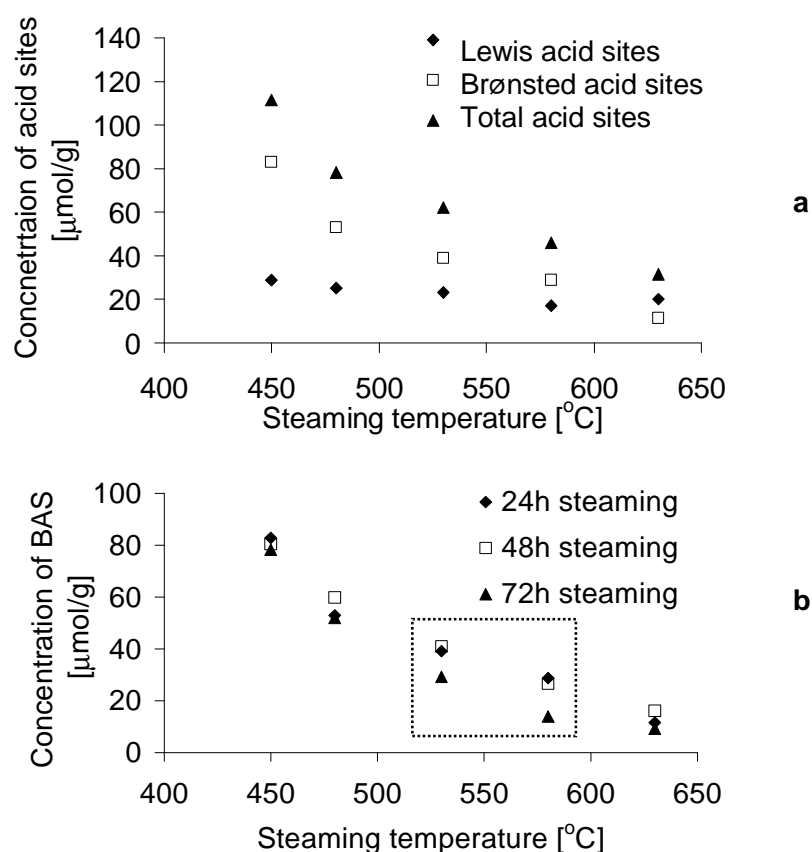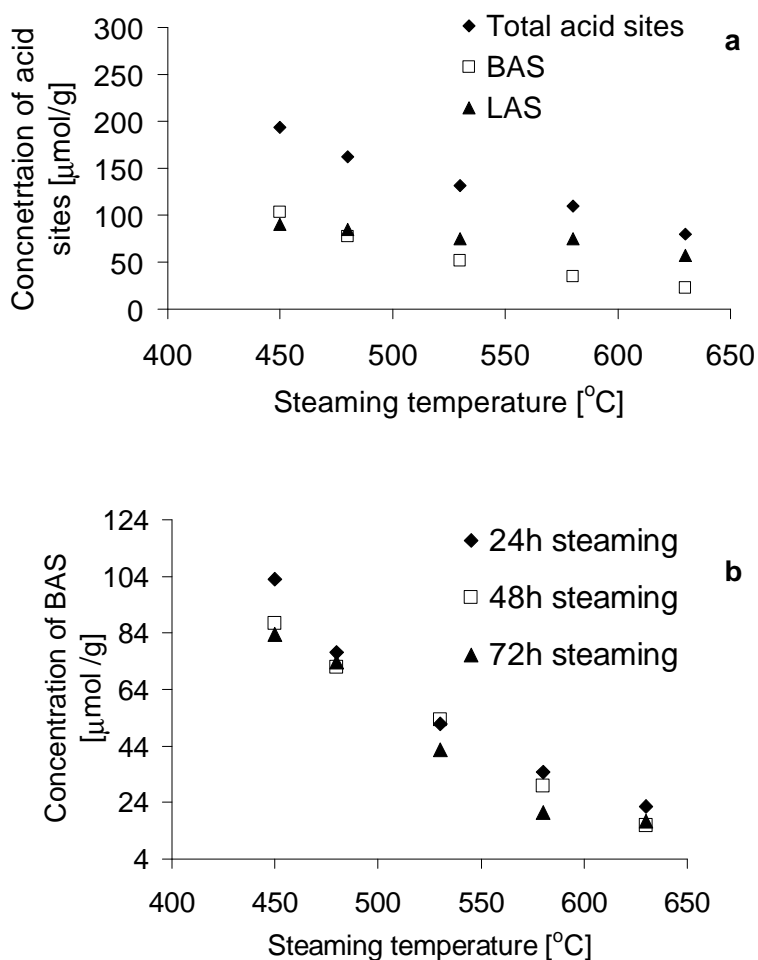
Figure 5.16. a) Acid sites concentration of extrudate HZSM-5 after 24 h steaming at different temperatures (101.5 kPa H_2O:) and b) Effect of steaming duration at different steaming temperatures on extrudate HZSM-5.

Figure 5.16b shows that the concentration of BAS remained relatively constant after 48 h steaming. However, there was a further decrease after 72h steaming at steaming temperatures between 530 and 580 ℃. It is interesting to note that this was also observed for the powder samples. Thus, a comparison between extrudate and powder after 72 h steaming is shown in Figure 5.17. Note that all the intercrystalline sites in the extrudates were removed within 24 h steaming duration. The concentration of BAS of 1 g of powder was compared with that of 1.25 g of extrudate to account for the dilution effect by the presence of binder (20 wt%) in the extrudate. Despite the fact that the extrudates suffered a higher loss of BAS at mild steaming conditions and short steaming

time, after 72 h, the BAS in the extrudate are slightly more stable than are those in the powder HZSM-5 at harsher steaming temperatures.
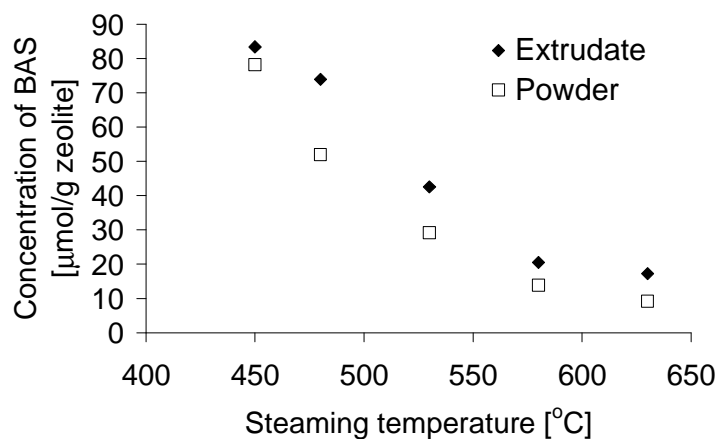
Figure 5.17. Comparison of Brønsted acid sites concentration in extrudate and powder HZSM-5 steamed for 72 h at different temperatures (101.3 KPa H_2O). The amount of BAS has been normalized to the amount of zeolite for the extrudate and powder.

5.2.2.1. ^{27}Al MAS NMR of steamed powder HZSM-5

^{27}Al MAS NMR analysis was carried out on HZSM-5 powder steamed for 24 h at different temperatures (Figure 5.18). Due to the high concentration of Al from the binder in the extrudates, a clear observation of the change in the framework Al_{HZSM-5} of the extrudate could not be unambiguously obtained. Hence, only the data of steamed powder HZSM-5 will be discussed here.
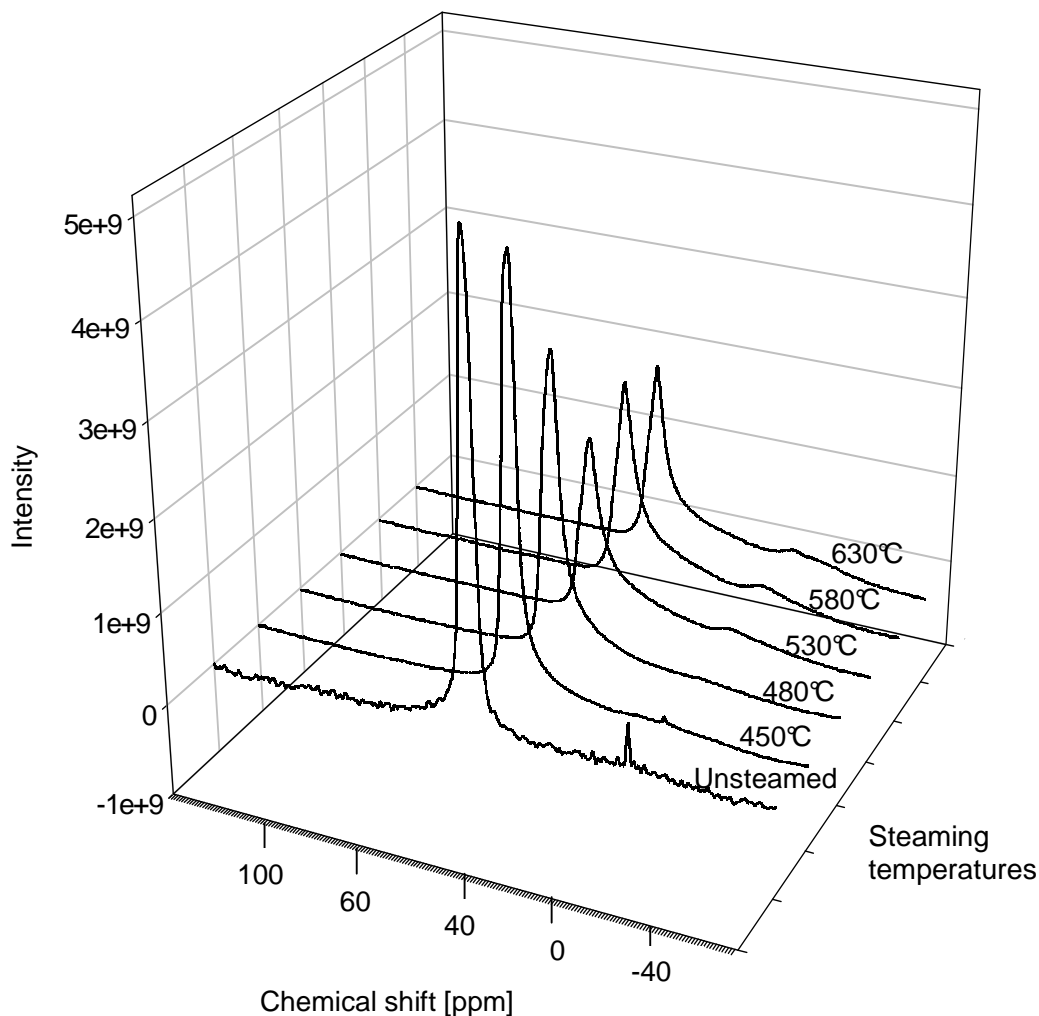
Figure 5.18. ^{27}Al MAS NMR spectra of 72 h steamed powder HZSM-5 steamed at different temperatures (pH$_2$O: 101.5 kPa).

At low steaming temperatures of 450 and 480 °C, on ly a small concentration of distorted tetrahedral aluminum (40-20 ppm) was formed. The small sharp peak at 0 ppm is an indication of extraframework aluminum with octahedral coordination. When steaming temperature was increased above 480 °C, an increase in the width of the tetrahedral peak was observed. This broadening is due to the progressive increase of distorted tetrahedral aluminum as hydrolysis of the framework progresses with higher temperature. In addition, the concentration of octahedrally coordinated aluminum at 0 ppm increased significantly. The broadness of this peak [32] indicates that the

octahedrally formed aluminum is in a distorted environment. Part of these species could still be partially attached to the framework [33-35].

The progressive loss of intensity with increase in steaming temperatures prior to stabilization at 530 ℃ is due to further developme nt of "NMR invisible" Al species. These are in a non symmetric environment resulting in high quadrupolar coupling constant that broadened the peak beyond detection in the current arrangement.

5.2.2.2. ^{27}Al MQMAS NMR of steamed powder HZSM-5

2D [27]Al MQMAS measurements were performed to distinguish the coordination of Al species in the steamed powder samples. The isotropic projection in the F1 dimension gives a 1D high resolution spectrum of aluminum without quadrupolar second order broadening (Figure 5.19a).This spectrum can be deconvoluted into three peaks (Figure 5.19c). Peak IV_1 and IV_2 represent Al in 2 T-sites in the HZSM-5 while peak IV_3 corresponds to distorted tetrahedral extraframework Al species.

The contour of the tetrahedral peak in the 2D spectrum lying close to the isotropic diagonal line indicates the similar excitation efficiency of Al represented by Peak IV_1 and Peak IV_2. Hence, the two peaks were deconvoluted by assigning them to have similar quadrupolar coupling constants of around 2100 MHz (Figure 5.19b). As shown in figure 5.19d, increasing steaming temperature resulted in the preferential removal of Al represented by Peak IV_1. The greatest change in the ratio between Peak IV_1 and Peak IV_2 occurred at mild steaming conditions, which is for temperatures below 480 ℃. For higher temperatures, the dynamic change in the Al at the 2 T-sites approaches to an equilibrium.

Al in distorted tetrahedral environment represented by Peak IV_3 formed on steaming and remained approximately constant after 450 °C steaming temperature. These species are most likely extraframework Al which adopt tetrahedral coordination as partially hydrolyzed framework Al should be removed by 72h steaming time.
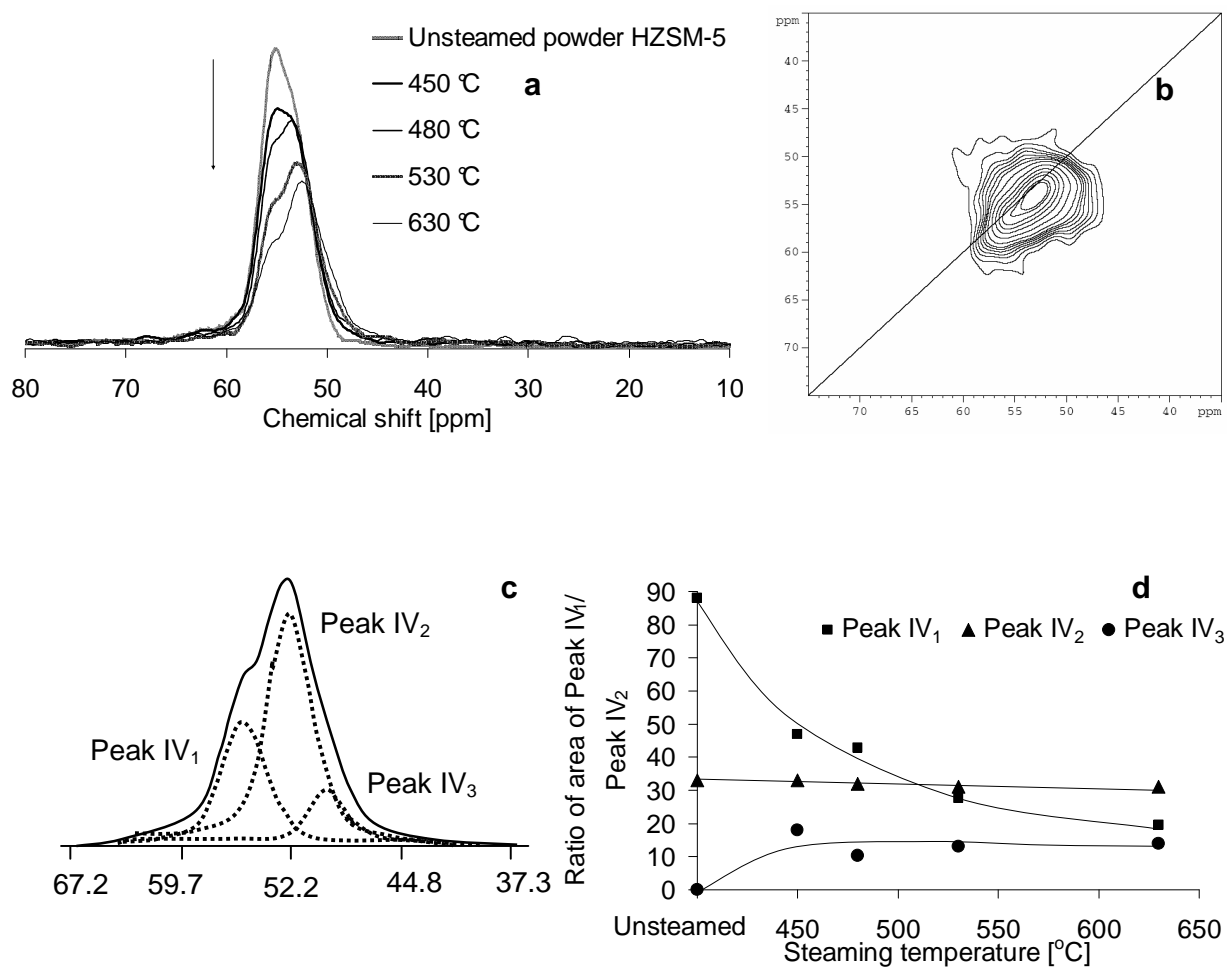
Figure 5.19 a) Comparison of F1 projection of unsteamed and 72 h steamed HZSM-5 powder (Arrow indicates decrease in Al at 57.3 ppm b) 2D MQMAS spectra of powder HZSM-5 steamed at 450 °C for 72 h, c) Deconvolution of F1 projection of powder HZSM-5 steamed at 530 °C and d) Change in concentration of different Al species as function of different steaming temperatures.

5.2.2.3. XRD measurements of steamed powder and extrudate HZSM-5

XRD measurements were carried out to determine the degree of crystallinity of the steamed samples. The resulting diffraction patterns are shown in Figure 5.20 and 5.21.
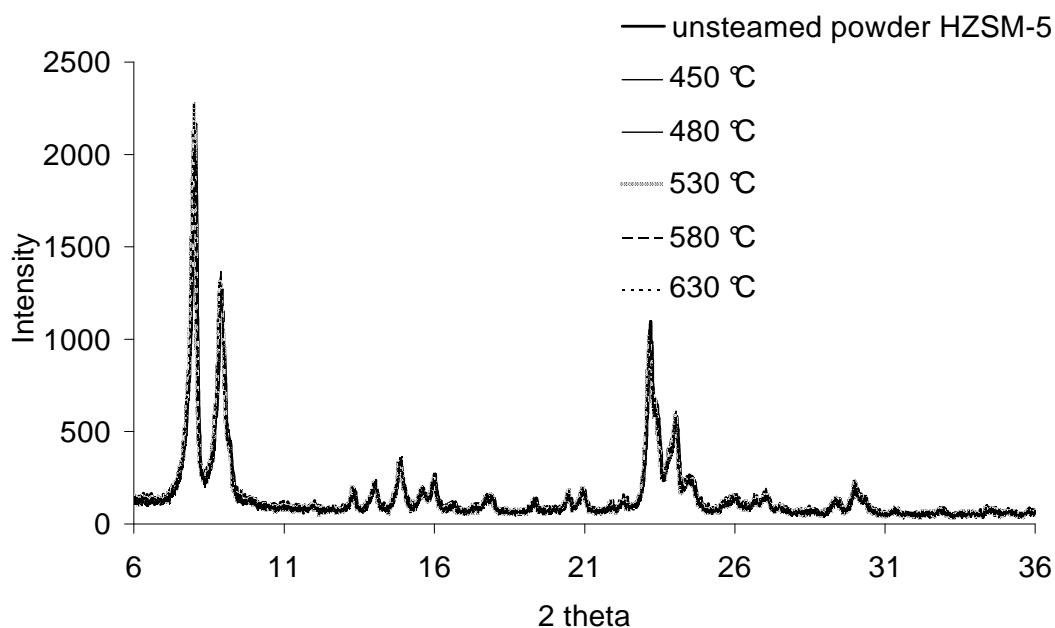
Figure 5.20. XRD powder diffraction patterns of 24 h steamed powder HZSM-5.
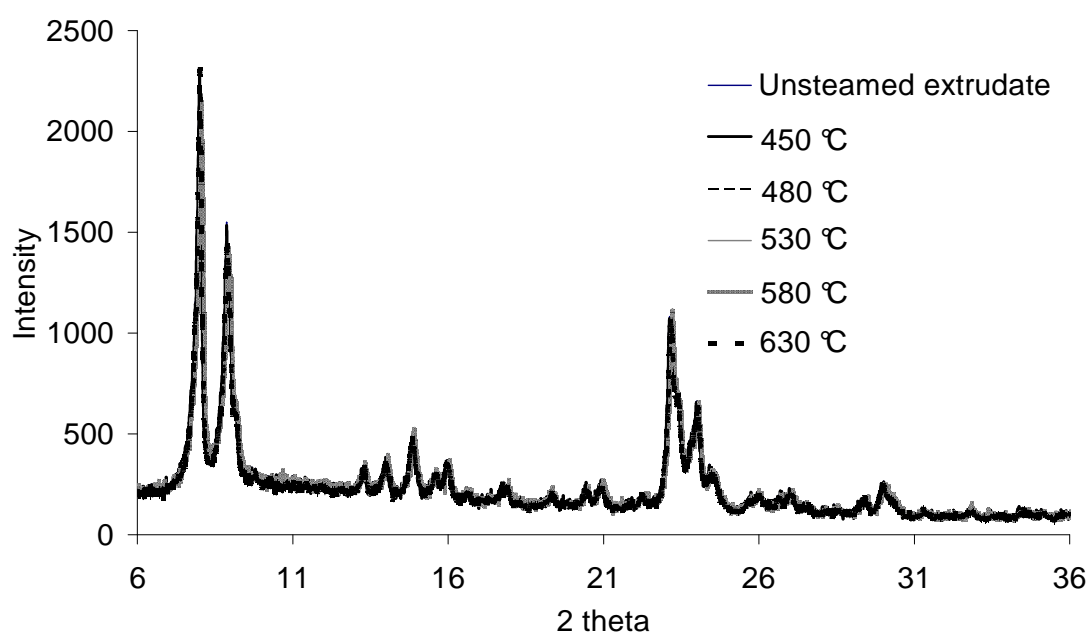
Figure 5.21. XRD powder diffraction patterns of 24 h steamed extrudate HZSM-5.

Only a small decrease in crystallinity was observed for the samples steamed from 450 until 580 °C. The degree of crystallinity in these samples was calculated to be

94% of that of the parent unsteamed zeolite. However, upon steaming at 630°C, a further decrease in intensity of the XRD reflexes was observed with the HZSM-5, retaining only 90% crystallinity. This is attributed to slow thermally induced structural decomposition of the zeolite forming amorphous material at severe steaming conditions [30]. The extrudates maintained approximately 95% crystallinity after 630°C (Figure 5.21). Note that this agrees perfectly with the higher concentration of Brønsted acid sites found in these materials

5.2.2.4. N$_2$ adsorption measurements of steamed powder and extrudate HZSM-5

Nitrogen physisorption data show the relatively constant micropore volume of powder HZSM-5 for all steaming temperatures (Table 5.3.).

The change in the mesopore volume is more complex. At mild steaming temperature of 450 °C, an increase in the mesopore volume was observed indicating that part of the lattice structure is hydrolyzed, forming defect sites. A further increase was observed for the powder samples steamed at 480 °C. At the intermediate steaming temperature (530 °C) the mesopore volume decreased. This is tentatively explained with a rearrangement and densification of the intercrystalline space between primary zeolite particles. Note that the slight increase in the pore volume at high steaming temperatures (580 to 630 °C) suggests that the rearrangement of the inter particle matter leads to increase in mesopore volumes. The rate of healing of the defect sites by silica species generated from the thermal destruction of the framework (a diffusion controlled process) is not sufficient to fill in the formed defects.

Table 5.3. Textural properties of 48 h steamed HZSM-5 powders.

Steaming temperature/ °C	BET surface area [m^2/g]	Mesopore volume [cc/g]	Micropore volume [cc/g]
Unsteamed	335	0.15	0.15
450	338	0.18	0.15
480	357	0.26	0.16
530	333	0.16	0.16
580	341	0.19	0.15
630	336	0.20	0.15

Table 5.4 compiles the nitrogen physisorption data of steamed extrudate HZSM-5. The 35% increase in mesopore volume at mild steaming temperature of 450 ℃ indicates the agglomeration of alumina binder into clusters at the beginning of steaming. However, no significant change in the pore morphology and structure after 450 ℃ steaming was observed.

Table 5.4. Textural properties of 48 h steamed HZSM-5 extrudates

Steaming temperature/ ℃	BET surface area [m^2/g]	Mesopore volume [cc/g]	Micropore volume [cc/g]
Unsteamed	353	0.15	0.15
450	323	0.23	0.10
480	338	0.22	0.11
530	318	0.24	0.10
580	319	0.24	0.10
630	303	0.24	0.10

5.3. Discussion

During steaming, a complex series of events changes the acid site distribution as well as pore structure. This network of kinetic reactions strongly depends on the nature of the starting material, and the external parameters such as temperature, partial pressure of water and the duration of the process. We account for these parameters here in the most detailed way, laying a basis for later kinetic modeling of the processes.

Acid functional groups
Tetrahedrally coordinated aluminum and Brønsted acid sites

The concentration of Brønsted acid sites decreased upon steaming as a result of expulsion of Al from the framework. However, we have shown in Chapter 4 that the two phenomenons are not always quantitatively equivalent. Both the HZSM-5 and the formed catalysts showed a marked decreased in the BAS concentration within the first 24h steaming followed by a very slow decrease thereafter. The two different rates are attributed to the removal of at least two groups of Al species, which differs in their location within the lattice.

The onset of the initial dealumination process involves the participation of more than 1 Al, given the rate order of 2 with respect to BAS for both powder and extrudate

HZSM-5. For the parent zeolite sample, these Al atoms are located in a zone of higher aluminum concentration. Upon removal from the lattice, the alumina species interact with nearby sites still in the lattice. It should be noted that tetrahedral aluminum species exist (peak IV_2 in ^{27}Al MASNMR) that hardly change in concentration with time (refer to Chapter 4) and temperature of steaming. As the concentration of BAS decreases under all circumstances steadily, we conclude that these sites must be stabilized eventually by extra lattice alumina species.

After the removal of the labile Al species in the first 24h, the subsequent dealumination process involves the Al that is more isolated and stable, and hence requires more energy to hydrolyze the Al-O bond manifested in the slower dealumination rate after 24h.

In the case of the formed material, this fast step would also involve the labile surface/intercrystalline acid sites. These non-isolated Al species, once removed, cap onto neighboring BAS and neutralized their Brønsted acidity, also causing a rapid decrease in the detected BAS concentrations.

Previous IR spectroscopy investigations on the effect of binder on the acidity of HZSM-5 (see Chapter 3) indicate that these intercrystalline acid sites are formed as a result of interaction of the alumina binder with $SiOH/SiO_2$ phase in the zeolite during extrusions/calcinations at high temperature. Comparison between the powder and the extrudate indicate a higher initial rate of decrease of BAS in the extrudate. This is primarily due to the facile removal of intercrystalline acid sites. As the formation of intercrystalline sites requires the contact of the alumina clusters with the zeolite crystals on an atomistic level, we conclude that hydrothermal treatment disrupts such contact, resulting in changes in pore morphology and subsequently the stability of such acid sites at the interface.

The tetracoordinated framework Al forming Brønsted acidity is influenced by the presence of extra lattice Al in its vicinity. Even though part of the framework Al is stabilized by extra lattice Al, their Brønsted acidity is neutralized. This is detrimental in reactions requiring the participation of BAS. The interaction of the extra lattice Al with neighboring sites, previously possessing Brønsted acidity, is apparently sufficient to stabilize them in their present form. Such interaction is sufficient to prevent them from being leached out even at severe steaming temperatures of more than 500 ^{o}C. This is concluded from NMR data in which tetracoordinated extra lattice Al is detected in all the steamed materials.

The preferential removal of Al from T-sites with lower T-O-T angle of around 150° (δ= 57.3 ppm in ^{27}Al NMR) compared to T-O-T angle of around 155° (δ= 53.1 ppm in ^{27}Al NMR) gives an insight to the stability of Al with different T-O-T angles. This information is useful towards the systematic design of zeolites that have higher hydrothermal stability especially when paired sites are avoided.

Lewis acid sites

Lewis acidity is mainly related to hexacoordinated extraframework Al, by the alumina binder (in the formed material), and to a small extent, by the presence of cationic impurities present in the parent material. If the species would remain fully dispersed, the removal of Brønsted acid sites should result in an equivalent increase in the concentration of Lewis acid sites. However, the disparity in the quantification of the two indicates that most of the expelled Al species hydrolyzed and condensed to form larger alumina nanoclusters. This is on top of the small amount of Al that was hydrolyzed out from regions of high Al concentrations and is deposited within the parent material.

Blockage of the micropore structure is not observed, despite the dealumination process. This is a result of the 3D network of pore channels of HZSM-5 zeolites, which enabled probe molecules e.g. pyridine used in IR spectroscopy measurements to enter through various pathways to the acid sites.

The Lewis acid sites of the alumina binder continue to decrease with increase in steaming temperatures. In this aspect, the agglomeration of alumina clusters via dehydroxylation and condensation took place upon steaming, thus changing the contact between the zeolite and the binder. The rearrangement of the interparticle material destabilizes the intercrystalline acid sites, thus contributing to the higher initial decrease in the BAS present in the extrudates.

Pore structure and lattice integrity

An increase in the mesopore volumes for both the parent and formed HZSM-5 is observed upon steaming. This increase is attributed to the rearrangement of interparticle materials and, to a smaller extent, to the destruction of the structural integrity, forming defect sites in the zeolite crystals.

Dehydroxylation and thermal destruction on the HZSM-5 starts at 500 ℃. This structural decomposition, which is slower than dealumination, may proceed for certain duration and once a threshold level of structural degradation is reached. The remaining

framework Al becomes destabilized and is further hydrolyzed from the zeolite lattice. This is supported by the further decrease in BAS concentration after 72h steaming at 530 and 580 °C. Hence, structural integrity is vita l for the stability of the framework Al, without which, they would be easily hydrolyzed from the lattice structure.

At 630 °C, framework decomposition takes place as a result of thermal induced degradation of the structure. This is evident from the loss of intensity of the main reflexes of the diffraction pattern and the formation of further mesoporous structure. At this stage, the healing of defect sites by diffusion of hydroxylated silicic species from amorphous silica phase is too slow to compensate the increase in the number of defect sites.

The retaining of 90% crystallinity in the parent HZSM-5 indicates that the structural integrity of the crystals is largely retained. The 95% crystallinity in the formed catalysts shows an even more superior stability of the final material against structural degradation during steaming. This is also indirect evidence that explain for the retaining of a higher concentration of Brønsted acid sites at severe steaming conditions compared to the unformed material.

Specific influence of the binder

Embedding HZSM-5 powder into an alumina binder leads to higher stability of the zeolite at severe steaming conditions. It is interesting to note that the changes in mesopore structures of the steamed extrudates upon further increase of steaming temperatures are minute compared to that exhibited by the unbound HZSM-5.

The matrix retarded the interparticle rearrangement of the zeolite aggregates as observed in the powder HZSM-5. This protecting effect requires the intimate contact between the matrix and the zeolite particles which has been shown by the generation of intercrystalline acid sites in the unsteamed extrudates. The zeolite crystal aggregates are surrounded by small aggregates of alumina clusters. Thus, the individual zeolite aggregates are no longer in direct contact.

The intimate contact between the zeolite crystals and the alumina binder also gives rise to limited realumination of vacancies created during dealumination. This is related to the metastable aluminum species present in the zeolite that can undergo reversible coordinations [37]. Such realumination only takes place if there is interaction between the matrix and the zeolite surface. Thus, for realumination to take place, the defect sites formed from structural degradations should most probably be located near to the pore mouth of the zeolite crystals.

The location of defect sites near to the zeolite surface can arise from the apparent migration of vacancies via the T-jump mechanism, when neighboring Si refills the vacancies (Figure 5.21) The Al from the binder can then insert into these vacancies near to the zeolite crystal surface. Further studies should be performed to confirm, if these realuminated sites possess Brønsted acidity of comparable acid strength with that of the zeolitic acid sites.
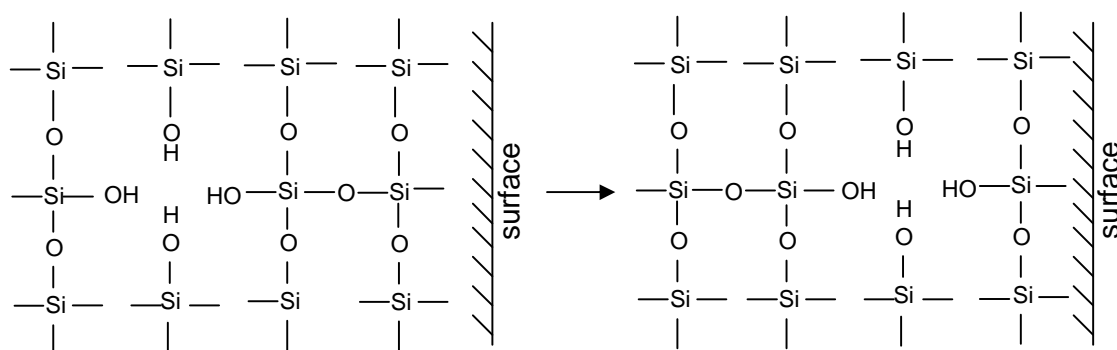
Figure 5.22. T-jump mechanism of Si migration or apparent migration of the framework vacancy [38].

Segregation of vacancies
form defect sites

Realumination of vacancies at
surface of zeolite crystals

H_2O

H_2O

Realuminated site at surface
of zeolite crystal

H_2O

.... Steam

HZSM-5 crystal

Aggregates of alumina binder

○ Defect sites

--▶ Segregation of vacancies to surface of zeolite crystal via T-jump mechanism

⊗ Enlarged schematic drawing of $Al(OH_x)^{y+}$ species migrate to fill in vacancies

⊙ Realuminated sites

Figure 5.23. Schematic drawing of the realumination of zeolite crystals by hydroxylated Al species from binder.

5.4. Conclusions

It is commercially attractive to perform post synthesis modification of zeolites via steaming to achieve a material of higher hydrothermal stability with the desirable Si/Al ratio. The effect of steaming is the decrease in BAS concentration accompanied by a minor decrease in LAS concentration. The existence of Al paired sites resulted in a rapid decrease of BAS concentration after the initial steaming duration. This is due to neutralization of neighboring sites by extra lattice Al that originates from the paired sites. Presence of intercrystalline acid sites can also contribute to the rapid decrease as

demonstrated in the formed materials. Hence, the avoidance of such paired sites is essential when hydrothermal conditions are applied.

The agglomeration of extra lattice Al and also alumina binder results in the decrease of the detected Lewis acid sites concentration. The former phenomenon did not result in significant pore blockage while the latter resulted in the destabilization of previously formed intercrystalline acid sites. Minimal changes in the crystallinity of the steamed materials indicate the superior structural stability of high silica zeolite for use in hydrothermal conditions.

The results further demonstrate that embedding of zeolite crystals in a matrix created a protecting effect which retards the sintering and structural degradation of zeolite crystals. Hence, more Brønsted acid sites are retained in the formed material after steaming compared to the unformed material on the same zeolite weight basis. The limited realumination of defect sites that segregated to the surface of the zeolite crystals by hydroxylated Al species from the binder during steaming also contributes to the enhanced hydrothermal stability of the formed materials.

5.5.   References

1.   Guisnet, M. and Magnoux, P., Appl. Catal., **1989**, 54**,** 1, 1-27.

2.   Rollmann, L.D. and Walsh, D.E., J. Catal., **1979**, 56**,** 1, 139-140.

3.   Langner, B.E., Appl. Catal., **1982**, 2**,** 4-5, 289-302.

4.   Guisnet, M., Magnoux, P., and Martin, D., Catalyst Deactivation, **1997**, 111, 1-19.

5.   Gayubo, A. G., Aguayo, A. T., Moran, A. L., Olazar, M. and Bilbao, AIchE. J., **2002**, 48, 7, 1561-1571.

6.   Benito, P. L., Gayubo, A. G., Aguayo, A. T., Olazar, M. and Bilbao, J., Ind. Eng. Chem. Res., **1996**, 35, 11, 3991-3998.

7.   Aguayo, A. T., Gayubo, A. G., Ortega, J. M., Olazar, M. and Bilbao, J., Catal. Today, **1997**, 37, 239-248.

8.   Masuda, T., Fujikata, Y., Mukai, S. R. and Hashimoto, K., Appl.Catal., A, **1998**, 172, 1, 73-83.

9.   Campbell, S. M., Bibby, D. M., Coddington, J. M. and Howe, R. F., J. Catal., **1996**, 161, 1, 350-358.

10.   Choudhary, V. R., Devadas, P., Kinage, A. K., Sivadinarayana, C. and Guisnet, M., J. Catal., **1996**, 158, 2, 537-550.

11. Salman, N., Ruscher, C. H., Buhl, J. C., Lutz, W., Toufar, H. and Stocker, M., Microporous Mesoporous Mater., **2006**, 90, 1-3, 339-346.

12. Zhang, Y. W., Zhou, Y. M., Yang, K. Z., Li, Y., Wang, Y., Xu, Y. and Wu, P. C., Microporous Mesoporous Mater., **2006**, 96,1-3, 245-254.

13. Kühne, M. A., Babitz, S. M., Kung, H. H. and Miller, J. T., Appl. Catal., A, **1998**, 166, 2, 293-299.

14. Calero, S., Schenk, M., Dubbeldam, D., Maesen, T. L. M. and Smit, B., J. Catal., **2004**, 228, 1, 121-129.

15. Baeck, S.H. and Lee, W.Y., Appl. Catal., A, **1998**, 168, 1, 171-177.

16. Corma, A., Grande, M., Fornes, V. and Cartlidge, S., Appl. Catal., **1990**, 66, 2, 247-255.

17. Corma, A., Grande, M., Fornes, V., Cartlidge, S. and Shatlock, M. P., Appl. Catal., **1990**, 66, 1, 45-57.

18. Emeis, C.A., J. Catal., **1993**, 141, 2, 347-354.

19. Massiot, D., Fayon, F., Capron, M., King, I., Le Calve, S., Alonso, B., Durand, J. O., Bujoli, B., Gan, Z. H. and Hoatson, G., Magn. Reson. Chem, **2002**, 40, 1, 70-76.

20. Loeffler, E., Lohse, U., Peuker, C., Oehlmann, G., Kustov, L. M., Zholobenko, V. L. and Kazansky, V. B., Zeolites, **1990**, 10**,** 4, 266-271.

21. Loeffler, E., Peuker, Ch. and Jerschkewitz, H. G., Catal. Today, **1988**, 3, 415-420.

22. Knözinger, H. and Ratnasamy, P., Cat. Rev. - Sci. Eng., **1978**, 17, 1, 31-70.

23. Lercher, J.A., Ritter, G., and Vinek, H., J. Colloid Interface Sci., **1985**, 106, 1, 215-221.

24. Dědeček, J., Kaucký, D., and Wichterlová, B., Chem. Comm., **2001**, 11, 970-971.

25. Kaucký, D., Dědeček, J. and Wichterlová, B., Microporous Mesoporous Mater., **1999**, 31, 1-2, 75-87.

26. Marques, J. P., Gener, I., Ayrault, P., Bordado, J. C., Lopes, J. M., Ribeiro, F. R. and Guisnet, M., Comptes Rendus Chimie, **2005**, 8, 3-4, 399-410.

27. Sarv, P., Fernandez, C., Amoureux, J. P. and Keskinen, K., J. Phys. Chem., **1996**, 100, 50, 19223-19226.

28. van Bokhoven, J. A., Roest, A. L., Koningsberger, D. C., Miller, J. T., Nachtegaal, G. H. and Kentgens, A. P. M., J. Am. Chem. Soc., **2000**, 122, 51, 12842-12847.

29.   Wang, Q. L., Giannetto, G., Torrealba, M., Perot, G., Kappenstein, C. and Guisnet, M., J. Catal., **1991**, 130, 2, 459-470.

30.   Gola, A., Rebours, B., Milazzo, E., Lynch, J., Benazzi, E., Lacombe, S., Delevoye, L. and Fernandez, C., Microporous Mesoporous Mater., **2000**, 40, 1-3, 73-83.

31.   Jacobs, P.A. and Uytterhoeven, J. B., J. Chem. Soc., Faraday Trans. I, **1973**, 69, 2, 373-386.

32.   L. Yingcai, J.M., S. Yaojun, W. Tailiu, W. Liping, F. Lun, J. Chem. Soc., Faraday Trans., **1996**, 92, 1647-1651.

33.   Bourgeatlami, E., Massiani, P., Direnzo, F., Espiau, P., Fajula, F. and Courieres, T. D., Appl. Catal., **1991**, 72, 1, 139-152.

34.   Wouters, B.H., T.H. Chen, and P.J. Grobet, J. Phys. Chem. B, **2001**, 105, 6, 1135-1139.

35.   Wouters, B.H., T.H. Chen, and P.J. Grobet, J. Am. Chem. Soc., **1998**, 120, 44, 11419-11425.

36.   Lippmaa, E., Magi, M., Samoson, A.,Tarmak, M. and Engelhardt, G., J. Am. Chem. Soc., **1981**, 103, 17, 4992-4996.

37.   Chang, C. D., Hellring, S. D., Miale, J. N., Schmitt, K. D., Brigandi, P. W. and Wu, E. L., J. Chem. Soc., Faraday Trans. I, **1985**, 81, 2215-2224.

38.   Hunger, M., Karger, J., Pfeifer, H., Caro, J., Zibrowius, B., Bulow, M., and Mostowicz, R., J. Chem. Soc., Faraday Trans. I, **1987**, 83, 3459-3468

Chapter 6

Summary

More than 60 years have passed since the first introduction of zeolites as adsorbent, catalysts and ion exchanger in various applications of science and technology. Of the members of the zeolite family, HZSM-5 with its ten-membered ring pores and high acid strength are ideal materials for selective sorption and catalytic reactions. Its outstanding property in terms of thermal stability, coke resistivity and shape selectivity resulted in several industrial applications for hydrocarbon conversion.

The key to the successful application of HZSM-5 as a catalyst requires a careful control of the synthesis process to tailor desirable acid sites strength, distribution and concentration of the aluminum within the framework. The understanding of zeolites in terms of its inherent acidity has matured tremendously over the past 50 years with a vast number of publications and proceedings which enhanced our understanding of these aluminosilicate materials.

However, one often observes different results with slight variations of the preparation methods. In addition, the application of pure HZSM-5 as a catalyst is not possible due to the poor self binding property. The requirement of embedding into a matrix resulted in the contribution of the binder to the overall observed stability and activity of the bound HZSM-5. It is no longer possible to extrapolate the properties of the pure powder to the bound catalysts as the intimate contact of the matrix and the zeolite crystals involves complicated physicochemical processes.

With this in mind, the subtle variations in a series of HZSM-5 with varying Si/Al ratios were explored in Chapter 2 of the thesis. In-depth characterizations of the change in acidity was done using temperature programmed desorption of ammonia, IR spectroscopy of adsorbed pyridine, ^{1}H NMR and thermogravimetry. Heterogeneity of acid sites was observed in all samples despite the relatively low concentration of Al in the unit cell ranging from about 4.5 to 0.4 Al/u.c.. In addition, the HZSM-5 with highest Al content exhibited highest strength while that with the lowest number of framework Al has the highest proportion of weak acid sites. This is in contrary to the general notion of higher acid strength in high silica zeolite due to localization of aluminum charge density.

The observed peculiarities are explained by the presence of extraframework Al in the vicinity of the Brønsted acid sites resulting in the inductive enhancement of its acid strength. A constant number of weak sites are present in all the HZSM-5 investigated, suggesting a fortuitous formation of paired Al sites at local gradients in which their non-statistical distribution and location is influenced by the energetics of the synthesis process. It is likely that the formation of such paired sites takes place at specific T

positions within the framework, resulting in the lower protonic reorientation in the AlO_4 tetrahedra and hence lowers the protonic mobility. These findings suggest that estimation of acid strength purely based on the number of framework Al is too simplistic. The distribution and location of framework Al appears to precede the concentration in the overall observed acid strength.

Since the application of most HZSM-5 in commercial use requires the binding with a matrix, the physicochemical properties of HZSM-5 extrudates bound with alumina binder is studied in Chapter 3. Results show that the overall effect of the pelletization process is the increase in the total acid sites concentration as a result of an increase in the Lewis acid sites contributed by the binder. In addition, the effect on the Brønsted acid sites concentration differs, depending on the Si/Al ratio of the zeolites. It is shown that new intercrystalline Brønsted acid sites are formed at the outside of the crystals or with silica between the crystals for the high silica HZSM-5. In addition, apparent acid sites are formed which takes place only on adsorption of a strong base like pyridine when Lewis acid sites of unsaturated Al from the binder is in the vicinity of terminal SiOH groups.

The decrease in Brønsted acid sites concentration of the low silica sample is attributed to the partial charge compensation of bridging oxygens by anionic alumina species near the pore entrance. This kind of exchange may be the reason for the slightly lowered acid strength of the extrudates compared to the unbound powder. The different effects on the final acidity of the extrudates with the same binding conditions imply the non homogenous distribution and location of Al in the parent HZSM-5. The complex interplay of physical and chemical interaction between the binder and the HZSM-5 crystals shows that the contribution from the binder and the zeolite is not a mathematical summation of the two. Tailoring of the final bound catalyst properties to impart desirable properties is possible when a careful selection of the binder and the method is employed.

Another method for tuning the Si/Al ratio of the HZSM-5 is through post synthetic hydrothermal treatment which dealuminates the framework Al resulting in a more hydrothermal stable zeolite. However, the mechanistic aspects of dealumination proposed in the past years vary among the different works which can be due to the influence of pore structure and the inherent tendency towards defect sites formation in different zeolites. Since high silica HZSM-5 is of practical interest for the industry due to

its higher thermal stability, the dealumination mechanism of the unbound HZSM-5 (SAMPLE C) is investigated in Chapter 4.

The rapid dealumination in the first 24h followed by a slow dealumination rate thereafter is due to the preferential removal of the unstable Al populated at sites with lower T-O-T angle. Conceptually, the Al atom with lower T-O-T angle should be more stabilized within the framework but the above observations indicate that hydrolysis is localized at the weakest Al-O bond after which the extraction of the partially hydrolyzed Al from the framework is very rapid. NMR results indicated that most of the Al adopts tetrahedral coordination but data from IR spectroscopy indicated a drastic decrease in the Brønsted acid sites concentration. This implies that the extraframework Al formed are tetrahedrally coordinated and that the cationic exchange onto neighboring Brønsted acid sites contributed to the drastic decrease of Brønsted acidity. The weak/unstable Al is most likely located in the more crystalline part of the zeolite in the form of paired Al sites.

The higher resistance of the remaining Al against dealumination is due to the greater hydrothermal stability of Al populated at sites with higher T-O-T angle and the stabilization of cationic exchanged Brønsted acid sites by extraframework Al. The structural integrity of the steamed HZSM-5 is maintained at 94% crystallinity which suggests the robustness of the zeolite under steaming conditions.

Following the work in Chapter 4, the hydrothermal stability of the extrudate HZSM-5 (EXT C) bound with alumina binder was investigated. The motivation for this is the observed difference in the physicochemical properties of the bound HZSM-5 compared to the unbound counterpart. Hence, the dealumination behavior of the bound and unbound HZSM-5 may vary. The work is divided into two parts in Chapter 5 to investigate the stability of the Al against hydrolysis. The first part studies the dealumination kinetic of the powder vs. the extrudate. It was found that the initial rate of dealumination is more rapid in the extrudate compared to the powder HZSM-5. This is explained by the removal of the weak Brønsted acid sites situated at the external of the crystals that is formed by the interaction of the alumina binder with silica phase of the HZSM-5 upon binding. The determined rate order with respect to water was 1.4 for the extrudate vs. 1.6 for the powder, indicating a complex reaction.

The rate order of 2 with respect to Brønsted acid sites in the dealumination process implied that Al located at local gradients forming paired Al sites are preferentially hydrolyzed. The non statistical distribution of Al in the parent material has already been

observed in Chapter 2 of this thesis. In addition, ^{27}Al NMR results indicated the preferential loss of Al populated at sites with lower T-O-T angles. Despite the higher initial dealumination rate of the extrudate, the bound HZSM-5 exhibited greater thermal stability at more severe hydrothermal conditions with respect to the temperature and steaming duration.

The stabilization effect imparted by the binder requires the intimate contact between the zeolite crystals and the alumina clusters. This is because migration of hydroxylated aluminic species form the binder can then fill the zeolitic defect sites that segregate or are formed near to the surface of the crystals in the presence of water and high temperature. In addition to the limited reinsertion of the Al into defect sites, the formed extrudates retarded the sintering of the zeolite particles, hence resulting in higher structural stability.

Complex changes in the mesoporosity were also observed which can be taken advantage of via the careful application of pore engineering to produce zeolites of lower diffusion resistivity. Optimal post synthetic modifications can be achieved by the tuning of the hydrothermal conditions (temperature and duration) to produce thermally stable catalyst for applications where water is fed or produced.

Curriculum Vitae

Lay Hwa, Ong was born on the 9th of September, 1979 in Singapore. After the completion of her junior college studies, she joined the department of Applied Chemistry in the National University of Singapore for her bachelor degree. Subsequently, she enrolled into the GIST (German Institute of Science and Technology) for a Master in Industrial Chemistry. The theme of her diploma thesis is: Hydroformylation in multiphasic systems of supercritical carbon dioxide and ionic liquids under the guidance of Professor Walter Leitner in collaboration with Celanese AG. After her Masters, she joined the department of Technical Chemistry in the Technical University of Munich working under Professor Johannes A. Lercher for her PhD. The work involves the study of subtle variations of Al distribution and location in HZSM-5 and the influence of hydrothermal dealumination on powder and extrudate prototypes.

List of publications